PET/PP-Based Polymer Composites: Effects of Compatibilizer and Nanofillers on the Processing-Structure-Property Relationships

Beim Fachbereich für Maschinebau und Verfahrenstechnik
der Technischen Universität Kaiserslautern
zur Erlangung des akademischen Grades

Doktor-Ingenieur (Dr.-Ing.)

genehmigte Dissertation

von

M.Sc. Wenjing Li

aus Shandong, China

Tag der mündlichen Prüfung: 27th, November, 2009

Prüfungvorsitzender: Prof. Dipl.-Ing. Dr. techn. habil. H.-J. Bart
1. Berichterstatter: Prof. Dr.-Ing. Alois K. Schlarb
2. Berichterstatter: Prof. Dr.-Ing. P. L. Geiss

Acknowledgement

The present work was completed between January 2009 and August 2009 at the Institute for Composite materials (Institut für Verbundwerkstoff GmbH, IVW) of the University of Kaiserslautern, Germany.

First and foremost, I would like to express my special gratitude to my supervisor Prof. Dr.-Ing. Alois K. Schlarb for his scientific support and concern about the progress of my work. I would also like to thank Prof. Dr. h.c. Karger-Kocsis József and Prof. Dr.-Ing. Evstatiev for the fruitful discussions on polymer science and technology. I am thankful to Prof. Dipl.-Ing. Dr. techn. habil. H.-J. Bart for accepting the presidency of the examination committee and to Prof. Dr.-Ing. P. L. Geiss for the co-referent of this PhD thesis.

I would like to thank the RLP Graduate School for the financial support. I am grateful to the IVW for providing me the opportunity of working in an outstanding environment from the scientific and technical point of view. Many thanks to Mr. Rolf Walter, Mr. Hermann Giertzsch, Mr. Stephen Schmitt, Mr. Ralf Schimmele, Ms. Pia Eichert for their kind help in the experiments. I would also like to express my appreciation for the help and friendship to M.Sc. Lada Gyurova, Dr. Ga Zhang, Dr. Suchart Siengchin, Dr. Zhenyu Jiang, Dr. Sergiy Gryshchuk, Dr. Nuria Castellá, Dipl.-Chem. Ruijuan Zhou, Dipl.-Ing. Zdravka Rasheva, Dipl.-Ing. Nicole Knör, Dipl.-Ing. Martin Priebe. Especially I would like to thank Dr. Martin Weber (BASF SE) for his support and helpful discussion during our cooperation.

I would like to convey my special thanks to my parents who constantly supported and encouraged me.

Table of Contents

Abstract

Microfibrillar reinforced composites (MFC) have attracted considerable academic and practical interests after the concept was introduced more than a decade years ago. This new type of composites will be created by blending of two polymers with different melting temperatures and processing the blend under certain thermo-mechanical conditions to generate in-situ formed microfibrils of the higher melting polymer grade of temperature in the blend. The compression molded microfibrillar composites were reported to possess excellent mechanical properties and thus they are promising materials for different applications.

In the present work, a typical immiscible polymer blend PET/PP was selected for the preparation of PET/PP, PET/PP/TiO$_2$ microfibrillar reinforced composites. The objective of this study is to analyse the processing-structure-property relationship in the PET/PP based MFCs.

The morphology of the PET microfibrils and the dispersion of the TiO$_2$ nanoparticles were characterized by scanning electron microscopy (SEM) and transmission electron microscopy (TEM), and discussed. The crystallization behaviour of PET and PP was studied by means of differential scanning calorimetry (DSC). The thermomechanical and mechanical properties of the composites were determined by dynamic mechanical thermal analysis (DMTA) and uniaxial tensile tests and the related results discussed as a function of the composition of the corresponding system.

During stretching of the PET/PP extrudate, the PET dispersed phase was deformed into microfibrils. These microfibrils were still well persevered after compression molding of the drawn strands. Therefore the PET microfibrils acted as the reinforcement for the PP matrix. Compared with neat PP, the tensile properties of the PET/PP MFC were greatly improved. For the PET/PP/TiO$_2$ MFC, the effects of polypropylene grafted maleic anhydride (PP-g-MA, introduced as

compatibilizer) and TiO_2 particles on the structure and properties of drawn strands and composites were investigated. Upon the addition of PP-g-MA, the preferential location of TiO_2 particles changed: they migrated from the PET dispersed phase to the continuous PP matrix phase. This was accompanied with structural changes of the drawn strands. The microfibril formation mechanism was also investigated. After injection molding of the microfibrillar composites, the preferential location of TiO_2 particles was still preserved. DMTA analysis of drawn strands, the tensile and impact tests of the composites demonstrated that the mechanical properties of the drawn strands of the microfibrillar composites were strongly dependent on the respective structures of the tested materials.

To further investigate the preferential location of TiO_2 particles in the PET/PP blend which were discovered during the preparation of PET/PP/TiO_2 MFCs, PET/PP/TiO_2 ternary nanocomposites were prepared according to four blending procedures. The preferential location of TiO_2 nanoparticles was influenced by the blending sequence and the amount of PP-g-MA incorporated. Furthermore, it was discovered that TiO_2 nanoparticles exerted a compatibilizing effect on the morphology of the composites. Three different compatibilization mechanisms of nanoparticles were proposed depending on the location of the nanoparticles.

Kurzfassung

Microfibrillar verstärkte Komposite (MFC) haben nach Vorstellung des Konzeptes vor mehr als zehn Jahren ein beachtliches akademisches sowie anwendungstechnisches Interesse geweckt. Diese neuartige Art von Verbundwerkstoffen wird über ein Blend zweier Polymere mit unterschiedlichen Schmelztemperaturen und anschließender Verarbeitung unter bestimmten thermisch-mechanischen Bedingungen realisiert. Dabei bilden sich in-situ erzeugte Mikrofibrillen, die aus dem höherschmelzenden Polymer des Blends bestehen.

Die über entsprechende Pressverfahren hergestellten microfibrillaren Komposite (MFC) sollen exzellente mechanische Eigenschaften aufweisen wodurch sie ein vielversprechendes Anwendungspotential haben.

In der vorliegenden Arbeit wurde ein typisches, nicht mischbares Polymergemisch, PET/PP, für die Herstellung von PET/PP, PET/PP/TiO$_2$ mikrofibrillar verstärkten Kompositen ausgewählt. Ziel dieser Studie ist es, die Prozess-Struktur-Eigenschaften von auf PET/PP basierenden MFCs zu erforschen.

Die Morphologie der PET Mikrofibrillen und die Dispersion der TiO$_2$ Nanopartikel wurden mit Hilfe von Rasterelektronenmikroskopie (SEM) und Transmissions-Elektronenmikroskopie (TEM) charakterisiert und erörtert. Das Kristallisationsverhalten von PET und PP wurde über dynamische Differenzkalorimetrie (DSC) untersucht. Die thermomechanischen und mechanischen Eigenschaften der Komposite wurden durch dynamisch-mechanische Thermoanalyse (DMTA) und einachsige Zugprüfungen bestimmt und die entsprechenden Ergebnisse wurden als Funktion des Blends erörtert

Während des Streckens des PET/PP Extrudates wurde die PET disperse Phase

in Mikrofibrillen verformt. Diese Mikrofibrillen waren nach dem Pressverfahren noch vorhanden. Wodurch die PET Mikrofibrillen eine Verstärkung für die PP-Matrix darstellen. Im Vergleich zu reinem PP, waren die Zugeigenschaften des PET/PP MFCs deutlich verbessert. Bei PET/PP/TiO$_2$ MFCs, wurde der Einfluss von mit Maleinsäure anhydrid gepfropftem Polypropylen (PP-g-MA, als Kompatibilisator) und TiO$_2$ über Struktur-Eigenschafts-Beziehungen analysiert. Nach der Zugabe von PP-g-MA, veränderte sich die bevorzugte Position der TiO$_2$ Partikeln: Sie wanderten aus der PET dispersen Phase zur kontinuierlichen PP-Matrix Phase. Dies war mit strukturellen Veränderungen von gezogenen Fasersträngen verbunden. Der Mechanismus zur Bildung von Mikrofibrillen wurde ebenfalls untersucht. Nach dem Spritzgießen von mikrofibrillaren Kompositen hatten die TiO$_2$ Partikel ihre bevorzugte Position beibehalten. Die DMTA Analyse der gezogenen Faserstränge, Zugprüfungen und der Schlagzähigkeitstest der Komposite demonstrierten, dass die mechanischen Eigenschaften der gezogenen Faserstränge und der mikrofibrillaren Komposite stark von den Strukturen der getesteten Materialien abhängig waren.

Um die bevorzugte Position der TiO$_2$-Partikel in der PET/PP Mischung, die während der Herstellung von PET/PP/TiO$_2$ MFCs festgestellt wurden, weiter zu untersuchen, wurden ternäre PET/PP/TiO$_2$-Nanokomposite nach vier Mischverfahren hergestellt. Die bevorzugte Position der TiO$_2$ Nanopartikel wurde über die Mischfolge und die Menge des eingearbeiteten PP-g-MA beinflusst. Darüberhinaus wurde festgestellt, dass die TiO$_2$ Nanopartikel eine kompatibilisierende Wirkung auf die Morphologie der Komposite ausübten. Drei verschiedene Kompatibilisierungsmechanismen der Nanopartikel wurden in Abhängigkeit der Position der Nanopartikel vorgeschlagen.

List of Abbreviations and Symbols

Abbreviations

CB	Carbon black
DSC	Differential scanning calorimetry
DMTA	Dynamic mechanical thermal analysis
GMA	Glycidyl methacrylate
LCP	Liquid crystalline polymer
MA	Maleic anhydride
MFC	Microfibrillar composite
OH	Hydroxyl (group)
PA6	Polyamide 6
PBT	Polybutylene terephthalate
PC	Polycarbonate
PE	Polyethylene
PEMA	Polyethyl methacrylate
PET	Polyethylene terephthalate
PMMA	Polymethyl methacrylate
PO	Polyolefin
PP	Polypropylene
PP-g-MA	Polypropylene grafted maleic anyhydride
PPS	Polyphenylene sulfide
PS	Polystyrene
rpm	Revolution per minute
SAN	Styrene acrylonitrile copolymer
SEM	Scanning electron microscopy
SiO_2	Silicon dioxide
TEM	Transmission electron microscopy
TiO_2	Titanium dioxide
vol.%	Volume percent

wt.%	Weight percent

Symbols

a	[nm]	Radius of a particle
C	[s^{-1}]	Frequency of collisions
D_0	[cm^2/s]	Diffusion coefficient
D_f, D_n	[nm]	Diameter of a microfibril, droplet
E*	[MPa]	Complex elastic modulus
E', E''	[MPa]	Storage-, loss modulus
ΔG_m	[kJ/mol]	Free energy of mixing
ΔH	[kJ/mol]	Activation energy
k_B	J/K	Boltzmann constant
L	[mm]	Length
L/D	[1]	Length/diameter
R	[mm]	Radius
T, T_0	[ºC]	Actual-, reference temperature
T_g, T_c	[ºC]	Glass transition-, crystallization temperature
t	[s]	Time
t_D	[s]	Time of diffusion
tan δ	[1]	Mechanical loss factor
X_c	[%]	Crystallinity

Greek symbols

$\dot{\gamma}$	[s^{-1}]	Shear rate
η_d, η_m	[Pa.s]	Viscosity of dispersed phase, matrix
Φ	[%]	Volume fraction of the dispersed entity
λ	[1]	Viscosity ratio
ω	[1]	Wetting parameter

1 Introduction

Immiscible polymer blends usually exhibit poor mechanical properties due to weak interfacial adhesion between their constituents. The lack of adhesion between the blend constituents is generally considered as a disadvantage [1]. However, it becomes a critical factor in the successful creation of a new type of fibrillar polymer-polymer composite from immiscible blends. Microfibrillar reinforced composites (MFC) are comprised of an isotropic polymer matrix reinforced with an even dispersion of micro- or nanofibrils with high aspect ratio. The fibrils made from the secondary dispersed polymer after the blend has been subjected to a hot stretching procedure. This is accompanied with the orientation of the matrix polymer as well. The orientation of the matrix is then released through an isotropization process whereby keeping the disperse phase aligned, i.e. in fibril form [2].

Blends of poly(ethylene terephthalate) (PET) and polyolefin (PO) have attracted considerable research activities since both materials are among the most frequently used thermoplastics, especially as packaging materials. PET may enhance the stiffness of polyolefin at higher temperatures while the polyolefin could facilitate the crystallization of PET by heterogeneous nucleation affecting the blend stiffness. However, owing to the differences in chemical nature and polarity, the PET/polyolefin blends exhibit very poor impact strength. Hence, appropriate compatibilization is needed to achieve better adhesion between the two phases and to improve mechanical properties. A compatibilizer typically has two parts so that each part can interact with one of the polymers in the blends. This allows blending of immiscible polymers and creating a homogenous mixture.

PET fibers are known as high performance fibers which possess high tensile strength and modulus, while polypropylene (PP) is of low tensile properties. Immiscible with PP and having a much higher melting temperature than the PP,

PET is considered as ideal reinforcement material for preparing PET/PP-based MFC.

Incorporation of nanofillers into immiscible polymer blends was reported to exert a compatibilization effect on the blend morphology, which usually contributes to improvement of mechanical properties [3]. The incorporated nanofillers usually have a preferential location in the polymer blends (either located in one phase or at the interface). The location of nanofillers is greatly influenced by the following factors: the interfacial tension of the two polymers, the viscosities of the two polymers, blending procedures, mixing time and the incorporation of additives. Due to large difference in polarity and viscosity, PET/PP is considered as the ideal blend to investigate the migration and compatibilization mechanisms of nanofillers.

2 State of the Art

2.1 Polymer blends

2.1.1 Phase morphology

Blending of polymers is an effective route to develop new materials with novel properties. The ability to combine existing polymers into new compositions with improved novel properties offers the advantage of reduced research and development expense compared to the development of new monomers and polymers. Therefore, great attention has been paid to investigate polymer blends.

The types of polymer blends are very broad, from simple binary mixture to combinations of block copolymers and homopolymers, interpenetrating networks, reactive compatibilized systems, molecular composites, impact modified polymers, emulsion blends, engineering polymer blends and countless other systems [1]. The primary difference of polymer blends is linked with their phase structure: completely miscible blends, partially miscible blends and fully immiscible blends. In completely thermodynamically miscible blends, homogeneity is observed at least on nanometer scale, if not on the molecular level. This type of blend exhibits only one glass transition temperature, which is between the glass transition temperatures of both blend components in a close relation to the blend composition. In partially miscible blends a (small) part of one blend component is dissolved in the other. Both blend phases are homogeneous, and have their own glass transition temperatures. The glass transition temperatures are shifted, however, from the values for the pure blend components towards the glass transition temperature of the other blend component [4].

Most of polymer blends are known as phase separated systems. Depending on the complex interplay of material parameters and processing conditions, various types of useful morphologies can be obtained for a given blend (Figure 1.1). The

related morphologies generate different end properties such as high strength and toughness, toughness coupled with stiffness, good barrier properties, and high melt flow. However, from the point of view of a broader classification, multiphase polymer blends may be divided into two major categories:

- Blends with a discrete phase structure (i.e., droplets in matrix),
- Blends with a bi-continuous phase structure (i.e., co-continuous).

Other types of morphologies include fibrillar, core shell and onion ring-like morphologies [5, 6].

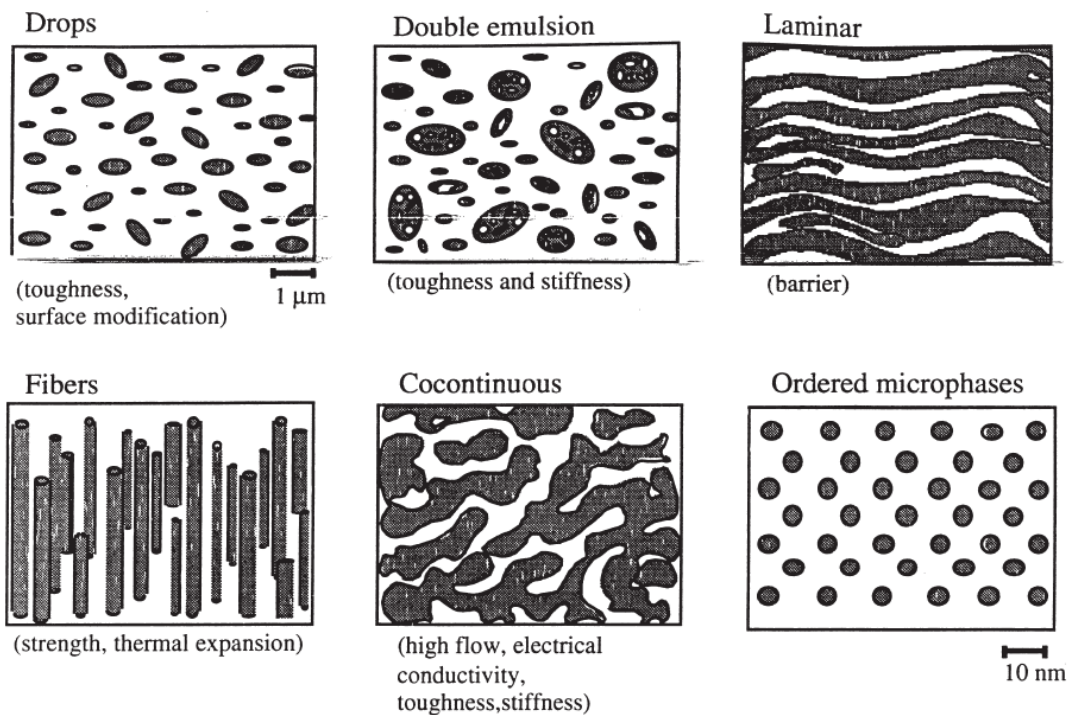**Figure 2.1**: Schematic of useful morphologies of polymer blends [6].

2.1.2 Compatibilization of immiscible blends

Due to the weak adhesion at the interface, immiscible polymer blends exhibit unstable phase morphologies and poor mechanical properties. In order to create a blend with useful properties, its compatibilization is necessary. Two general methods are used for compatibilizing immiscible polymers:

- incorporation of suitable block or graft copolymers (nonreactive compatibilization),
- reactive compatibilization.

Usually the chains of a block or graft copolymers a have a blocky structure, with one constitutive block miscible with one blend component and a second block miscible with the other blend component. These blocky structures can be premade and added to the immiscible polymer blend, but they can also be generated in-situ during the blending process. The incorporated copolymers tend to enrich at the interface between the two polymers. The copolymers anchor their segments in the relevant polymer, reducing the interfacial tension and stabilizing dispersion against coalescence [7-9]. However, their ability to stabilize the phase structure is limited [10]. The conformation of different block, graft, or random copolymers at the interface is schematically drawn in Figure 1.2.
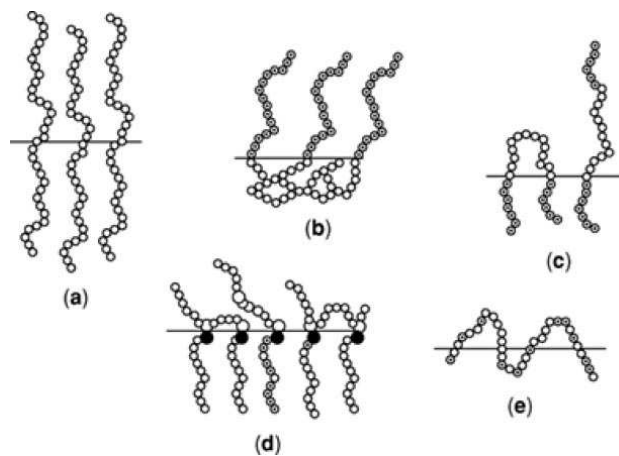
Figure 2.2: Possible localization of A-B copolymer at the A/B interface. Schematic of connecting chains at an interface, (a) diblock copolymers, (b) end-grafted chains, (c) triblock copolymers, (d) multiply grafted chain, (e) random copolymer [11].

Reactive compatibilization is the process that allows generating graft or block copolymers acting as compatibilizers in-situ during melt blending. There are different types of reactive compatibilization. If the two blended polymers contain

reactive groups, their reaction is straightforward. Another type of reactive compatibilization is realized by incorporating a reactive polymer which is miscible with one blend component and reactive towards functional groups attached to the second blend component. A block or grafted copolymer is thereby formed in-situ at the interface [11].

One of the primary methods of reactive compatibilization is to utilize maleic anhydride (MA) grafted polymers. The anhydride group can react with the amine end groups of polyamides (PA) and the hydroxyl end groups of polyester [12-15]. The other reactive groups such as carboxyl, oxazoline, isocyanate and epoxy are also employed as grafts or in copolymers to compatibilize immiscible polymer blends [16-20]. Figure 1.3 lists some reactive groups involved in reactive processing.
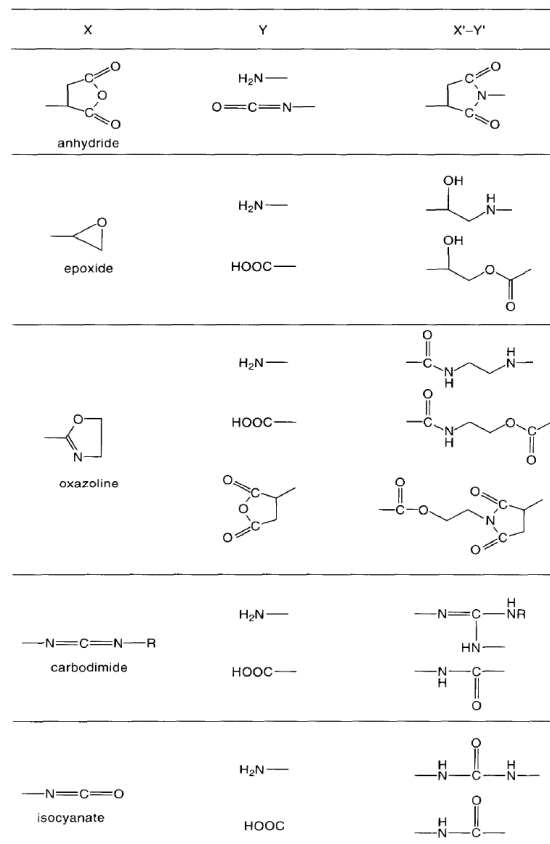
Figure 2.3: Reactive groups involved in reactive processing [4].

The mechanism of stabilization against coalescence for compatibilized polymer blends is shown schematically in Figure 1.4. The interface of the polymer blends consists of a layer (or layers) of copolymers. The block segment of the matrix phase polymer is located in the outer surface of the droplet since it is incompatible with the droplet. Therefore, the dispersed phase droplet is covered with a shell of copolymer with the outside consisting of matrix phase block segments. When the matrix fluid tries to drain as the droplets come together, the copolymers at the interface do not allow the dispersed phase in the two droplets to meet and the droplets recoil. In order for the dispersed phase in the two droplets to meet, the copolymers must be moved out of the contact area. Since the interfacial viscosity increases upon adding a compatibilizer, it will be difficult to move the copolymers, thus, coalescence is retarded. If there is enough copolymer at the interface, then it may form an "interphase" which must be overcome for coalescence to occur.

Broader Interface

Figure 2.4: Suppression of coalescence. Two droplets which have a layer of diblock or grafted copolymer at the interface are less likely to coalesce since copolymer molecules form shells around the droplets [8].

2.1.3 Control of blend morphology

The morphology of immiscible blends depends on many factors, such as blend composition, viscosity ratio of the two components, the capillarity number, interfacial tension, mixing time, geometry of the screw and screw rota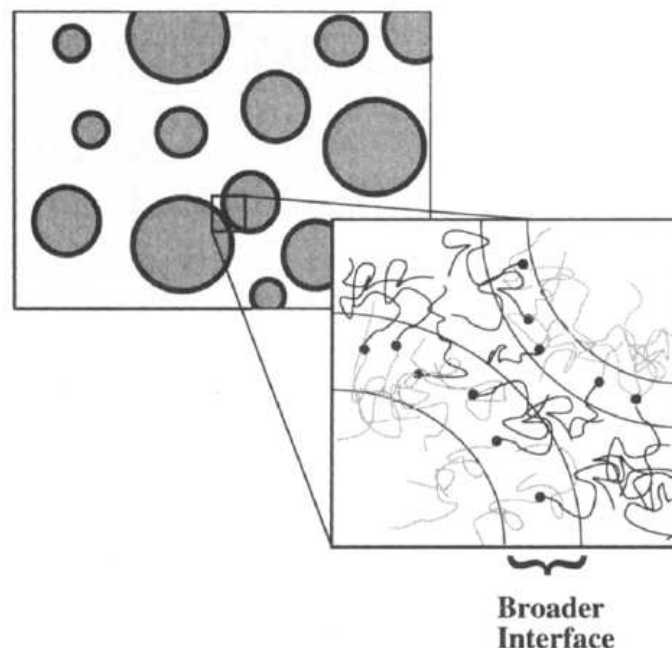tion speed [21-23]. During processing, a wide range of size and shapes of dispersed phase can be obtained. In the immiscible polymer blends, the domains range in size from submicron to hundreds of microns. Moreover, spherical, ellipsoidal, cylindrical, ribbon-like, co-continuous, and sub-inclusion types of morphology can be obtained under various conditions. The final morphology is balanced between the droplet breakup and coalescence processes [24-30].

Viscosity ratio

The viscosity of the dispersed phase/the viscosity of the matrix (λ) is one of the most critical variables for controlling blend morphology. Generally, a high viscosity ratio results in a coarse morphology, while low viscosity ratio results in a fine morphology. It is generally accepted that a viscosity ratio of 1 leads to the smallest diameter of the dispersed phase and the finest morphology [24].

Blend composition

In polymer blends, the minor component usually forms the dispersed phase while the major component forms the continuous phase. However, when the contents of the two polymers are comparable, more viscous component tends to form the dispersed phase, and the less viscous component tends to form the continuous phase [23, 24, 31].

Interfacial modification

Interfacial modification of polymer blends reduces the droplets size of the dispersed phase and narrows the droplet size distribution [24].

Processing parameter

Blending immiscible polymers in an extruder at high screw speed leads to a finer morphology, since high screw speed generates an intensive shear stress field that facilitates efficient droplet breakup. Longer mixing time also favors a finer phase morphology. Figure 1.5 describes the mechanism of morphology development during the melt blending of immiscible polymer blends [7, 24].
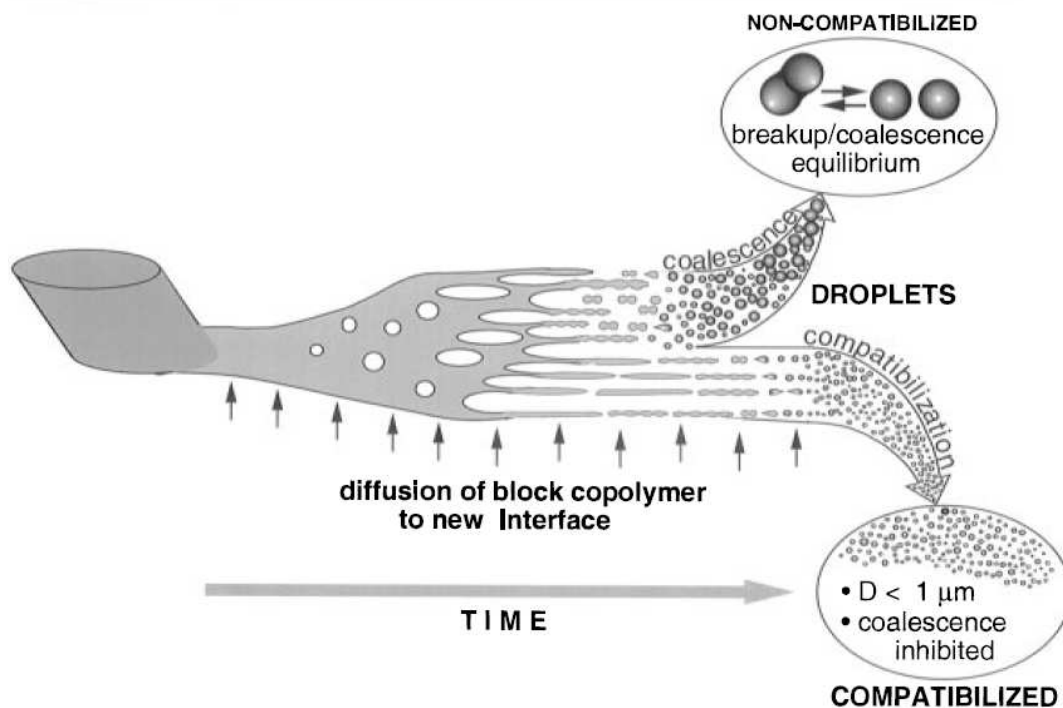

Figure 2.5: Schematic of morphology development during melt blending of miscible polymer blend. As pellets or powder of the minor phase soften, layers peel off. These stretch out into sheets which break up into fibers and then droplets. Unless block copolymer can rapidly cover the new interface, these droplets will coalesce to larger particles [7].

2.2 Microfibrillar composites

2.2.1 Polymer fibers

It is well known that melt-spinning or solid-state drawing of polymers produces high-modulus high-strength polymer fibers [32, 33]. Clark and Scott [34] using acetal resin, found that the drawing process consists of two stages. In the first stage, the unoriented billet is drawn at a rapid rate; a neck forms and propagates along the entire specimen until, at this rapid draw rate, the process is terminated by fracture. This first stage of draw is termed "natural draw" with the draw ratio of the necked specimen being about 7 at fracture for acetal polymer. The natural draw rate can be several hundred percent per minute. The second stage of draw (super draw) which elongates the sample several hundred percent beyond the natural draw ratio, appears to be a distinctly separate process requiring a much slower draw rate (several percent per minute) and careful control of temperature. Figure 1.6 shows the morphology of natural drawn fiber and super drawn fiber. The undrawn crystalline polymer consists of folded chain lamellae joined by a small but important fraction of tie molecules. On drawing, the lamellae break into folded chain blocks on the order of 20 nm in breadth which subsequently aggregate to form the fundamental unit of the drawn structure: the microfibril. The microfibril is composed of alternating crystal blocks and amorphous layers, the latter consisting of chain folds (of varying loop length), chain ends (cilia) and tie molecules connecting the chain folded blocks along the longitudinal direction in the drawn microfibril. The tie molecules which connect the blocks in the longitudinal (draw) direction provide the principal source of strength and modulus in the microfibril [35].
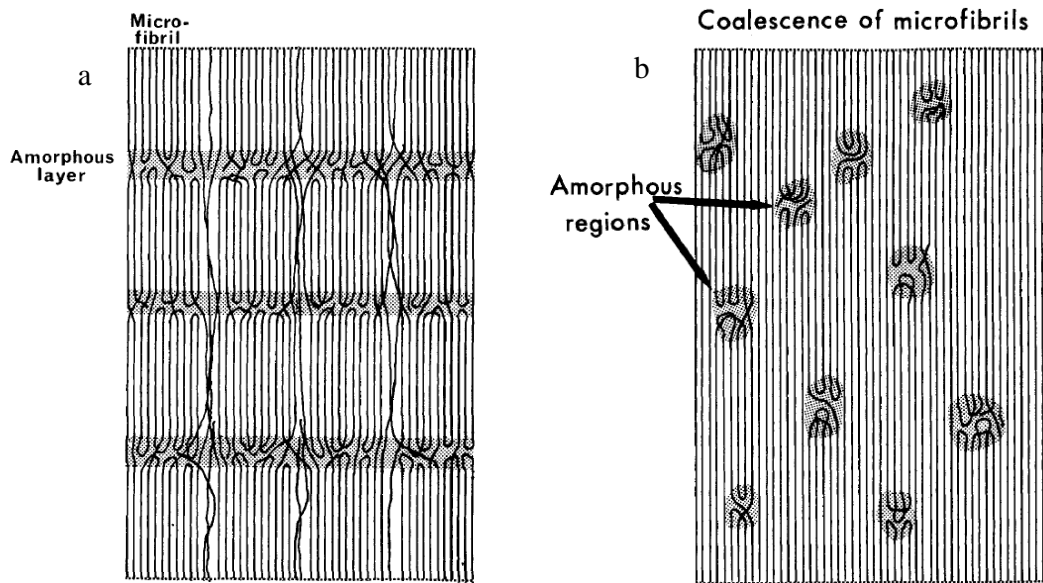
Figure 2.6: Proposed morphology of (a) natural drawn filament and (b) morphology of super drawn filament illustrating the concept of a continuous crystal matrix [35].

There are different types of polymer fibers available on the market. The tensile properties of some polymer fibers are summarized in Table 1. The performance of polymer fibers are greatly improved compared with the bulk polymers. The superior properties of polymer fibers are attributed to the high crystallinity and high degree of orientation of the polymer chains. Demonstrating excellent tensile properties, light weight and good compatibility with polymers, polymer fibers are considered as promising candidates for the reinforcement of polymer matrices. When these fibers are incorporated into a suitable polymer, the resulting composite materials are light weight, strong and deformation resistant.

Table 2.1: Typical examples of polymer fiber

Polymer fiber	Type and Manufacturer	Tensile strength	Tensile modulus
PE fiber	Spectra® fiber 1000 (Honeywell)	3000 MPa	172 GPa
	Dyneema® (Toyobo)	3500 MPa	110 GPa
	HDPE monofilament (Esbjerg Thermoplast)	3500-5000 MPa	-
PP fiber	HY-strength (Fiber Visions)	1700-2000 MPa	-
	PP-Fiber (Taian Modern Plastic)	7700 MPa	-
Polyester fiber	High Tenacity-510 (Wellman)	6000 MPa	-
	High tenacity (INVISTA)	6000 MPa	-
Aramid fiber	Kevlar 49 (DuPont)	-	112 GPa
	Nomex 430 (DuPont)	4400 MPa	
	Meryl® Techno (Nylstar)	14900 MPa	-
PLA fiber	(IngeoTM PLA fiber) Nature Works LLC	3200-3600 MPa	
Acrylic fiber	CFF Fiber (Sterling Fibers)	450 MPa	6 GPa

2.2.2 Concept of microfibrillar composites

With respect to the size of the reinforcing components, polymer composites can be divided into two extreme groups:

- Macro-composites (e.g. glass fiber reinforced ones);
- Molecular composites (with single rod-like macromolecules entities, like in liquid crystalline polymers).

The interest in molecular composites is driven by the fact that by increasing aspect ratio (either by raising the length or by decreasing the diameter of the fibers) of the reinforcement, the mechanical behavior of the respective material can be improved substantially [36]. Following this reasoning, theoretically the

ultimate reinforcement would be achieved by single, extended rigid-rod polymer molecules [37].

Thermotropic liquid crystalline polymer (LCP) is essentially a rigid-rod long-chain molecule. The molecular chain contains some irregularity ("flexibility") to lower the melting point below the decomposition temperature. The rigid-rod molecular structure allows these materials to exhibit molecular order in a liquid mesophase. The highly oriented nature of LCP yields highly anisotropic physical properties and makes thermotropic LCP quite attractive for a potential dispersed phase in in-situ reinforced materials. In the first try to produce molecular composites, LCP was combined with a commercial engineering polymer matrix. The composite was produced by melt blending of the LCP and the thermoplastic matrix, usually in an extruder, followed by a processing step characterized by high elongational flow. The LCP phase was elongated into oriented microfibrils due to the elongational stress field and these microfibrils serve as reinforcing elements (phase) in the polymer matrix [38-44]. Although LCP in-situ composites have some advantages compared to conventional short fiber reinforced composites, they also have some disadvantages: (1) they are generally immiscible with other thermoplastics and form a two-phase structure; (2) they are expensive, and processing from the solution of lyotropic LCP complicates the processing; and (3) the application of the self-reinforcing approach on a commercial scale requires a well-defined set of processing conditions [45].

Unlike LCP, the molecules of common thermoplastics relax during melt processing. Therefore a good molecular orientation can hardly be guaranteed. In order to overcome this problem, Fakirov and Evstatiev introduce a novel concept for developing in situ formed fibril-reinforced composites from polymer blends. The so-called microfibrillar reinforced composites (MFC) satisfy to a great extent the above mentioned represents (aspect ratio and compatibility) that achieved with the LCP-reinforced composites [2, 46-49]. Unlike the classical macro-composites (e.g., fiber reinforced macro-composites), this group of polymer

composites is reinforced with polymer fibrils or, more frequently, bundles of them. The selected polymer pairs for preparing MFC should meet the following requirements:

- The two (or even more) polymers are immiscible;
- The melting temperature gap between of the polymers should be at least 30 K;
- The polymer pairs should demonstrate good drawability.

The preparation of MFC includes three basic steps as shown in Figure 1.7:

- **Mixing and Extrusion**: Melt blending extrusion of two immiscible polymers having different melting temperatures (T_m), which produces an isotropic and continuous blend filament.
- **Drawing and Fibrillation**: Cold drawing of the blend in order to get orientation of the two phases. This step creates highly oriented microfibrils with properties biased predominantly along the axial direction (or symmetry axis).
- **Post-processing**: Thermal treatment at a temperature between the melting temperatures of the two polymers to ensure the formation of an isotropic matrix while still retaining the highly oriented reinforcing fibrils.
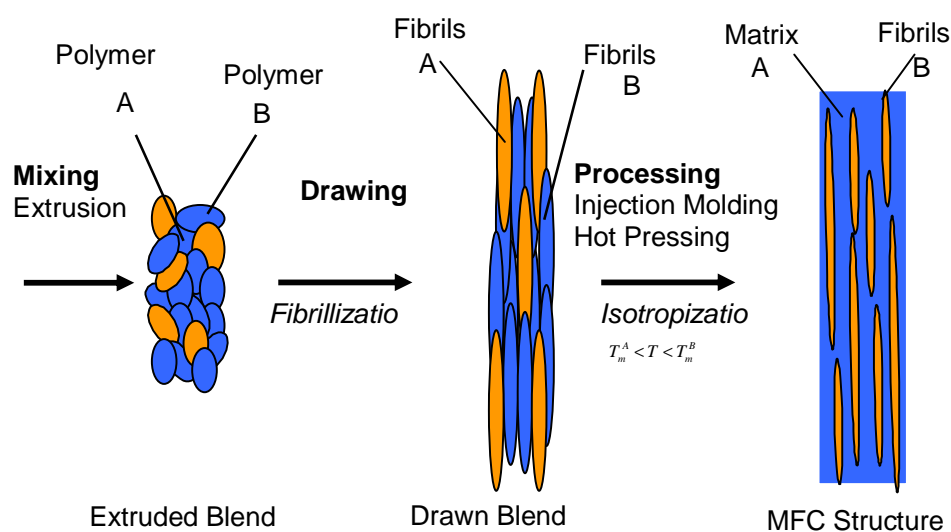
Figure 2.7: Preparation of microfibrillar composites [50].

During the drawing and fibrillation step, the two polymers are converted into a highly oriented state. With the progress of cold drawing, the originally spherical particles are transformed into rotational ellipsoids. As the drawing continues, these ellipsoids become thinner and longer transforming into cylindrical bristles and are brought closer to each other initiating end-to-end coalescence to build up uniform microfibrils. A qualitative mechanism of fibril formation during cold drawing in immiscible blends is proposed as shown in Figure 1.8.
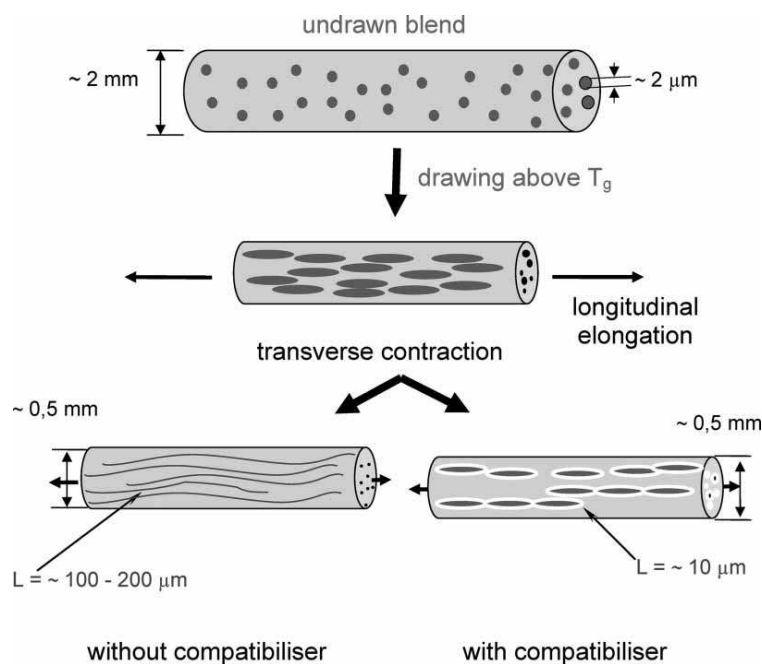
Figure 2.8: Schematic the microfibril formation mechanism in polymer blends during cold drawing (transformation of the spherical particles into microfibrils via coalescence under transverse contraction) [51].

The post-processing step, usually realized by injection molding or compression molding (where the processing window should not be too close to the melting temperature of the microfibrils), results in melting of the lower-melting-point component and its transformation into an isotropic matrix, reinforced with the microfibrils of the higher melting polymer component.

Compared with standard polymer composites, microfibrillar composites demonstrate the following advantages [52]:

- reinforced by in-situ formed polymer microfibrils;
- ease of processing;
- reduced weight in comparison to glass fiber reinforced composites;
- recyclability and repetition of processing.

2.2.3 Development of microfibrillar composites

2.2.3.1 PET/polyolefin MFC

Many immiscible polymers have been explored for preparing MFC, however, the PET/polyolefin combination received special attention [21, 53-57]. PET fibers exhibit superior tensile properties which make it as ideal reinforcement for the tough but less stiff polyolefin. Li has made extensive investigation on the morphology, crystallization behavior, rheological and mechanical properties of PET/polyolefin MFC. He reported that the morphological characteristics of the fibrillized PET phase, such as diameter and its distribution were dependent on the hot stretch ratio at a fixed blend composition [58]; at a fixed stretch ratio the microfibrils became larger with the increase of PET concentration [59]. Furthermore, he proposed three nucleation origins in microfibrillar reinforced blends under an elongational flow field: (a) the classical row nuclei model; (b) fiber nuclei; (c) nuclei induced by fiber assistant alignment. In the microfibrillar PET/PP blend, PET in-situ microfibers had significant nucleation ability for the crystallization of the PP matrix phase. The non-isothermal crystallization kinetics of the PET/PP microfibrillar blend was investigated by applying the theories proposed by Jeziorny, Ozawa, and Liu, and agreement was found between the experimental results and Liu's prediction [60]. For the PET/polyethylene(PE) MFC, in general, the tensile strength and modulus of the composites increased with increasing PET concentration. Needless to say that the strength of MFC was higher than those of the conventional PET/PE blends. The tensile strength and modulus reached a maximum at ca. 15 wt.% of PET [61].

By incorporating carbon black (CB) into PET/PE MFC, Li successfully fabricated a new conductive composite. In the composite, the CB particles were located in the surfaces of the PET microfibrils. The conductive network was built by the contact and overlapping of the CB particles coated PET microfibrils, which led to a very low percolation threshold and a good conductivity [62]. In addition, the CB particles, remaining in the PE matrix also contributed to the conductive paths, especially at high CB content of the corresponding microfibrillar composites.

In order to improve the interfacial adhesion between the PET microfibrils and the polyolefin matrix, Fakirov et al. [51] incorporated ethylene-glycidyl methacrylate (E-GMA) and polypropylene grafted maleic anhydride (PP-g-MA) as compatibilizers into the PET/polyolefin blends during melt extrusion. It was discovered that the MFC blends with compatibilizer had shorter fibrils, because the compatibilizer formed a thin shell around the PET spheres and this did not allow their coalescence. Friedrich et al. [63] prepared uncompatibilized and compatibilized PET/PP MFC by compression molding and injection molding of the drawn strands. They concluded that the compression molded samples possessed better mechanical properties than the injection molded specimens. This was due to the uniaxial orientation of the PET fibrils in the unidirectionally laid drawn strands during compression molding. The impact energy of the injection molded uncompatibilized PET/PP MFC was lower than that of the neat PP because of the incompatibility between PET and PP. However, the toughness of PET/PP MFC increased with increasing amount of the compatibilizer. Fuchs et al. [56] studied the extent of Tsai-Hill equations applicability to microfibrillar composites for characterizing their mechanical behavior. The tensile tests on specimens cut at various angles of MFC with unidirectional PET microfibrils alignment showed a good agreement with Tsai-Hill predictions.

During the investigation on PET/PE MFC, Fakirov and Evstatiev observed the formation of PE transcrystalline lay on the surface of the PET microfibrils. The lamellae in the transcrystalline layer were parallel to each other and laid

perpendicularly to the PET fibril surfaces (as shown in Figure 1.9). They attributed the impressive mechanical properties of the injection molded PET/PE MFC to the transcrystallization and the relatively high aspect ratio of the PET fibrils [64]. The PP transcrystallites in in-situ microfibrillar PET/PP blends were also observed by Li [57]. The cited author further proposed a model for the transcrystalline structure of the microfibrillar composites as schematically presented in Figure 1.10.
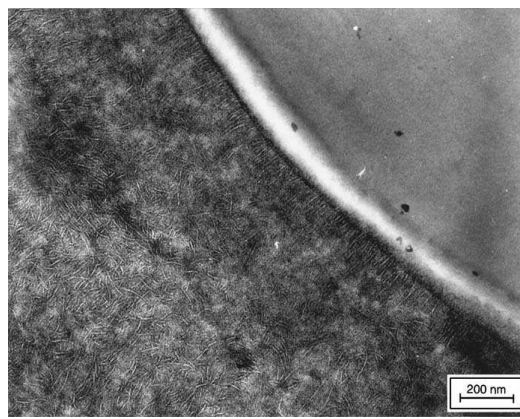

Figure 2.9: TEM micrograph of an ultrathin, stained section of an injection molded dog bone sample of PET/PE (50/50 by weight ratio) with an MFC structure [57].
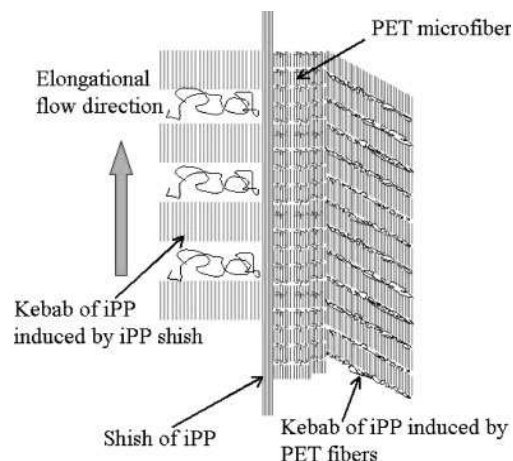

Figure 2.10: Scheme of the transcrystalline layers in the stretched microfibrillar PET/PP blend. The row structures of PP can be induced by a simple flow field and the combination with PET fibers [57].

Other researchers also investigated the PET/polyolefin MFC. Taepaiboon et al. reported that diameters of the in-situ formed PET microfibrils decreased with increasing draw ratio, and the initial size of ground PET flakes did not affect the mechanical properties of the final MFC. Flexural modulus, tensile modulus, and tensile strength of PP/PET MFC were improved by the presence of PET microfibrils and further improvement could be achieved by the addition of PP-g-MA [54]. Jayanarayanan reported that the tensile, flexural and impact properties of injection molded PET/PP increases with stretch ratio. However, a too high stretch ratio was not desirable for the reinforcement of PP. The PET microfibrils with high aspect ratio and good orientation were obtained for samples drawn at stretch ratio 5. Beyond stretch ratio 8, the breakage of the fibrils was observed during stretching which produced very short randomly distributed fibrils after injection molding [55]. Similar observation was also reported by Lin: during cold drawing, there was a critical drawing speed below which the natural draw ratios of the polymers remained constant, but above which the draw ratios first decreased slightly because of suppression of molecular relaxation and then increased because of breakage of highly strained molecules and disintegration of lamellar crystals into finer mosaic blocks [65].

2.2.3.2 MFC based on other polymer blends

Besides the PET/polyolefin combinations, other polymer blends were also explored for preparing MFC. More than a decade years ago, Fakirov and Evstatiev successfully developed other MFC from binary and ternary blends of polyesters/PA 6, PET/polybutylene terephthalate (PBT), PBT/PA, and PET/PA/PBT MFC. These studies are the pioneering works to prepare MFC [2, 47]. Soon afterword, the PET/PA MFC was also developed in which the PET microfibrils existed as reinforcement. Compared with neat PA6, the elastic modulus and the strength of injection molded MFC blends increased by factors of 2.5 and 1.7, respectively. In the case of the compression molded ones, depending on laminate lay-up, modulus and strength were three to five times higher than the corresponding values of the neat PA6 [37, 45]. Evstatiev

investigated the possibility to prepare PA66/PA6 and PET/PA6/PA66 MFC. However, due to the miscibility of the two polyamides, separate PA6 or PA66 microfibrils were not observed [66].

Pesneau [67] and Huang [68] prepared PA66/PP-based MFC. Huang reported that the increase in the viscosity ratio between PA66 and PP was favorable for the fibrillization of PA66, while the elevation in the compatibilizer concentration (PP-g-MA) was unfavorable for the fibrillization.

Xu [70] prepared poly(phenylene sulfide) (PPS)/PP MFC. It was reported that at the same PPS concentration, diameter of most PPS fibrils in the microfibrillar blend was comparable to that of the PPS particles in the common blend [69]. Polycarbonate (PC)/high density polyethylene (HDPE) MFC was successfully fabricated by Li despite of the high viscosity ratio between PC and HDPE, which is usually disadvantageous for fibrillation.

2.3 Ternary nanocomposites

2.3.1 Preferential location and migration of nanoparticles

In the last 20 years, the development of polymeric nanocomposites became under the spot of interest. This is due to the fact that nanocomposites often exhibit remarkable improvement in materials properties when compared with the corresponding neat polymer or conventional micro- and macro-composites. These improvements include high stiffness [71, 72], increased strength and heat resistance [73], decreased gas permeability [74]. However, in the recent years considerable research attention has been focused on introducing nano-scale fillers into polymer blends. It turned out that the nanofillers always had a preferential location either in one polymer phase or at the interface, which may exert some compatibilization effect on the polymer blends.

Many researchers have investigated the preferential location of the nanofillers in the polymer blends. Most of them attributed this phenomenon to a strong chemical affinity between the nanofillers and the corresponding polymer. As the nanofillers were usually surface modified, they tended to be "chemically bonded" to a given polymer [75-79, 80]. On the other hand, some other researchers offered different explanations. For polymer blends filled with CB, the interfacial tension was the key factor determining the location of CB [81-83]. Elias investigated a PP/polystyrene (PS) blend filled with hydrophilic and hydrophobic nanosilica. The cited author attributed the preferential location of silica (hydrophilic silica in PS phase and hydrophobic silica in PP phase) to the lower interfacial tension between the nanoparticles and the preferred polymers [84]. Wu reported that the preferential location of nanofillers in the melts of two chemically different polymers was not always determined by the surface tension of polymers. Location of the nanoparticles may also be governed by the flexibility of polymer chains. This implies that the entropy penalty may play a decisive role in competitive adsorption of polymers on the surfaces of nanofillers [85]. Lee studied the SiO_2/LCP/PP ternary composites, and argued that the preferential

location of the hydrophilic silica in the LCP phase was due to the polar interaction between them [86].

To explain the preferential location of nanofillers, in addition to the above mentioned thermodynamic factors, the blending sequence should also be considered. This covers the kinetic aspect of the nanofiller location (migration). To investigate the blending sequence on the preferential location of nanofillers, most of the researchers adopted the following blending procedures to incorporate the nanofillers into the polymer blends: compounding the three components simultaneously; blending the nanofillers with one polymer and add the second polymer during a second step extrusion. These investigations showed that the blending sequence did not basically influence the preferential location of nanofillers: the nanofillers either stayed in or migrated to the preferred phase irrespective of the blending sequence [84, 86, 87].

Elias et al. have investigated the migration of particles in polymer blends, and proposed three migration mechanisms [88, 89]:

- Brownian motion of the particles (self-diffusion of the particles).
  According to Larson [90] when the shear rate is high enough to disturb the equilibrium state of the particle, the rate at which the particle equilibrium is regained is controlled by the particle diffusion coefficient (D_0), given by

  $$D_0 = \frac{k_B T}{6\pi\eta a} \tag{1.1}$$

  Where k_B is the Boltzmann constant, η is the viscosity of the medium at temperature T and a is the radius of the particle.

  The time for a particle to diffuse a distance equal to its radius a is therefore

  $$t_D \approx \frac{a^2}{D_0} = \frac{6\pi\eta a^3}{k_B T} \tag{1.2}$$

By assuming the size of diffusing particle aggregates is a = 100 nm, t_D is calculated to be 7500 s for η = 2.5×10^3 Pa.s (usual PP viscosity) and T = 473 K. This rough calculation shows that the order of magnitude of the motion time is very large and consequently not matched with the mixing time which is in the range of few minutes. Generally speaking, the high viscosity of the molten polymer impedes the particle movement by Brownian motion.

- The second possibility for the particle movement is induced by the shear. Actually, the inorganic particles and the droplets of the dispersed phase are moving in the matrix so that collisions between particles and drops occur. The frequency of collisions may be roughly approximated by the following equation:

$$C = \frac{8\,\dot{\gamma}\,\Phi}{\pi} \tag{1.3}$$

Φ is the volume fraction of the considered dispersed entity (particle or polymer drops) and $\dot{\gamma}$ is the shear rate.

- A third mechanism can also be proposed where particles are trapped in the inter-droplet zone during a collision between two dispersed polymer drops. In this latter case, it is the coalescence of polymer droplets that is playing a role in the transfer of the solid particles from one phase to the other

2.3.2 Compatibilization effect of nanofillers

Many researchers investigated the compatibilization effect of nanofillers on immiscible polymer blends. From a historically point of view, the compatibilization of immiscible blend by nanofillers was first reported for CB particles dispersed in elastomers [91, 92]. Clarke et al. [93] showed that CB had a powerful compatibilizing effect when the particles were present at the interface between natural rubber and acrylonitrile butadiene rubber phases. Other inorganic

nanoparticles and nanoclays also exert the same effect on polymer blends. Zhu et al. [94] observed that in spin-cast films prepared from PS/polymethyl methacrylate (PMMA), addition of organoclays has resulted in a reduction of the micro-domain size of the dispersed phase. In another report, Ferreiro et al. [95] showed similar behavior in PS/poly(ethyl methacrylate) (PEMA) blends, modified with organoclays. Liu and Kontopoulou [96] showed that the addition of nanosilica particles into PP/polyethylene-co-octene blend decreased the size of the dispersed elastomer phase. Elias et al. [84] and Zhang et al. [97], observed also for PP/PS blends a drastic reduction of the size of the PS phase corresponding to a concentration of hydrophobic fumed silica at the interface. Si et al. [3] and Ray et al. investigated the PC/styrene acrylonitrile (SAN) and PC/PMMA blends respectively. They reported that at the concentration of organoclays around 5 wt.% the blends, normally immiscible depicted the characteristics of a ''miscible'' blend with only one alpha relaxation (in that case, glass transition temperature) peak [98].

Lipatov et al. have made extensive investigations on the compatibilization effect of nanoclays on polymer blends [99, 100]. The cited authors proposed that the compatibilizing effect of nanofillers depended on the change in free energy of mixing between the two polymers. The free energy of mixing for a filled system including three components, inorganic filler S and polymers A and B, can be given as

$$\Delta G_m = \Delta G_{AS} + \Delta G_{BS} + \Delta G_{AB} \tag{1.4}$$

where the subscripts identify the interacting pairs. The system is thermodynamically stable when $\Delta G_m < 0$. If both polymers are strongly absorbed onto the filler surface, ΔG_{AS} and ΔG_{BS} become negative. In this case the introduction of fillers decreases the ΔG_m, whereby the thermodynamic stability of the system is enhanced, and a finer phase morphology is achieved. This theory is further proved by Si [3] and Ray [98].

However, many other researchers offered different explanations for the compatibilization effect of nanofillers. In polymer blends, the nanofillers are observed to be located either in one phase or at the interface. Some researchers argued that when located at the interface the nanofillers (especially the nanoclays) acted as a physical barrier, which slowed down the coalescence of the dispersed phases [90, 101, 102]. Other researchers believed that the nanofillers at the interface stabilized the blend morphology by reducing the interfacial tension [103, 104]. If the nanofillers are preferentially located in one phase (usually in the matrix) the viscosity ratio between the matrix and dispersed phase is changed, which can significantly affect the phase morphology. On the other hand, nanofillers (especially the nanoclay platelets having large aspect ratio) in the matrix prevent the coalescence of the dispersed droplets, thus resulting finer phase morphology [105]. Hong [106] reported that in the PBT/PE blend the nanoclays were mostly located in the dispersed PBT phase when their concentration was high. Therefore the deformability of the PBT droplets filled with organoclays was significantly reduced. The less likelihood of breakup of the droplet hindered the effect of the organoclays in the size reduction of PBT. So, an increase in the mean droplet size of PBT was observed at high nanoclay loading.

2.4 Summary

Numerous investigations on microfibrillar composites have been carried out since the concept of MFC was proposed more than a decade years ago. As reviewed before, the morphology, mechanical properties, crystallization behavior and rheology of the MFC were widely studied. However, there are still many scientific (fibril formation mechanism, morphology-property relationship, the influence of compatibilizer on fibril formation and the possibility of exploring possible polymer blends for preparing MFC) and technical questions (large scale production of MFC, materials feeding problem during injection molding, the effect of processing parameters) unsolved. In addition, incorporation of nanofillers into MFC-structured materials may open a new perspective for enhancing the properties of these materials. Therefore it is of particular interest to investigate the effect of nanofillers on the morphology and properties of MFC. Such work will not only expand our knowledge of polymer composites but also present a detailed and direct reference for the application of MFC.

At present, most of the investigations on ternary nanocomposites focus on introducing nanoclays to compatibilize the polymer blends. However, spherical nanoparticles are also reported to be able to act as effective compatibilizing agents for polymer blends [97,107]. Despite of great efforts by various researchers, the preferential location of nanofillers in polymer blends is still not well understood and there is no widely accepted explanation for this interesting phenomenon. In addition, it is already known that the migration and preferential location of nanofillers in the polymer blends are both thermodynamically (interfacial tension) and kinetically (shear stress during compounding) controlled [87]. Few researchers have investigated the mechanism of nanofiller migration in polymer blends [76, 89], but little is know about the migration process. Furthermore, to our knowledge, all the published investigations on the preferential location and migration of nanofillers are centered on the uncompatibilized polymer blends. So, no investigation has been carried out concerning the location and migration of nanofillers in the compatibilized blends.

It is thus interesting and valuable to investigate the migration and compatibilization mechanisms of nanoparticles in the uncompatibilized and compatibilized blends prepared with different blending procedures.

2.5 Objective of the Study

2.5.1 Microfibrillar composites:

In the present work, PET and PP were selected for preparing the microfibrillar composites. Two types of TiO_2 particles were introduced into the PET/PP microfibrillar composites. The aim of the work was to prepare and investigate two groups of microfibrillar composites based on PET/PP, PET/PP/TiO_2 blends in absence (uncompatibilized) and presence (compatibilized) of compatibilizer (PP-g-MA) for the PET/PP pair.

PET/PP MFC

PET/PP MFC with different concentrations of PET and different amounts of PP-g-MA (as compatibilizer) were prepared under various processing conditions. The main aims of the work on PET/PP MFC are:

- To study the effects of blend composition and compatibilizer on the morphology of extrudates and drawn strands;
- To define the maximum concentration of PET in PET/PP MFC;
- To investigate the influence of processing parameters on the morphology of extrudates and drawn strands;
- To obtain PET/PP MFC with superior tensile properties by adopting optimized processing conditions and incorporating a suitable amount of compatibilizer.

PET/PP/TiO_2 MFC

PET/PP/TiO_2 MFC were prepared by using pre-compounded PP/TiO_2 composites and PET both in absence and presence of PP-g-MA. Two types of TiO_2 particles were incorporated (300 nm and 15 nm in diameter). The two basic targets of this work are:

- To investigate the fibril formation mechanism in filled polymer blends during stretching;

- To study the influences of TiO_2 nanoparticles (the size and concentration) on the morphology and properties of $PET/PP/TiO_2$ drawn strands and MFC;

2.5.2 PET/PP/TiO$_2$ composites

Two types of TiO_2 particles were incorporated into PET/PP (minor/major phases) blends in presence and absence of PP-g-MA via four different blending procedures. Major aims of this study are:

- To clarify the effect of blending procedure on the preferential location of TiO_2 particles;
- To investigate the effect of PP-g-MA on the preferential location of TiO_2 particles;
- To study the compatibilization effect of TiO_2 particles on the phase morphology.
- To study the effect of TiO_2 particles on the crystallization behavior and mechanical properties of $PET/PP/TiO_2$ composite.

3 Experimental

3.1 Materials

3.1.1 Selection of polymer pairs

PP (Moplen HP400H) was purchased from LyondellBasell (Rotterdam, Netherlands) with a melt flow rate of 2 g/10 min (230 °C/2.16 kg). Granulated PET (skyPET BL8050) was provided by SK Eurochem (Warszawa, Poland) with the intrinsic viscosity of 0.80 dl/g. The PP-g-MA (OREVAC CA 100 of Arkema, Colombes, France) was used as compatibilizer for PET and PP. The maleic anhydride content was 1 wt. %, and the melt flow rate was 10 g/10 min (190°C, 325 g).

3.1.2 Nanofillers

Two types of TiO_2 (RM 300 of Sachtleben Chemie GmbH, Duisburg, Germany; Kronos 2220 of Kronos, Leverkusen, Germany) nanoparticles served as fillers for PET/PP MFC. Their specifications are listed in Table 3.1.

Table 3.1: Specifications of TiO_2 nanoparticles

Type	Crystal size (nm)	Crystal form	TiO_2 content	Surface treatment
RM 300	15 (rodlike)	rutile	~ 87%	1 wt.% of trimethylolpropane aluminum and silicon compounds
Kronos 2220	300 (spherical)	rutile	≥ 92.5%	

3.2 Preparation of microfibrillar composites

3.2.1 Preparation of PET/PP MFC

Prior to processing, the PET was dried for 12 hours at 100 ℃ to avoid its hydrolytic degradation. PET/PP blend with different compositions were extruded with a Brabender co-rotating twin-screw extruder (PL 2000 of Brabender® GmbH & Co. KG, Duisburg, Germany). The diameter of the screw was 25 mm and the L/D (length/diameter) was 22. The screw configuration is shown in Figure 3.1. The temperature zones from hopper to die were set at 230, 270, 275, 275 ℃, and the screw speed was 14 rpm. The residence time was estimated to be about 2 minutes. During extrusion of the PET/PP blend with 40 wt.% of PET, different extrusion screw speeds were adopted and different amounts of compatibilizer were incorporated. The compositions of the polymer blends and processing conditions are listed in Table 3.2. After leaving of the extruder (2 mm capillary die), the extrudate was immediately quenched in a water bath at 15 ℃. After passing through the take-up device, the strand was heated in a hot water bath at 85 ℃ and then drawn by a stretching device (Figure 3.2). Necking of the extrudate took place in the water bath, resulting a dramatic decrease in the diameter of the extrudate. The draw ratio which is defined as the ratio between the cross section areas of the drawn strand and the die was always kept at 14.
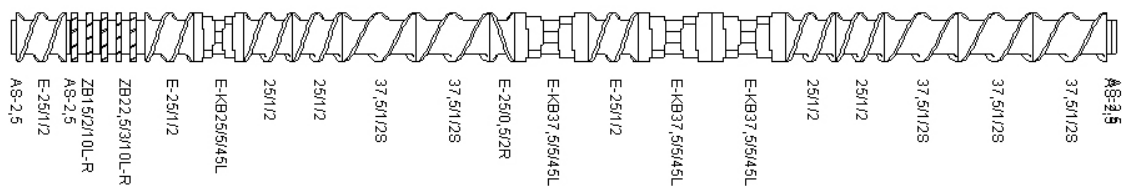

Figure 3.1: Screw configuration of Brabender co-rotating twin-screw extruder.
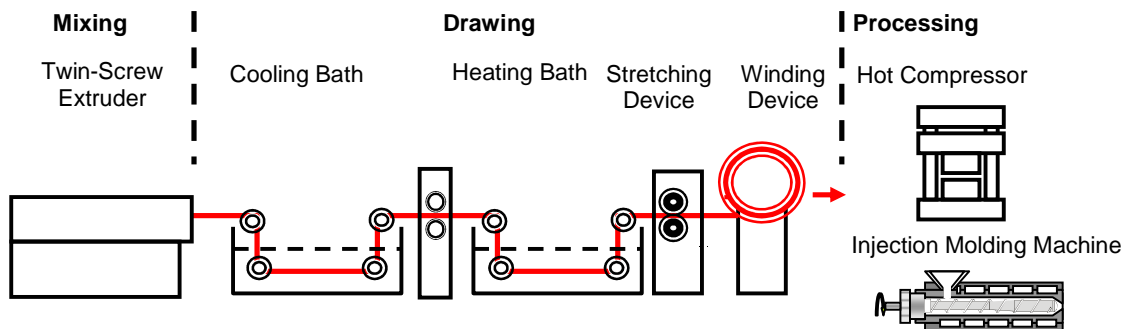
Figure 3.2: Manufacturing chain of microfibrillar composites.

The drawn strand was dried and wound unidirectionally onto a metal plate for compression molding. The compression molding of the drawn strands was carried out at 200 ℃ for 20 minutes under a pressu re of 3 MPa. The pressure was maintained until the plate cooled to room temperature. Each time, two sheets with a thickness of around 2 mm were obtained and the sheets were cut into strips along the strand alignment (unidirectional PET reinforcement) for mechanical testing.

Table 3.2: Material designation and composition of PET/PP MFC

Composition	Parts (weight ratio)	Screw speed (rpm)
PET/PP	30/70	40
PET/PP	40/60	20, 40, 80
PET/PP	50/50	40
PET/PP/PP-g-MA	40/59/1	80
PET/PP/PP-g-MA	40/57/3	80
PET/PP/PP-g-MA	40/54/6	80

3.2.2 PET/PP/TiO$_2$ MFC

The PET and PP-g-MA were dried for 12 hours at 100 ℃ and 80 ℃, respectively before processing. The TiO$_2$ nanoparticles (TiO$_2$-300nm and TiO$_2$-15nm) with different concentrations were firstly blended with the PP in a Berstorff co-rotating twin-screw extruder (ZE-25A UTX; KraussMaffei Berstorff GmbH, Hannover, Germany) at 200 ℃. The diameter of the screw was 2 5 mm and the L/D was 44. The obtained PP/TiO$_2$ nanocomposite was subsequently blended with PET in

absence and presence of PP-g-MA in the Brabender twin-screw extruder (cf. section 3.2.1) as the second step extrusion process. The extrusion temperatures from hopper to die were 230, 270, 275, 275 °C and t he screw speed was 40 rpm.

The extrudate was stretched by heating in hot water bath at 85 °C, the draw ratio was set for 10. The drawn strands were then pelletized into small pieces (3 mm in length) and injection molded into dog-bone specimens by an injection molding machine (Arburg 320S, ARBURG GmbH & Co KG, Lossburg, Germany). The temperatures of different zones were (from the hopper to the die): 175 °C, 190 °C, 190 °C, 195 °C, 200 °C. As injection speed 60 cm ^{3}/s was selected and the injection pressure was kept at around 600 bar. For comparison purpose, PET/PP MFC and PP were also prepared by injection molding. To subject the pure PP to the same mechanical history as that of the PP in the PET/PP/TiO_2 MFC, the PP was extruded twice before injection molding. The designation and composition of the injection molded PET/PP/TiO_2 and PET/PP MFC are given in Table 3.3.

Table 3.3: Material designation and composition of PET/PP/TiO_2 MFC

Designation	Composition	Parts (volume ratio)
PET/PP	PET/PP	25/75
PET/PP/MA	PET/PP/PP-g-MA	25/72/3
PET/PP/2T300	PET/PP/TiO_2-300nm	24.5/73.5/2
PET/PP/MA/2T300	PET/PP/PP-g-MA/TiO_2-300nm	24.5/70.5/3/2
PET/PP/4T300	PET/PP/TiO_2-300nm	24/72/4
PET/PP/MA/4T300	PET/PP/PP-g-MA/TiO_2-300nm	24/69/3/4
PET/PP/2T15	PET/PP/TiO_2-15nm	24.5/73.5/2
PET/PP/MA/2T15	PET/PP/PP-g-MA/TiO_2-15nm	24.5/70.5/3/2

3.2.3 PET/PP/TiO_2 nanocomposites

PET and PP-g-MA were dried before processing. Detailed information is given in section 3.2.1. The PET/PP/TiO_2 (24.5/73.5/2 by volume) and PET/PP/PP-g-MA/TiO_2 (24.5/70.5/3/2) composites were prepared with the following four blending procedures.

Blending Procedure 1: the TiO_2 particles were blended with the PP in the Berstorff twin-screw extruder first (cf. section 3.2.2). The diameter of the screw was 25 mm and the L/D was 44. The obtained PP/TiO_2 composite was subsequently blended with PET in absence (or presence) of PP-g-MA in a Brabender twin-screw extruder (cf. section 3.2.1) as the second step extrusion (diameter of the screw was 25 mm and L/D was 22). The extrusion temperatures from hopper to die were 230, 270, 275, 275 ℃ and t he screw speed was 40 rpm. It should be pointed out that the PET was extruded in the Berstorff extruder before blending with the PP/TiO_2 composite.

Blending Procedure 2: the PP, PET and TiO_2 (or PP, PET, PP-g-MA and TiO_2) were fed into the Berstorff extruder simultaneously. The obtained composite was granulated and then extruded in the Brabender extruder for the second time, whereby the same extrusion parameters, as given before were used. The purpose was to subject this composite to same thermo-mechanical history as the one prepared with Blending Procedure 1.

Blending Procedure 3: the TiO_2 particles were firstly blended with PET in the Berstorff extruder. The obtained PET/TiO_2 composite was subsequently extruded with the PP in absence (or presence) of PP-g-MA in the Brabender extruder.

Blending Procedure 4: the PET, PP and PP-g-MA were extruded with the Berstorff extruder as the first step extrusion. In the second step extrusion, the obtained PET/PP/PP-g-MA blend was blended with TiO_2 in the Brabender extruder.

All the four blending procedures were adopted to prepare the $PET/PP/TiO_2$-300nm nanocomposites, while only Blending Procedure 1 was adopted to prepare the $PET/PP/TiO_2$-15nm nanocomposites. For comparison purpose, PET/PP blends with and without PP-g-MA were also prepared under the same extrusion conditions. It should be underlined that the PP was firstly extruded with

the Berstorff extruder. This was reassured that PP experiences the same thermo-mechanical history as the PP in the PET/PP/TiO$_2$ nanocomposites.

After extrusion, the PET/PP/TiO$_2$ and PET/PP/PP-g-MA/TiO$_2$ composites were dried and injection molded into dog-bone specimens for tensile test. The molding temperatures of the Arburg injection molding machine from hopper to nozzle were 250, 275, 275, 275, 280 °C, and the screw spee d was 450 rpm. The designations of the PET/PP/TiO$_2$-300nm and PET/PP/TiO$_2$-15nm nanocomposites are given in Table 3.4 and Table 3.5, respectively. For the PET/PP/TiO$_2$-300nm nanocomposites, the components which were extruded in the first extrusion step are given within the brackets.

Table 3.4: Material composition and designation of PET/PP/TiO$_2$-300nm nanocomposites

Blending Procedure	Composition	Volume Ratio	Designation
1	PET/PP/TiO$_2$	24.5/73.5/2	(PP/T)/PET
	PET/PP/PP-g-MA/TiO$_2$	24.5/70.5/3/2	(PP/T)/PET/MA
2	PET/PP/TiO$_2$	24.5/73.5/2	PP/PET/T
	PET/PP/PP-g-MA/TiO$_2$	24.5/70.5/3/2	PP/PET/MA/T
3	PET/PP/TiO$_2$	24.5/73.5/2	(PET/T)/PP
	PET/PP/PP-g-MA/TiO$_2$	24.5/70.5/3/2	(PET/T)/PP/MA
4	PET/PP/PP-g-MA/TiO$_2$	24.5/70.5/3/2	(PET/PP/MA)/T

Table 3.5: Material composition and designation of PET/PP/TiO$_2$-15nm nanocomposites

Designation	Composition	Parts (volume ratio)
PET/PP	PET/PP	25/75
PET/PP/MA	PET/PP/PP-g-MA	25/72/3
PET/PP/2T	PET/PP/TiO$_2$	24.5/73.5/2
PET/PP/4T	PET/PP/TiO$_2$	24/72/4
PET/PP/3MA/2T	PET/PP/PP-g-MA/TiO$_2$	24.5/70.5/3/2
PET/PP/6MA/2T	PET/PP/PP-g-MA/TiO$_2$	24.5/67.5/6/2

3.3 Structural characterization

3.3.1 Scanning electron microscopy (SEM)

The fracture surfaces of the extrudates (strands) and injection molded (or compression molded) MFC were inspected using a JSM-6300 scanning electron microscope of JEOL Ltd (Tokyo, Japan) operating at an accelerating voltage of 25 kV. For PET/PP/TiO_2 specimens a high resolution Supra^{TM} 40VP (Carl Zeiss GmbH, Goettingen, Germany) SEM was used in order to show the dispersion of TiO_2 nanoparticles. For a better observation of fibrils, PET/PP and PET/PP/TiO_2 drawn strands and MFC specimens were etched by xylene at 120 °C for 10 hours to remove the PP fraction. All the specimens were sputtered with Pd/Pt alloy before SEM observation.

3.3.2 Transmission electron microscopy (TEM)

The dispersion of TiO_2 nanoparticles in the nanocomposites were examined by a Zeiss LEO 912 Omega transmission electron microscope (Oberkochen, Germany) operated at an accelerating voltage of 120 kV. Thin sections (about 50 nm) were cut at room temperature with a Diatome diamond knife (Hatfield, PA) using an Ultracut E microtome (Reichert and Jung, Vienna, Austria).

3.4 Rheology

Disks (25 mm in diameter and 2 mm in thickness) of the pure polymers and polymer nanocomposites were pressed at 275 °C. The rheology of the materials was assessed at 275 °C using an ARES parallel plate rheometer (Rheometric Scientific, NJ, USA) with a gap of 1mm. All the measurements were performed in frequency mode with a strain amplitude of 1%.

3.5 Thermal and thermo mechanical characterization

3.5.1 Differential scanning calorimetry (DSC)

Differential scanning calorimetry traces of drawn strands were obtained by using a Mettler Toledo (Giessen, Germany), DSC821 device. In the first heating run, the specimen was heated from room temperature to 200 °C and then cooled to 40 °C; in the second heating run, the specimen was reheated to 280 °C and kept at this temperature for 3 minutes, before cooling down to 40 °C. The heating and cooling rates were always kept at 20 °C/min.

For the PET/PP/TiO$_2$-300nm nanocomposites, the specimens were heated from room temperature to 280 °C. Kept at 280 °C for 3 mi nutes, the specimens were then cooled to 40 °C. The heating rate and the cool ing rates were 20 °C/min and 10 °C/min, respectively. The percent of crystallini ty was calculated by according to the following equation:

$$X_c = \frac{\Delta H_m}{\Delta H_m^0} \times 100\% \tag{3.1}$$

Where ΔH_m and ΔH_m^0 are the measured melt enthalpy and the theoretical enthalpy of the crystalline polymer, respectively. The percent of crystallinity was calculated by using ΔH_m^0 = 209 J/g for PP [24] and ΔH_m^0 = 140 J/g for PET [25].

3.5.2 Dynamic mechanical thermal analysis (DMTA)

Dynamic mechanical thermal analysis of drawn strands was carried out using a DMA Q800 apparatus (TA Instrument, New Castle, USA). The storage modulus (E') and mechanical damping factor (tan δ) of the drawn strands were measured as a function of temperature (from -50 °C to 150 °C). All measurements were conducted in tensile and strain control modes at a fixed frequency of 1 Hz with a heating rate of 3 °C/min. The strain was kept at 0. 1 %.

DMTA spectra of injection molded MFC were recorded in a Gabo EPLEXOR 100 N dynamic mechanical analyzer (GABO QUALIMETER Testanlagen GmbH, Ahlden, Germany) with a tensile mode. The E' and tan δ of the specimens were monitored as a function of temperature from -30 ℃ to 150 ℃ at a frequency of 10 Hz. The heating rate was 2 ℃/min and the specim en dimensions were 10 × 4 × 50 mm^3 (width × thickness × length).

3.6 Mechanical characterization

3.6.1 Tensile test

The tensile properties of drawn strands were characterized using a Zwick 1474 universal testing machine (Ulm, Germany) with a test speed of 5 mm/min. Special clamps were used to avoid the breakage of drawn strands at the clamping parts.

Tensile tests on the MFC specimens were done on the above Zwick 1474 universal testing machine according to the DIN EN ISO 527. The tests were run at room temperature with a crosshead speed of 5 mm/min. The strain range, require to determine the tensile modulus, was measured by an extensometer. All the data presented correspond to the average of five measurements.

3.6.2 Impact test

Charpy impact strength was determined on un-notched MFC specimens (4×10×80 mm^3) according to the DIN EN ISO 179. For this measurement an instrumented impact tester (AFS-MK fracto scope of Ceast, Torino, Italy). The striker energy was 4 J. Measurements were run at room temperature on 7 specimens.

4   Results and Discussion

4.1 PET/PP MFC

4.1.1 Morphology

4.1.1.1 Morphology of extrudates

Figure 4.1 shows the phase evolution of the PET/PP blend with increasing concentration of the PET extruded at the screw speed of 40 revolutions per minute (rpm). At low concentration of PET (< 30 wt.%), the PET is the dispersed phase in the PP matrix (Figure 4.1a). With further increase of the concentration of PET (to 40 wt.%) two types of phase morphology are observed. In Figure 4.1b large PET domains appear in the extrudate, which indicates the coalescence of the dispersed PET droplets. In Figure 4.1c the so-called double emulsion morphology can be observed: the PET forms the continuous phase and divides the PP into separated large areas, within these areas numbers of small PET droplets are distributed. When the concentration of PET reaches 50 wt.%, a strengthened PET continuous phase and numbers of finely separated PP domains are observed in Figure 4.1d. Few PET droplets can also be resolved within the PP domains.
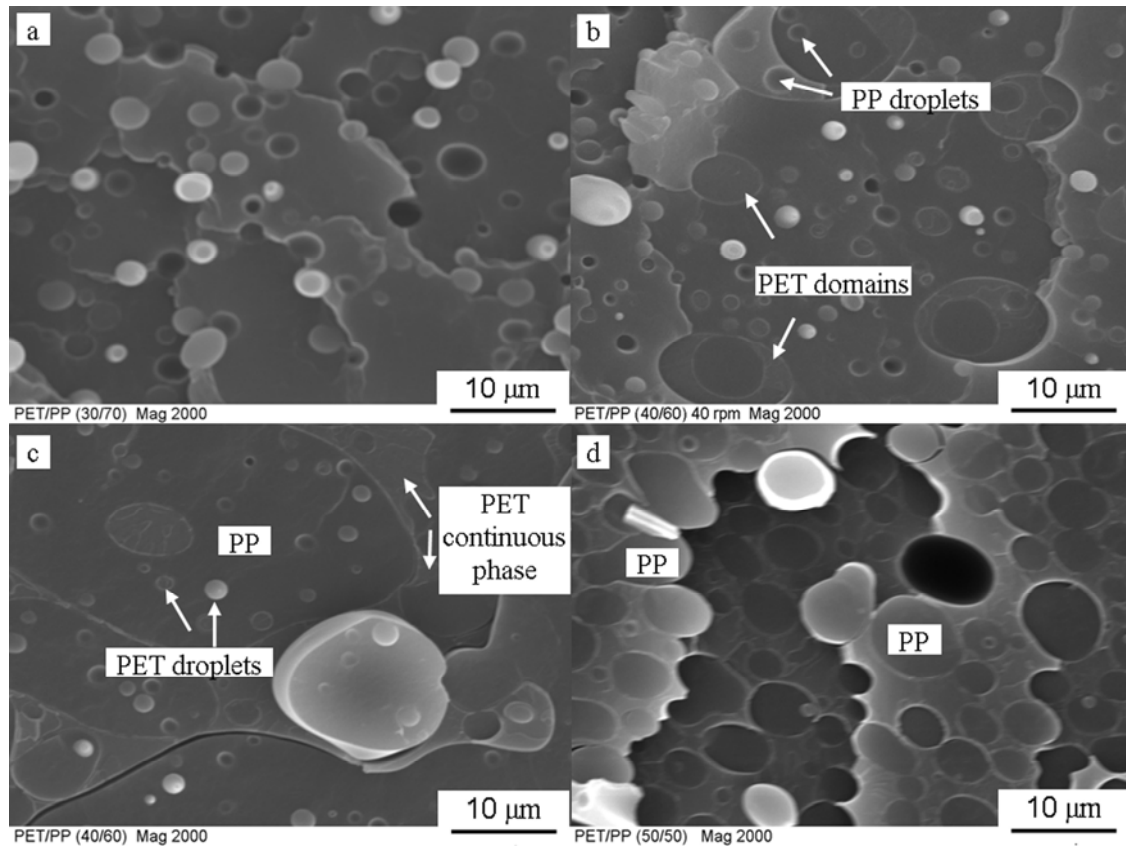
Figure 4.1: Phase morphology of PET/PP blend (fracture surfaces) with different compositions extruded at the screw speed of 40 rpm: (a) PET/PP (30/70), (b) and (c) PET/PP (40/60), (d) PET/PP (50/50).

The phase morphologies of the PET/PP blends extruded at different screw speeds are further verified by selectively removing of the PP phase. The morphology of the etched surfaces (by xylene) of the PET/PP extrudates is shown in Figure 4.2. For the PET/PP (30/70) extrudates, the PP matrix was removed and only the deformed PET droplets are observed (Figure 4.2a). As shown in Figure 4.2b-d, at higher PET concentrations (40 wt.% and 50 wt.%) the network of PET remains, and large cavities are left because of the removal of PP.
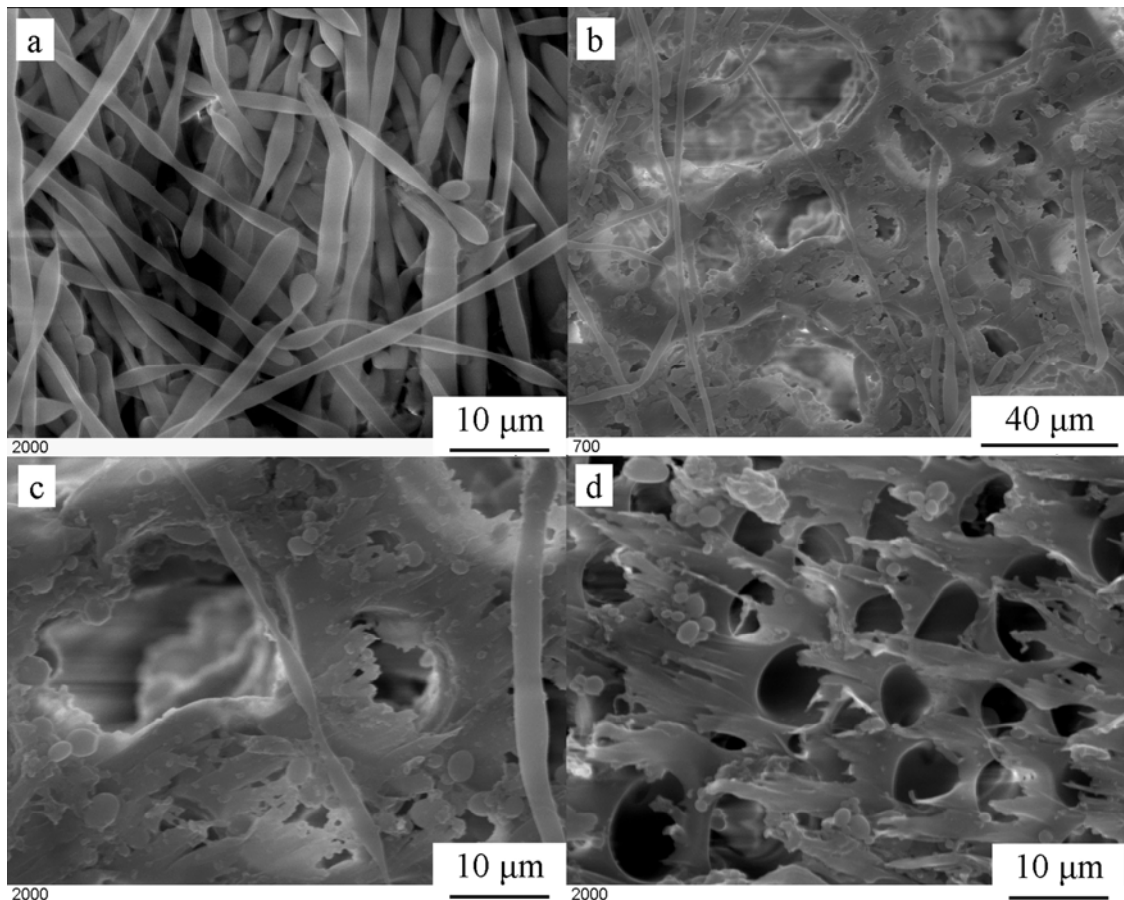
Figure 4.2: Phase morphology of PET/PP blend with different compositions extruded at the screw speed of 40 rpm (PP was removed by hot xylene): (a) PET/PP (30/70), (b) and (c) PET/PP (40/60), (d) PET/PP (50/50).

It is well known that during melt blending of immiscible polymers, the major component forms the continuous phase, while the minor component forms the dispersed phase. When the concentration of PET is 30 wt.%, it is the minor component, and forms dispersed phase in the PP matrix. However, at higher PET concentration, another effect should be taken into consideration in respect to the morphology development. According to the minimum energy dissipation principle, during melt blending of two immiscible polymers the more viscous component tends to form the dispersed phase, and the less viscous one tends to form the continuous phase. However, this principle is applicable only under the condition that the contents of the two polymers are comparable. Otherwise the

blend composition will overwrite the effect of viscosity [23, 31]. Melt viscosity versus shear rate curves are presented in Figure 4.3 for the neat PET and PP at 275 ℃. Having much lower viscosity than the PP the PET tends to form the continuous phase at high concentrations (40 wt.% and 50 wt.%).
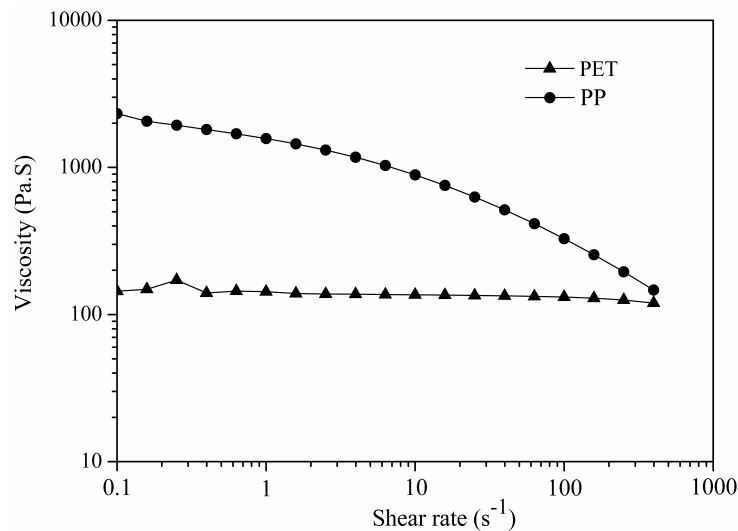

Figure 4.3: Viscosity of PET and PP at 275 ℃ as a function o f shear rate.

To investigate the influence of screw speed on the phase evolution, PET/PP (40/60 wt.%) were extruded at different screw speeds (20, 40 and 80 rpm). At the screw speed of 20 rpm, PET is the dispersed phase in the PP matrix as shown in Figure 4.4. However, higher screw speed leads to phase inversion: the PET remains the continuous phase when the screw speed is increased to 40 rpm, as shown in Figure 4.1b. Interestingly, extruded at the screw speed of 80 rpm, the PET/PP (40/60) extrudate shows a similar morphology (Figure 4.5) as that of the PET/PP (50/50) extruded at the screw speed of 40 rpm (Figure 4.1d).
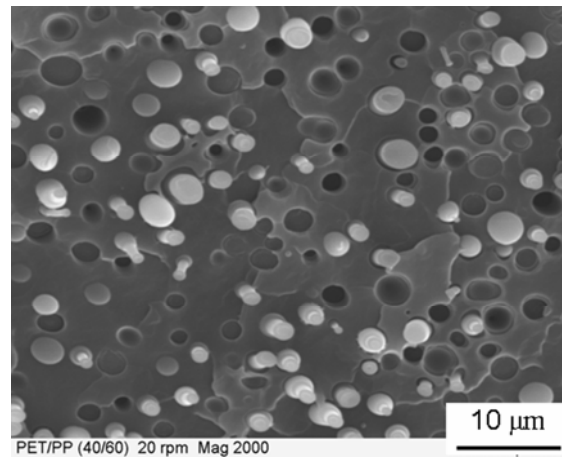
Figure 4.4: PET/PP (40/60) extruded at the screw speed of 20 rpm.
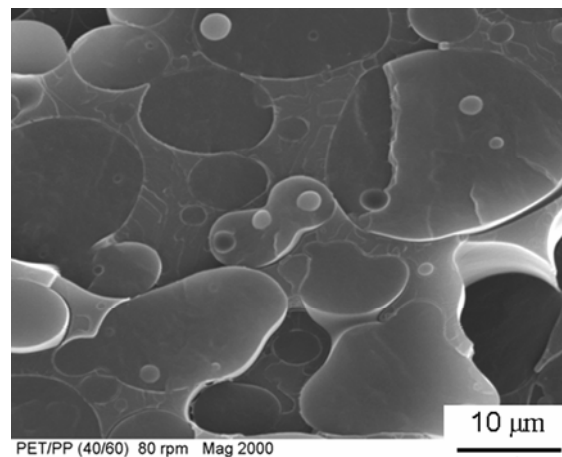
Figure 4.5: PET/PP (40/60) extruded at the screw speed of 80 rpm.

The main mechanism governing the phase morphology development of immiscible polymer blends is believed to be the droplet breakup and coalescence [108, 109]. Generally, the increase of screw speed leads to a finer morphology, since high screw speed generates intensive shear stresses that facilitate an efficient droplet breakup [110]. However, Willis reported an increase of brornobutyl rubber droplet size in polystyrene matrix at a higher screw speed [111]. Luciani also observed first a decrease before any increment in the PA droplet size in ethylene-propylene rubber matrix with increasing shear rate [112]. In fact, high shear rate not just favors the droplet breakup, it also accelerates the droplet coalescence process [31]. During melt blending, at low concentration of

the dispersed phase the droplet breakup dominates over droplet coalescence, since droplet-droplet interaction is less likely to take place. Therefore a finer morphology is usually achieved at high screw speed. However, at higher concentration of the dispersed phase, also the coalescence of droplets should be taken into consideration. The double emulsion morphology in Figure 4.1c demonstrates the coalescence tendency of the PET droplets. Under the screw speed of 40 rpm, most of the PET droplets have collided and formed the continuous phase. However, some droplets still remain in the large PP domains. When the screw speed reaches 80 rpm, the coalescence of the PET droplets is completed, since the intensive shear brings more chance for the coalescence of the PET droplets. The PET continuous phase is strengthened by incorporating more droplets (Figure 4.5). It is obvious that at high screw speed the droplet coalescence dominates over droplet breakup, partially because high screw speed enhances the probability for the coalescence of PET droplets, and partially because the less viscous PET tends to form the continuous phase during melt blending.

Addition of compatibilizer into immiscible polymer blends is known to be able to reduce the interfacial tension and diminish the droplet coalescence. In the present study, different amounts of compatibilizer (PP-g-MA) were incorporated into the PET/PP (40/60) blend which is extruded at the screw speed of 80 rpm. With 1 wt.% of compatibilizer, although the PET is still the continuous phase (Figure 4.6a), the double emulsion morphology appears (Figure 4.6b), note that its onset was formed at low screw speed (40 rpm) also appears. This morphology indicates that 1 wt.% of compatibilizer is able to reduce the coalescence of the PET droplets. Further increase of the concentration of the compatibilizer to 3 wt.% suppresses the coalescence of PET droplets in the center region of the extrudate (Figure 4.6d). However, on the surface of the extrudate where the shear is more intensive, the double emulsion-type morphology along with the PET as continuous phase become observable (Figure 4.6c). For the PET/PP/PP-g-MA (40/54/6) blend as shown in Figure 4.6e, the PET becomes the dispersed

phase. This finding confirms that the coalescence of the PET droplets is completely suppressed by adding 6 wt.% of compatibilizer.
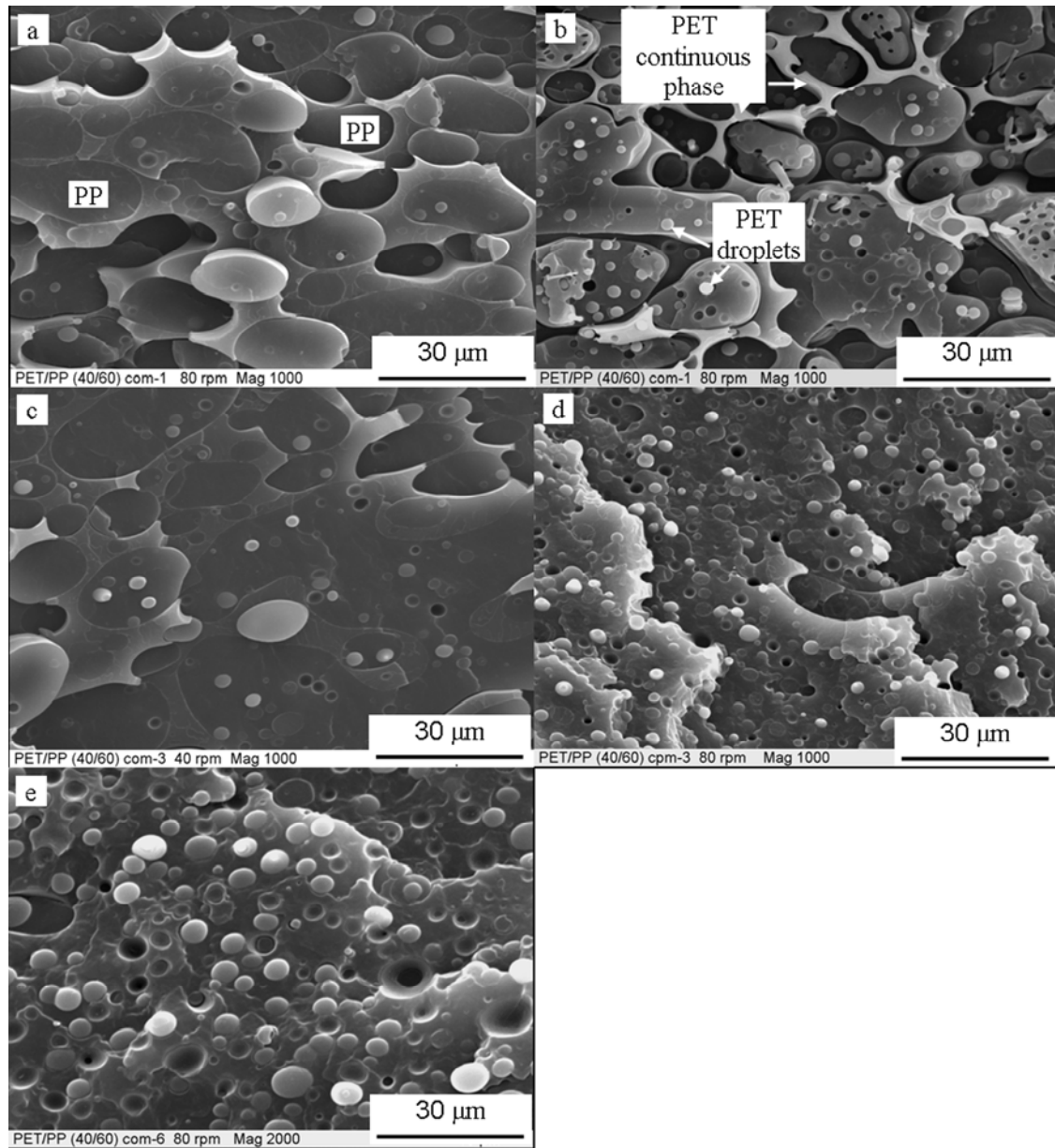

Figure 4.6: PET/PP blend with different amounts of compatibilizer extruded at the screw speed of 80 rpm: (a) and (b) PET/PP/PP-g-MA (40/59/1), (c) and (d) PET/PP/PP-g-MA (40/57/3), (e) PET/PP/PP-g-MA (40/54/6).

The effects of blend composition, screw speed and different amounts of compatibilizer on the phase evolution of the PET/PP blend can be summarized as schematically shown in Figure 4.7. Without compatibilizer, high screw speed (i.e. high shear rate) leads to a shift of matrix from the PP to PET; while under the screw speed of 80 rpm, increasing concentration of the compatibilizer results in an adverse effect, i.e. the role of the matrix is overtaking PP from PET.
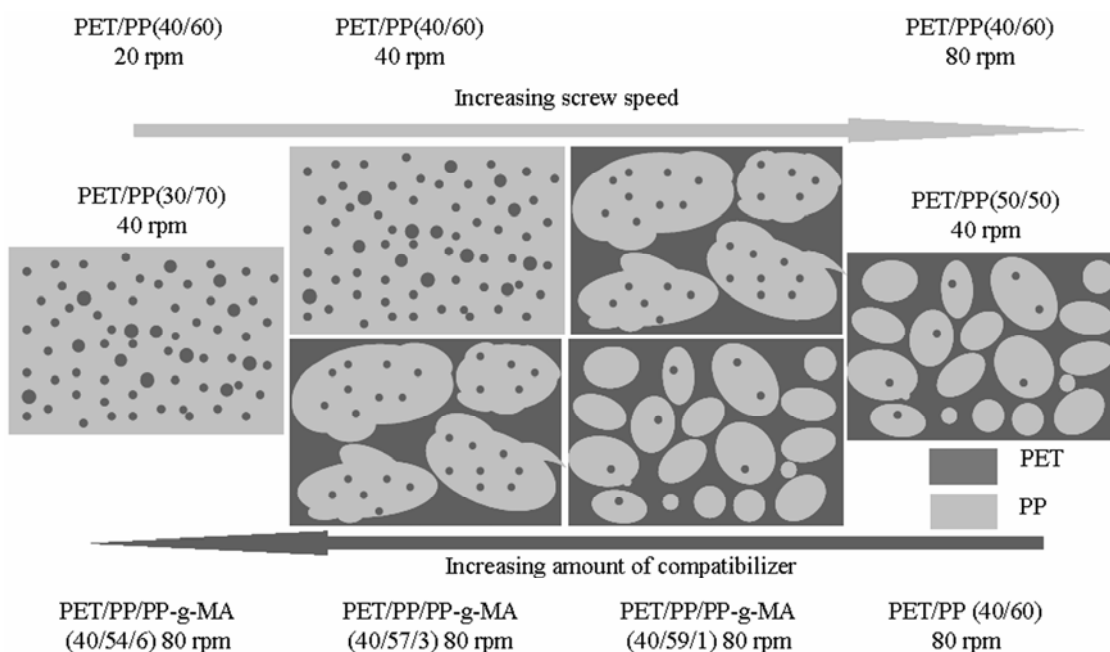
Figure 4.7: Effects of blend composition, screw speed and different amounts of compatibilizer on the phase evolution of the PET/PP blend.

4.1.1.2 Morphology of drawn strands

During melt blending of PET/PP, generally three kinds of morphologies are observed (Figure 4.7): the PET droplets in the PP matrix, the double emulsion morphology, and the PP domains in the PET continuous phase. The PET/PP (30/70), PET/PP (40/60) and PET/PP (50/50) blends extruded at 40 rpm demonstrate the three types of morphology, respectively. Upon stretching, both PET and PP phases are deformed; however, the stretching of extrudate does not change its fundamental phase structure. Therefore three different phase

structures can also be resolved in the drawn strands. Blends with the above mentioned three morphologies which are very representative, were stretched into drawn strands and their morphology inspected after etching the PP by hot xylene. The resulted morphologies are shown in Figure 4.8. After stretching, the dispersed PET droplets in the PET/PP (30/70) extrudate deform into long fibrils (Figure 4.8a). The PET/PP (40/60) extrudates possessed the double emulsion morphology. Therefore in their drawn strands cavities are observed as a result of the PP removal whereby the PET framework remians (Figure 4.8b). A few fibrils are noticed in some of the large cavities, and these fibrils are believed to be originated from uncollided PET droplets in the PP domains. The PET/PP (50/50) extrudate exhibits the "PP domains in PET matrix" morphology. When compared with Figure 4.1d the PP domains in PET/PP (50/50) are much smaller than those in the PET/PP (40/60) extrudate. This means some "strengthening" of the framework. Therefore in the PET/PP (50/50) drawn strands the size of the cavities is much smaller than those in the PET/PP (40/60) drawn strands, and the alignment of the PET framework becomes also thicker (Figure 4.8c).
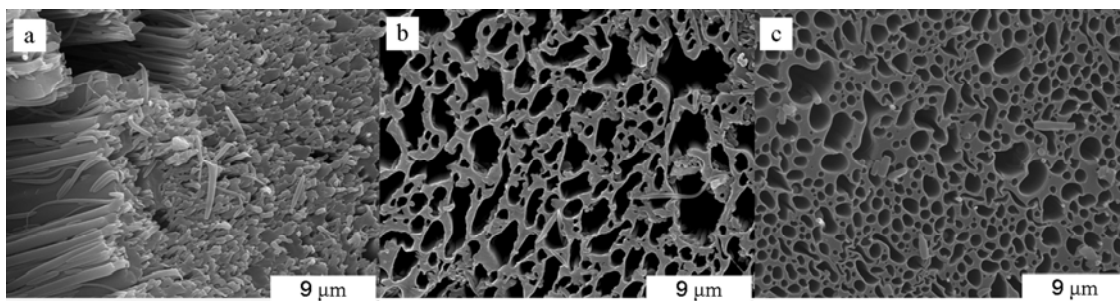
Figure 4.8: Morphology of PET/PP drawn strands (made from stretching the corresponding blends extruded at 40 rpm) after remove of PP: (a) PET/PP (30/70), (b) PET/PP (40/60) and (c) PET/PP (50/50).

The structures of drawn strands, shown in Figure 4.8b and c are, the undesired structures for preparing MFC, since the PET becomes the matrix instead of reinforcing fibrils. In order to obtain PET fibrils in drawn strand, the PET phase should be dispersed in the extrudate. The phase structure of PET droplets in PP

matrix can be obtained at low PET concentration (< 30 wt.%). When the concentration of PET reaches 40 wt.% (as shown in Figure 4.7) a low screw speed should be adopted or a suitable amount of compatibilizer should be incorporated at high screw speed in order to ensure the development of the "MFC-favored" initial morphology.

4.1.1.3 Morphology of compression molded MFC

The SEM images of the fracture surfaces of PET/PP (30/70) and PET/PP/PP-g-MA (40/54/6) MFC are shown in Figure 4.9. As seen in the images, after compression molding the PET fibrils are well preserved and act as desired reinforcement for the PP matrix.
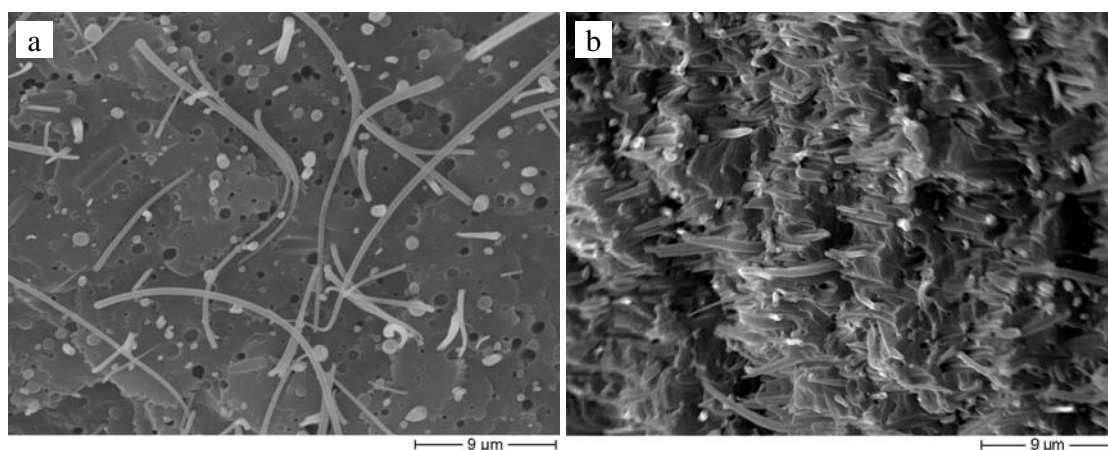
Figure 4.9: Fracture surfaces of (a) PET/PP (30/70) and (b) PET/PP/PP-g-MA (40/54/6) MFC.

4.1.2 DSC analysis of the extrudates

The compatibilization effect of PP-g-MA on the PET/PP blend is further verified by the DSC analysis of the extrudates. The crystallization exotherms of the uncompatibilzed and compatibilized PET/PP extrudates are shown in Figure 4.10. Two peaks are observed for the PET/PP (40/60) extrudates: with the intensive peak appearing at around 115 °C representing the crystallization of the PP, while

the small peak at around 190 °C reflects the crystallization of PET. The intensity of the crystallization peak of PET decreases upon the addition of PP-g-MA, which suggests a suppressed crystallinity of the PET. Upon addition of PP-g-MA, the in-situ generated PP-g-PET copolymer, which locates in the PET phase may act as a polymeric diluent to retard the crystallization of the PET. The consequence is a reduced heat of crystallization of the PET [113], as displayed by the DSC traces.
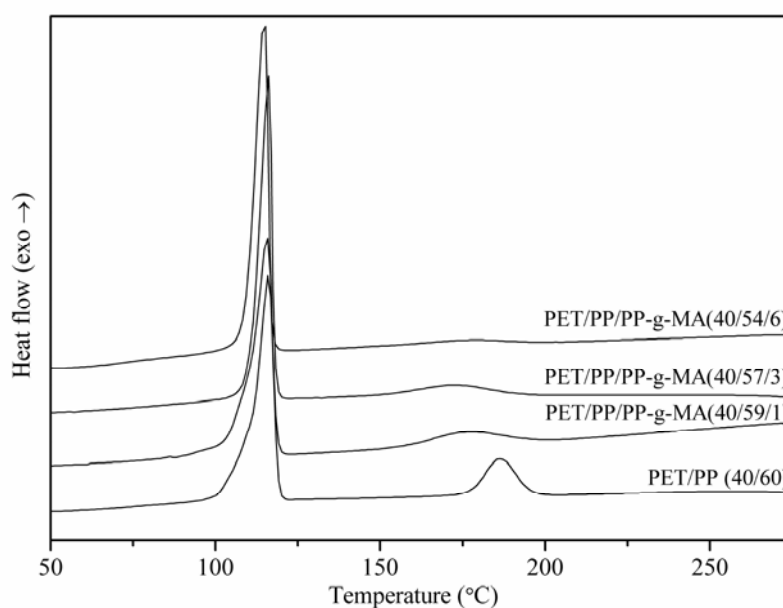
Figure 4.10: DSC traces of uncompatibilized and compatibilized PET/PP blends.

4.1.3 Tensile properties of compression molded MFC

Three types of drawn strands, PET/PP (30/70) extruded at the screw speed of 40 rpm, PET/PP (40/60) extruded at 20 rpm and PET/PP/PP-g-MA (40/54/6) extruded at 80 rpm, which possess the structure of "PET fibrils in PP matrix" were used to prepare MFC. The tensile properties of the compression molded MFC, are shown in Figure 4.11. For comparison purpose, the tensile properties of neat PP and PET are also presented. Because of the reinforcement effect of the uniaxially oriented PET fibrils, a great improvement in tensile properties of the PET/PP MFC is achieved compared with the neat polymers. Both tensile strength and modulus show a noticeable increase at a higher PET concentration, which is

attributed to the increasing amount of the PET fibrils. However, incorporation of compatibilizer does not further improve the tensile properties.
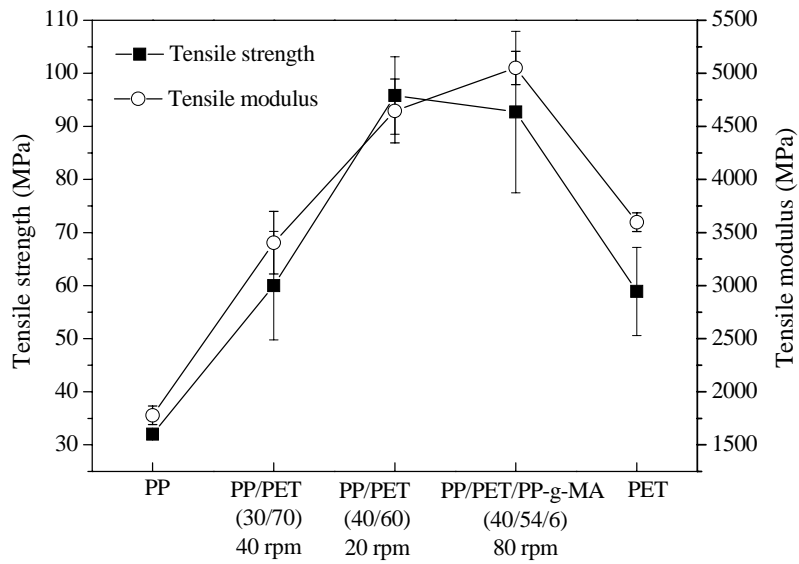
Figure 4.11: Tensile properties of compression molded PET/PP MFC.

4.2 PET/PP/TiO$_2$ MFC

4.2.1 Morphology

4.2.1.1 Morphology of the extrudates

Figure 4.12 shows the fracture surfaces of the PET/PP/TiO$_2$ extrudates. For comparison purpose, the SEM images of PET/PP and PET/PP/MA blend were also presented. The matrix is PP and the dispersed phase is PET. In the PET/PP/2T300 extrudate, the TiO$_2$-300nm particles are dispersed only in the cylindrical PET phase (Figure 4.12c). Interestingly, as can be seen from Figure 4.12d, in the compatibilized extrudate (PET/PP/MA/2T300), the TiO$_2$-300nm particles are only found in the PP matrix. When TiO$_2$-15nm nanoparticles are incorporated into the blend, without compatibilizer, all the nanoparticles migrate into PET phase in the extrudate (Figure 4.12e). With compatibilizer, however, the nanoparticles are found in the PET dispersed phase, in the PP matrix, as well as at the interface (Figure 4.12f).
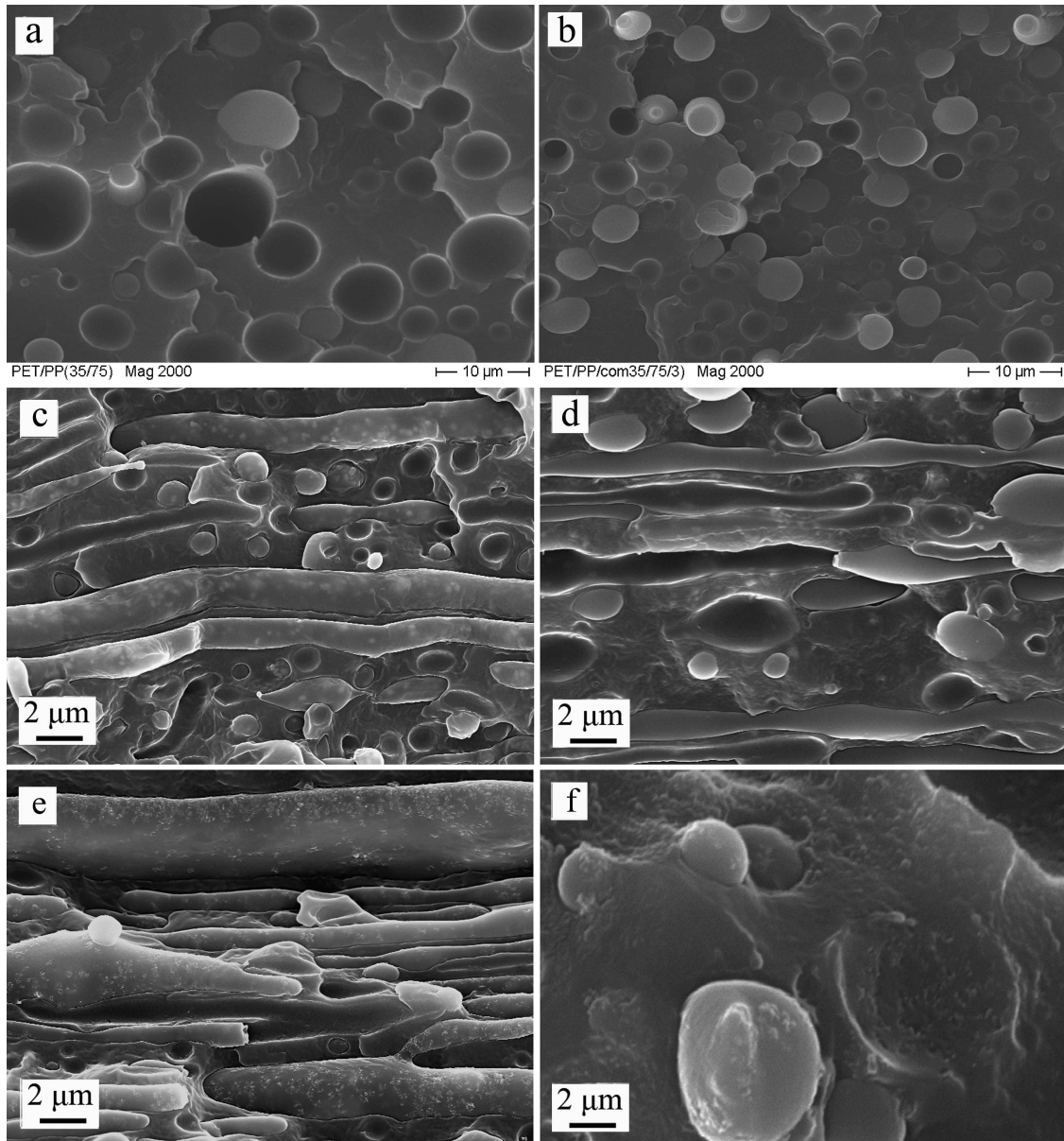
Figure 4.12: SEM images of PET/PP and PET/PP/TiO$_2$ extrudates: (a) PET/PP, (b) PET/PP/MA, (c) PET/PP/2T300, (d) PET/PP/MA/2T300, (e) PET/PP/2T15, (f) PET/PP/MA/2T15.

4.2.1.2 Morphology of drawn strands

As is well known, during cold drawing of the immiscible PET/PP blends both phases transform into fibrils [2, 46, 47, 114, 115-118]. In order to obtain more information of the size and aspect ratio of the PET fibrils in the drawn strands, the PP phase was removed by hot xylene. Figure 4.13a shows microphotograph taken from the PET fibrils. The diameter of the fibrils is in range of 0.5-1.5 µm and they exhibit a high aspect ratio. However, for the PET/PP/MA drawn strand, some short needle-like PET formations are also resolved besides the long fibrils (Figure 4.13b). Figure 4.13c and Figure 4.13d show the PET fibrils in the PET/PP/2T300 and PET/PP/MA/2T300 drawn strands, respectively. The observation confirms that the TiO_2-300nm particles have a preferential location in one polymer phase as already noticed in the extrudates (Figure 4.12). In the PET/PP/2T300 drawn strand, it is clearly seen that the TiO_2-300nm particles are in the PET phase. While in the PET/PP/MA/2T300 one, the particles are preferentially located in PP and thus partially removed by hot xylene. Therefore only those TiO_2 particles which are located at the PET/PP interface can be seen. Similarly, for the etched PET/PP/MA/2T15 drawn strand the PET fibrils are covered with small agglomerates of the TiO_2-15nm nanoparticles (Figure 4.13f). By contrast for the etched strands composed of PET/PP/2T15, no TiO_2 agglomerates can be recognized on the surface of the residual fibrils (Figure 4.13e).
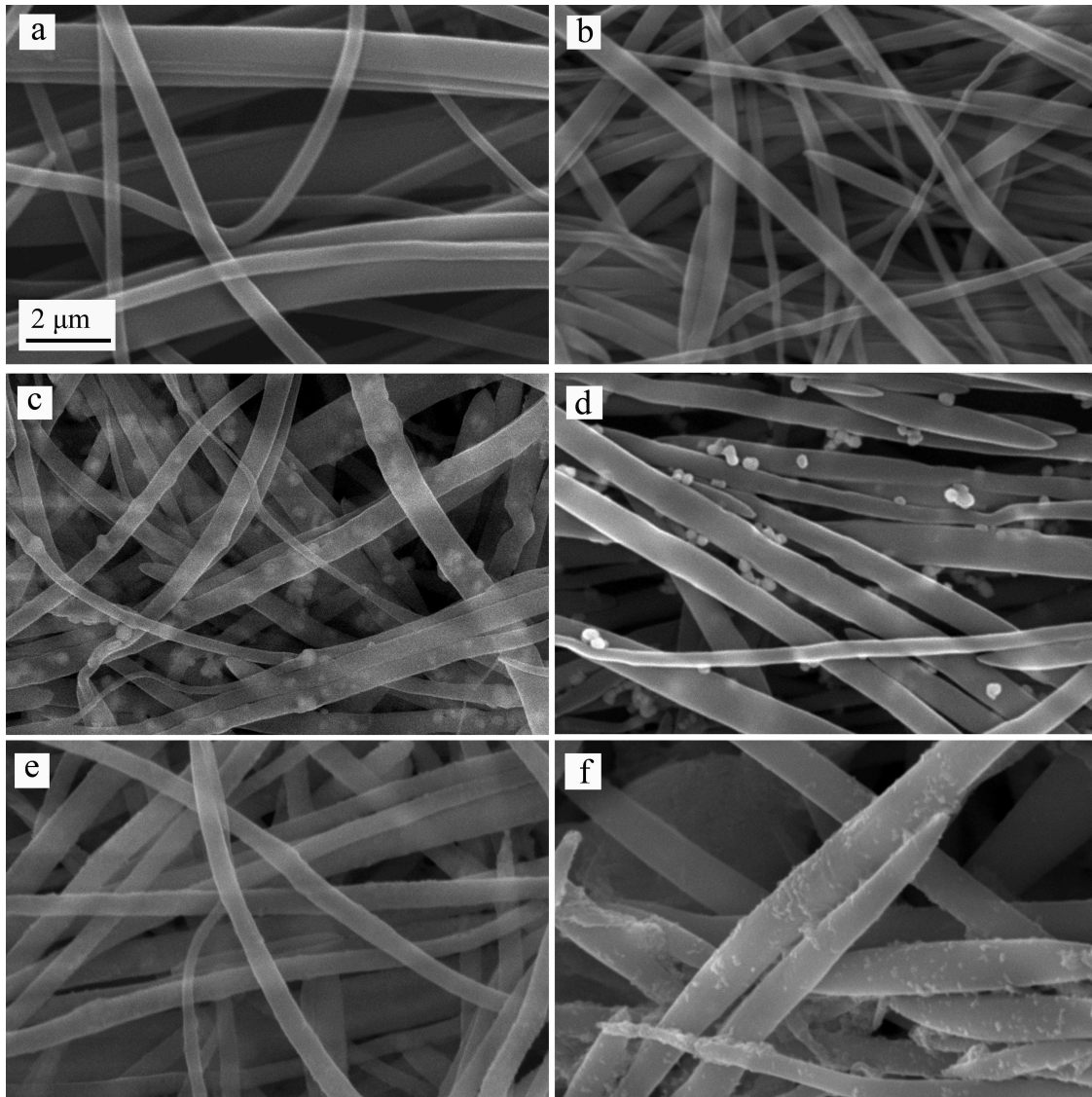
Figure 4.13: SEM images of the PET fibrils in drawn strands, note: PP was removed by hot xylene: (a) PET/PP, (b) PET/PP/MA, (c) PET/PP/2T300, (d) PET/PP/MA/2T300, (e) PET/PP/2T15, (f) PET/PP/MA/2T15.

As shown in Figure 4.14, in the PET/PP/T drawn strand all the PET fibrils are of high aspect ratio, only few needle-like PET formations of low aspect ratio can be observed. The diameters of the PET fibrils are in range of 0.5 μm to 2 μm. In the PET/PP/MA/T drawn strand as it is seen in Figure 4.14c, the diameter distribution of the PET fibrils is quite uniform (0.4-1 μm). Beside some short, needle-like PET domains are also present.
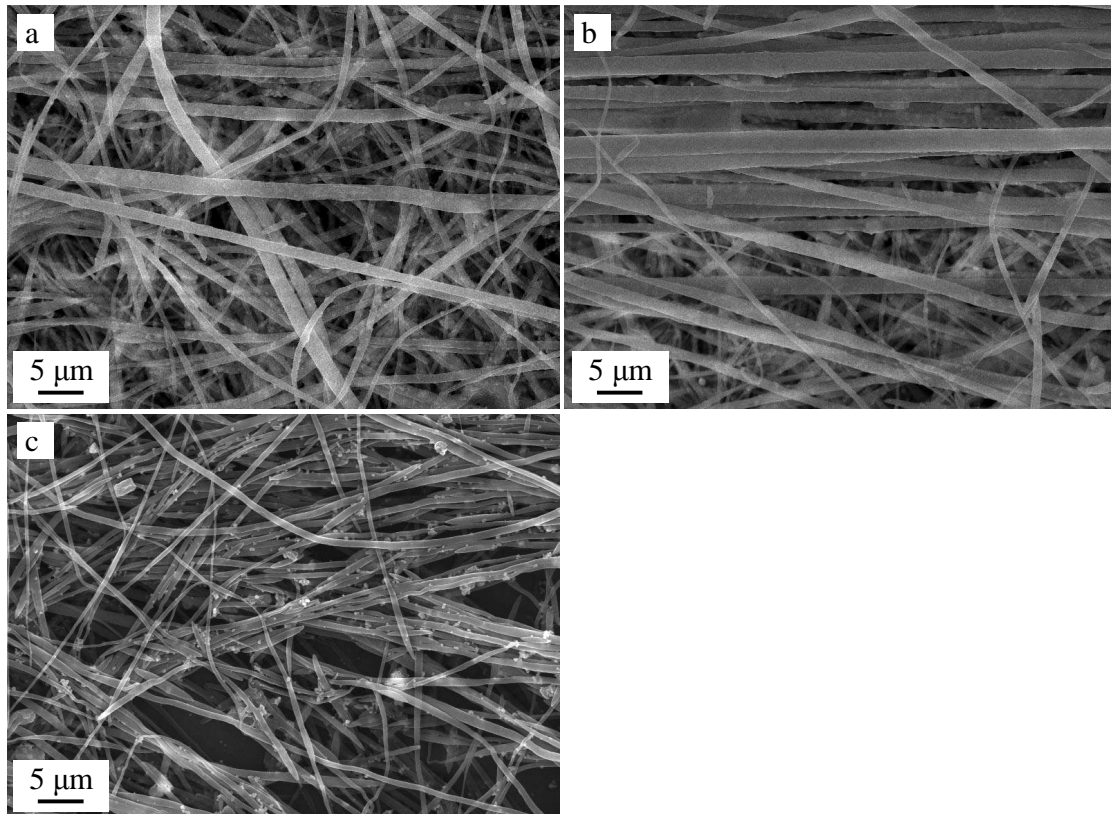
Figure 4.14: SEM images of PET microfibrils in the drawn strands, PP was removed by hot xylene: (a) and (b) PET/PP/2T300, (c) PET/PP/MA/2T300.

Drawing of the extrudate is the most critical step to generate PET fibrils with large aspect ratio. In the hot water bath where water temperature was kept at 85 °C, the extrudate underwent necking upon drawing and it become highly elongated. Consequently, the dispersed PET droplets in the extrudate were transformed either into fibrils or into short need-like domains. To explain the morphological difference of the PET fibrils in the PET/PP/2T300 and PET/PP/MA/2T300 drawn strands, two factors should be taken into consideration: the original PET droplet size in the extrudate and the coalescence of the PET droplets during stretching. Upon stretching large PET droplets deform into large microfibrils with high aspect ratio; while small droplets result in microfibrils with small diameter and low aspect ratio. Fakirov [51] reported that during stretching the PP/PET blend, breakdown of PET fibrils is excluded because of the very high viscosity and the moderate flow conditions during the

cold drawing. However, during stretching the PET/PP blend, long PET microfibrils can be created due to the end-to-end coalescence of the contacting elongated particles; while the PET/PP/MA drawn strand shows much shorter PET microfibrils because the PP-g-MA which presents on the PET droplets surface inhibits the coalescence process. In the present study, as discussed before in the PET/PP/MA/2T300 the PP-g-MA does not act as the compatibilizer for the PET and PP, instead it interacts with the TiO_2. Consequently there is no compatibilizer coating on the PET droplets. Therefore it is believed that during stretching the coalescence of the elongated PET droplets takes place both in the PET/PP/2T300 and PET/PP/MA/2T300.

However, the different morphologies of the PET microfibrils in the PET/PP/T and PET/PP/C/T drawn strands indicate that although the PET microfibril size is influenced by the coalescence of the PET droplet during stretching, the original size of the PET droplets is the key factor that controls the size of the PET microfibrils.

Figure 4.15 shows the dispersion of PET droplets in the PET/PP/2T300 and PET/PP/MA/T extrudates. The TiO_2 particles can not be discerned due to the low magnification. The number average diameter and the size distribution of dispersed droplets in the extrudates were determined by analyzing the SEM images. In the PET/PP/2T300 extrudate numbers of large PET/TiO_2 droplets with a number average diameter of about 4.4 μm are distributed (Figure 4.15a). For the PET/PP/MA/2T300 extrudate (Figure 4.15b), the number average diameter of the dispersed PET droplets is 2.8 μm. Figure 4.15a' and b' present the size distribution of PET droplets in the PET/PP/T and PET/PP/MA/2T300 extrudates, respectively. It is seen from the two images that the size distribution of PET droplets in the PET/PP/MA/2T300 extrudate is more uniform than that in the PET/PP/T extrudate, and the distribution shifts to the smaller diameter range.
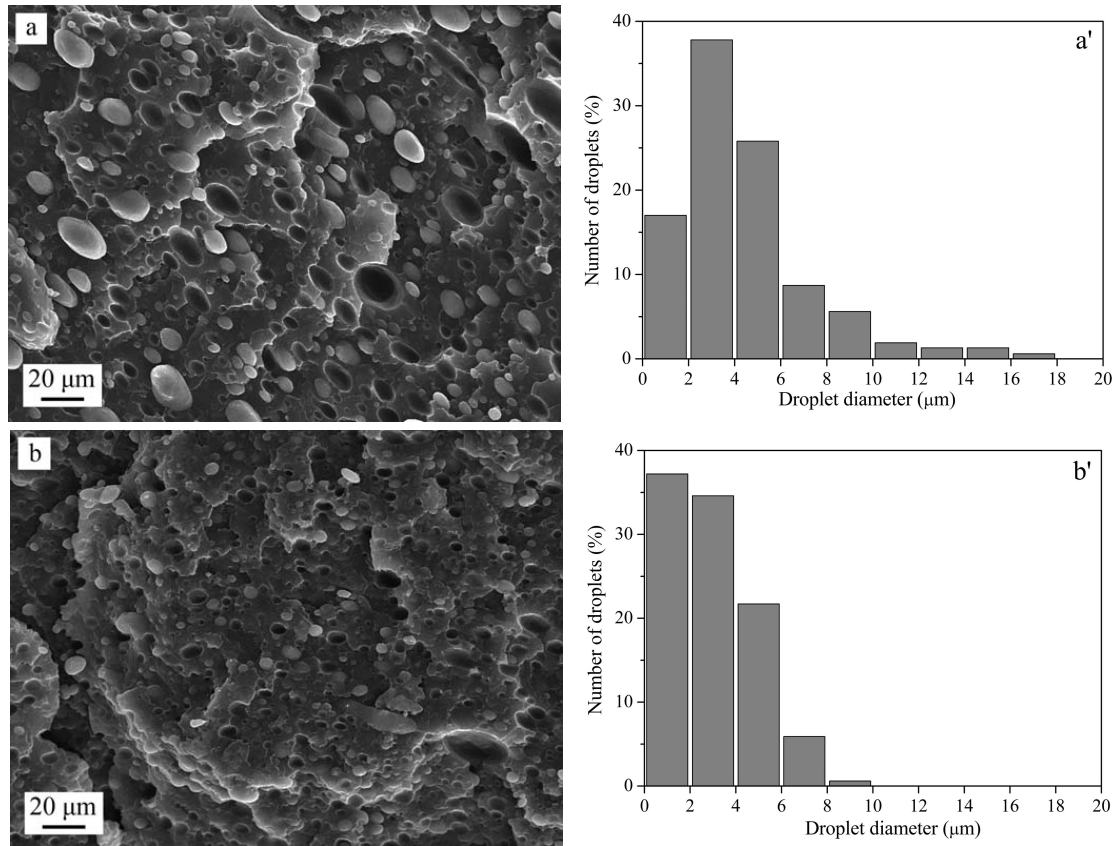
Figure 4.15: Cryofactured surfaces of the extrudates and the size distribution of PET droplets in the extrudates: (a) and (a') PET/PP/2T300, (b) and (b') PET/PP/MA/2T300.

Assuming the PET droplets in the extrudate are essentially spherical, the aspect ratio of PET fibrils in the drawn strand can be calculated by the following equation:

$$\frac{L}{D_f} = \frac{2}{3}\left(\frac{D_n}{D_f}\right)^3, \tag{4.1}$$

where L and D_f are the length and diameter of a fibril in the drawn strand, D_n is the diameter of a droplet in the extrudate. According to this equation, with a fixed D_f, a large D_n leads to a large aspect ratio of the fibril, and a small D_n results in a low aspect ratio. The PET droplet with a diameter of 2 μm in the extrudate is only able to deform into a short needle-like formation instead of a fibril. That is because the maximum aspect ratio of this deformed droplet can reach is only 10

(assuming the diameter of the deformed PET is 0.8 µm). In the PET/PP/MA/2T300 extrudate, the content of PET droplets with the diameter less than 2 µm is as high as 37% (Figure 4.15b'), consequently numerous short need-like PET formations appear in the drawn strand. In the case of the PET/PP/T extrudate, the content of PET droplets with the diameter below 2 µm is only 17% (Figure 4.15a'). Therefore few short need-like PET formations are observed in the drawn strand. In the PET/PP/T extrudates, although the diameter of most PET droplets is less than 8 µm, some droplets exist in large diameter range (from 8 µm to 18 µm). The PET fibrils with large diameter in the PET/PP/T drawn strand (Figure 4.14b) are believed to be either originated from those large droplets.

4.2.1.3 Morphology of injection molded MFC

Figure 4.16 shows the morphology of PET fibrils in the MFC specimens after extraction of the PP matrix. It is seen from Figure 4.16a-d that the PET fibrils are much shorter and thicker compared with the fibrils in drawn strands. Some fibrils almost retract back to their original spherical shape. In the injection molded MFC, the PET fibrils are no more unidirectionally aligned but highly curved (bent). During injection molding of the pelletized drawn strands, the processing temperature was 200 ℃ which is much higher than the T_g of PET. On the one hand, the PET fibrils tend to retract due to the high temperature; on the other hand, the PET fibrils may coalescence to some extent [54]. In addition, setting the screw rotation speed for 450 rpm during injection molding, the extensive shear stress inside the barrel may also break the fibrils. Consequently the PET fibrils in the MFC demonstrate larger diameters and much lower aspect ratios.
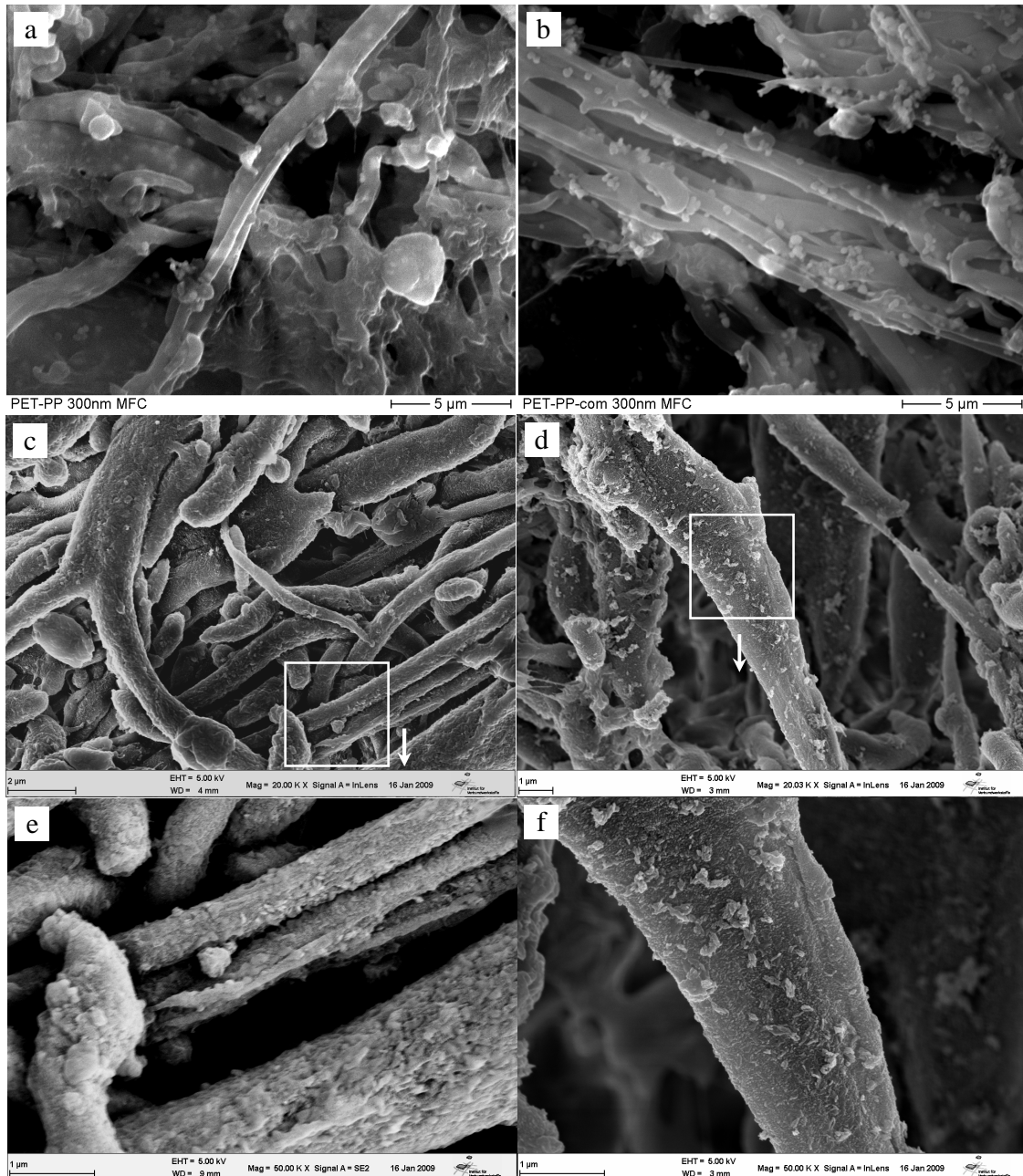
Figure 4.16: SEM images of PET fibrils in injection molded specimens (PP was removed by xylene): (a) PET/PP/2T300 MFC, (b) PET/PP/MA/2T300 MFC, (c) PET/PP/2T15 MFC, (d) PET/PP/MA/2T15 MFC, (e) high magnification image of the selected area in (c), (f) high magnification image of the selected area in (d).

After injection molding, the preferential location of TiO_2 is still preserved as shown in Figure 4.16. In the uncompatibilized PET/PP/TiO_2 MFC, the TiO_2-

300nm particles are found in the curved PET fibrils (Figure 4.16a); while in the compatibilized MFC the PET fibrils are quite "clean" and translucent, the TiO_2-300nm particles are located on the surface of PET fibrils (Figure 4.16b). High magnification SEM image (Figure 4.16e) show that in the PET/PP/2T15 MFC the PET fibrils contains lots of TiO_2-15nm. In the PET/PP/MA/2T MFC small agglomerates of TiO_2-15nm particles are noticed on the surface of PET fibrils (Figure 4.16f). These agglomerates TiO_2-15nm particles are believed to be from the PP matrix and remained on the PET fibrils' surface after the PP extraction.

4.2.2 Thermal and thermo mechanical properties

4.2.2.1 Crystallization behavior of drawn strands

The crystallization temperatures (T_c) and degree of crystallinities (X_{cr}) of the PP and PET in drawn strands are presented in Table 4.1. For comparison, neat PP and PP/TiO_2 (300 nm)-2 vol.% drawn strands were also subjected to DSC characterization. During the first cooling run (the PET fibrils are kept), the crystallization temperature of the PP in the PET/PP and PET/PP/TiO_2 drawn strands is about 10 °C higher than that of the neat PP. The heterogeneous nucleation effect of the PET fibrils on the PP matrix is believed to be responsible for this elevation of T_c. The preferential location of TiO_2 particles does not contribute to a further increase of the T_c of the PP matrix.

Table 4.1: Crystallization temperature (T_c) and crystallinity (X_{cr}) of PP and PET in drawn strands

Sample	First cooling run		Second cooling run	
	T_c of PP (°C)	X_{cr} of PP (%)	T_c of PET (°C)	X_{cr} of PET (%)
Neat PP	111.0	49.6	-	-
PET/PP	121.0	32.4	181.2	4.6
PET/PP/MA	121.5	32.8	-	-
PET/PP/2T300	121.5	29.4	184.0	5.6
PET/PP/MA/2T300	121.6	27.9	-	-
PET/PP/4T300	121.7	26.6	186.3	7.5
PET/PP/MA/4T300	122.4	27.8	-	-
PET/PP/2T15	122.1	28.2	185.5	6.4
PET/PP/MA/2T15	122.3	28.9	-	-

Incorporation of the TiO_2 particles into PET/PP moderately decreases the crystallinity of the PP irrespective of their preferential locations (in the PP phase or in the PET phase). The similar decrease in the crystallinity of PP was also observed for the PP/TiO_2 (300 nm)-2 vol.% drawn strand. Numerous researchers have reported similar observations: the crystallinity of polymer matrix decreased upon addition of nanofillers [119-121]. In the compatibilized PET/PP/TiO_2 drawn strands the TiO_2 particles are preferentially located in the PP matrix. The presence of the high concentration of TiO_2 particles prevents the development of large crystalline domains due to the restrictions imposed on polymer chains. This leads to smaller crystallite structures and more defect in crystalline lamella. Accordingly, the crystallinity of PP is decreased [121, 122]. In the uncompatibilized PET/PP/TiO_2 drawn strands, the TiO_2 particles are preferentially located in the PET. However, the crystallinity of PP is also decreased for the author can not give a simple explanation.

In the second cooling run, the crystallization peak of the PET disappeared upon addition of compatibilizer. Similar result was also found by Bae for PET/polypropylene grafted 2-hydroxyethyl methacrylate-isophorone diisocyanate (PP-g-HI) blend [113]. However, for the uncompatibilized PET/PP/TiO_2 drawn

strands where the TiO_2 particles are in the PET phase, the T_c and crystallinity of the PET are enhanced. Compared with PP, PET is of low crystallization ability. It is supposed that in the uncompatibilized PET/PP/TiO_2 drawn strands the TiO_2 particles serve as nucleation sites for the PET and elevate the crystallization temperature.

4.2.2.2 Thermal mechanical properties of drawn strands

Generally, incorporation of nanofillers into single-phase polymer or polymer blend increases the modulus of the composites [123, 124]. In our study, neat PP and PP/TiO_2 (300 nm)-2 vol.% drawn strands with the same draw ratio (draw ratio 10) were prepared and the corresponding DMTA results are presented in Figure 4.17. The storage modulus (E′) of the PP drawn strand shows a dramatic increase compared with bulk PP (generally the modulus of bulk PP at room temperature is less than 1800 MPa), which is attributed to the orientation of the molecular chains and the development of a supermolecular (semicrystalline) structure upon stretching. It is seen from Figure 17b that the tan δ versus temperature curves for the PP drawn strands show two relaxation transitions at 5 ℃ and 75 ℃, respectively. They are assigned to the α and β relaxation transitions, respectively. The relaxation at 5 ℃ corresponds to the glass/rubber transition of the amorphous region (T_g), and the second relaxation transition at 75 ℃ is attributed to the relaxation of polymer chains included in the crystallites and may involve lamellar slippage as well [125].

Incorporation of the TiO_2-300nm particles further increases the E′ of the PP drawn strand in the temperature range studied. It can be seen from Figure 4.17b that with TiO_2-300nm particles the T_g of PP shifts to a higher temperature. The elevation of T_g can be related to the reduction in mobility of the PP macromolecular chains in the vicinity of the fillers, which indicates a good filler-matrix interaction [126].
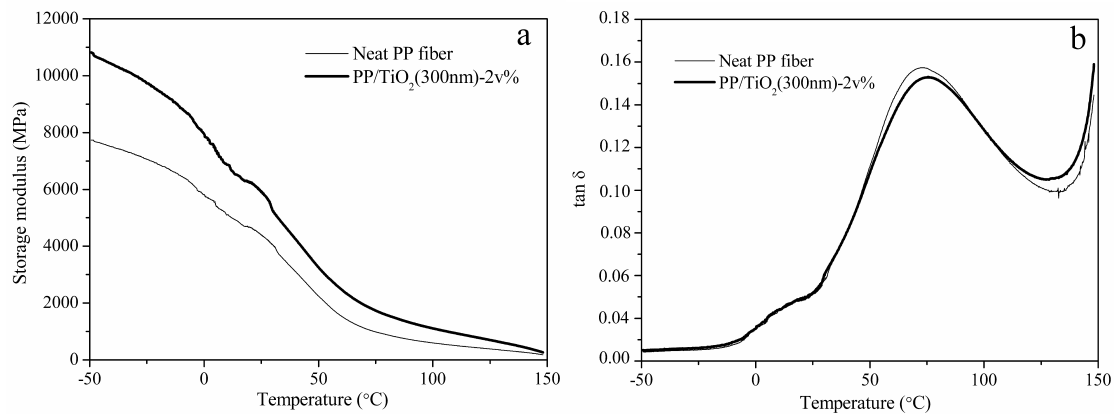
Figure 4.17: DMTA spectra of neat PP and PP/TiO₂ (300 nm)-2 vol.% drawn strands (draw ratio was 10): (a) storage modulus vs temperature, (b) tan δ vs temperature.

In case of the PET/PP/TiO₂ drawn strands both the PET and PP phases are oriented, therefore the interface between the two phases becomes very critical for the mechanical properties. The DMTA results of the drawn strands are presented in Figure 4.18a in form of E′ vs. T traces. The PET/PP drawn strand shows the highest modulus. This can be assigned to the reinforcement effect of PET fibrils and to the fairly good interfacial adhesion between the reinforcement and matrix. Incorporation of TiO₂ decreases the E′ for all drawn strands and the E′ drops even more with increasing concentration of TiO₂. The decrease of E′ by incorporating the TiO₂ particles is supposed to be mainly related to the decrease of matrix-fibril interfacial adhesion, and to the formation of defects at the interface. As a result, the stress transfer from the matrix to the fibrils less effective which is well resolved in the related E′ vs. T traces. This is associated with some reduction of E′.
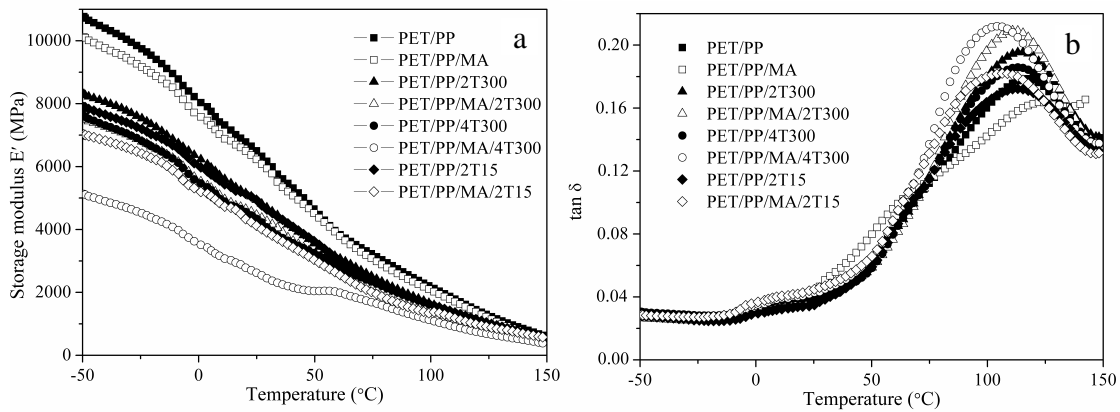
Figure 4.18: DMTA spectra of PET/PP and PET/PP/TiO$_2$ drawn strands: (a) storage modulus vs temperature, (b) tan δ vs temperature.

Figure 4.19a presents the morphology of the PET/PP/2T300 drawn strand. After stretching some TiO$_2$-300nm particles protrude out of the PET fibril, leaving pits on the interface. Therefore, the interface of the PET fibrils and the PP matrix is damaged, interfacial defects appear. Some TiO$_2$ particles even lose their adhesion to the PET, which creates large voids in the PET fibrils (indicated by arrows). Figure 4.19b shows that in the PET/PP/MA/2T300 extrudate, the thickness of the PP/TiO$_2$ phase between the neighboring elongated PET droplets is quite small (indicated by arrows), and in some parts it is less than 800 nm. In the drawn strand this thickness decreases dramatically. Finally a thin film forms which is not able to encapsulate the TiO$_2$-300nm particles (Figure 4.19c). Therefore these TiO$_2$ particles generate defects at the interface and result in the drop of the E$'$. To better illustrate the formation of the PP thin film and the voids at the interface, a schematic graph is presented in Figure 4.20.
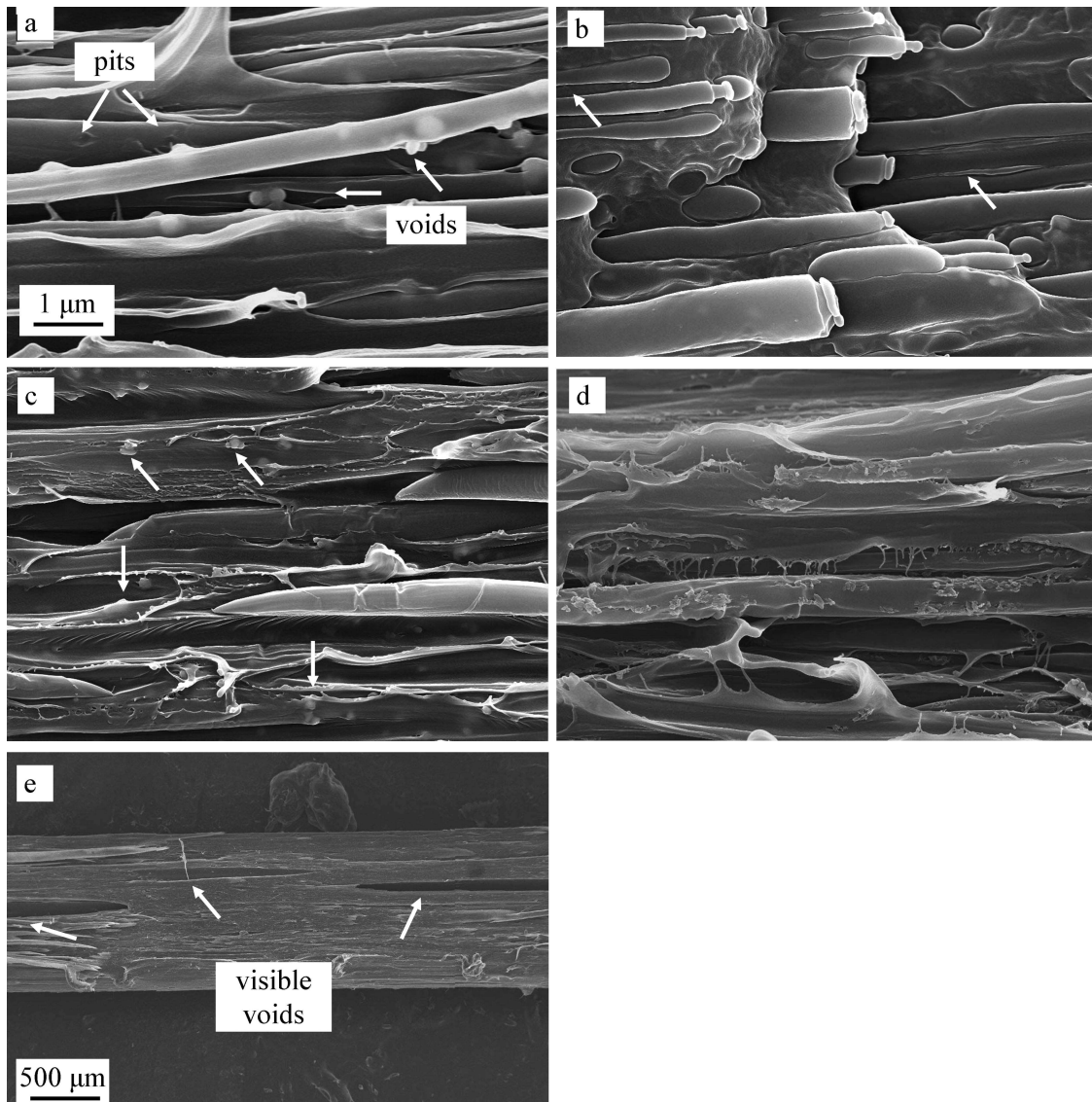
Figure 4.19: SEM images of the drawn strands and slightly drawn extrudates: (a) PET/PP/2T300 drawn strand, (b) PET/PP/MA/2T300 slightly drawn extrudate, (c) PET/PP/MA/2T300 drawn strand, (d) PET/PP/2T15 drawn strand, (e) PET/PP/2T15 drawn strand at low magnification.
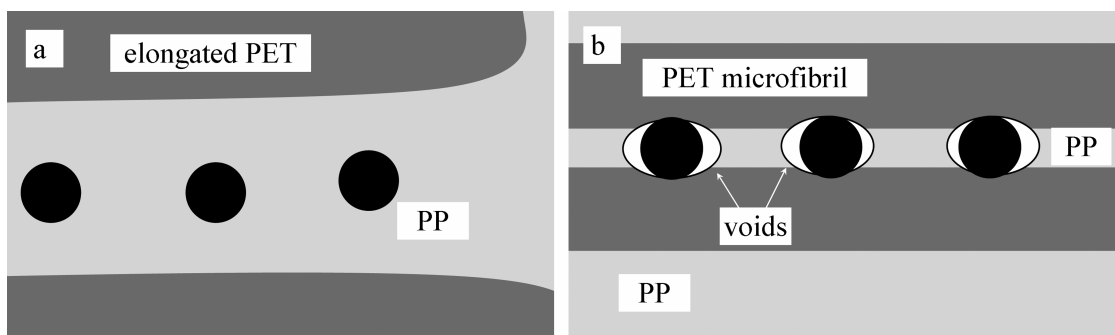
Figure 4.20: Schematic representation of (a) slightly drawn PET/PP/2T300 extrudate and (b) PET/PP/2T300 drawn strand.

For the PET/PP/2T15 and PET/PP/MA/2T15 drawn strands in which the TiO_2-15nm nanoparticles are always in the PET fibrils, the situation is even more complicated. Firstly, the PET fibrils are somehow damaged by the agglomerates of TiO_2-15nm nanoparticles as shown in Figure 4.19d. Secondly, visible voids appear in the drawn strands (see Figure 4.19e). Both structures result in the decrease of E′ (Figure 4.18a).

In general, the incorporated TiO_2 particles reduce the fibrillation ability of PET phase, resulting in a damaged fibril structure, which further affects the property enhancement of the PET/PP/TiO_2 drawn strand.

It is interesting to notice that the uncompatibilized drawn strands always exhibit higher modulus than the compatibilized ones irrespective of the presence of the TiO_2 particles. In the compatibilized drawn strands, as seen in Figure 4.14c, more short needle-like PET formations appear, therefore the fibrillar reinforcement is less effective. Besides, the elastomeric nature of the compatibilizer (PP-g-MA) may also decrease the E′ of the drawn strands [127].

Figure 4.18b shows the tan δ vs temperature curves for the drawn strands. As discussed earlier in this section, the β relaxation transitions of PP appear at about 75 ℃. It is known that the PET also exhibits α relaxation transitions at around 80 ℃. In Figure 4.18b, it is believed that the dominant peak, which

appears at around 100 °C, is associated to the glas s transition temperature of the PET as well as the β relaxation transitions of PP [128]. The small shoulder which locates in the vicinity of 10 °C is believed to be the β transition of the PP.

The T_g of the PET component in the compatibilized PET/PP/TiO$_2$ drawn strands is noticeably lower than that of the PET in the uncompatibilized ones. On the one hand, for the compatibilized drawn strands, the compatibility between the PET and the PP is improved upon addition of compatibilizer, therefore the T_g of PET shifts towards that of the PP. On the other hand, in the uncompatibilized PET/PP/TiO$_2$ drawn strands, the TiO$_2$ particles are located in the PET fibrils and the interaction between TiO$_2$ particles and the PET may result in the shifts of the T_g towards a higher temperature. Both the two factors account for the noticeable difference of the T_g for the PET phase in the compatibilized and uncompatibilized PET/PP/TiO$_2$ drawn strands.

The dominate damping peak of the PET/PP/TiO$_2$ drawn strands exhibits an increase magnitude compared with the PET/PP drawn strands, which also indicates the poor interfacial adhesion between the microfibrils and the matrix. In a composite system, damping is affected through the incorporation of fibers. The composite with poor interfacial bonding between fibers and matrix tends to dissipate more energy, thus resulting in an increase magnitude of damping peak [129].

4.2.2.3 Thermo mechanical properties of MFC

Dynamic mechanical spectra (storage modulus E′ and tan δ) as a function of temperature for the PET/PP and PET/PP/TiO$_2$ MFC are graphically represented in Figure 4.21. As shown in Figure 4.21a the storage modulus of MFC drops gradually in the whole temperature range. The storage moduli of PET/PP/TiO$_2$ MFC are very close to one another, these values are noticeably higher than that of the PET/PP MFC. This result seems to be contradictive to our earlier DMTA analysis of the PET/PP/TiO$_2$ drawn strands: incorporation of TiO$_2$ particles

decreases the E′ for all the PET/PP/TiO$_2$ drawn strands, and the E′ drops even more with increasing concentration of TiO$_2$ particles. Note in the drawn strands both PET and PP phases are well oriented, the decrease in E′ for the drawn strands is attributed to the damaged interface (by the TiO$_2$ particles), which results in poor stress transfer between the fibrils and matrix [130]. For the MFC, after injection molding the PP phase loses its orientation and forms the continuous phase. As demonstrated in Figure 4.22b showing the fracture surface of PET/PP/MA/2T300 MFC, the PET fibrils become much shorter and thicker, and some fibril bundles are also noticed. Accordingly, the interfacial area between the PET fibrils and PP matrix is greatly decreased. Compared with the PET/PP/TiO$_2$ drawn strands, the TiO$_2$ particles in both PET fibrils and PP matrix are less prone to protrude out in the PET/PP/TiO$_2$ MFC, less interfacial defects are expected. For the PET/PP/TiO$_2$ MFC the rigid TiO$_2$ particles contribute to the enhancement of storage modulus. Obviously, this positive effect of TiO$_2$ particles on the storage modulus surpasses the influence of the defects (caused by the TiO$_2$ particles) at the interface which decreases the storage modulus.
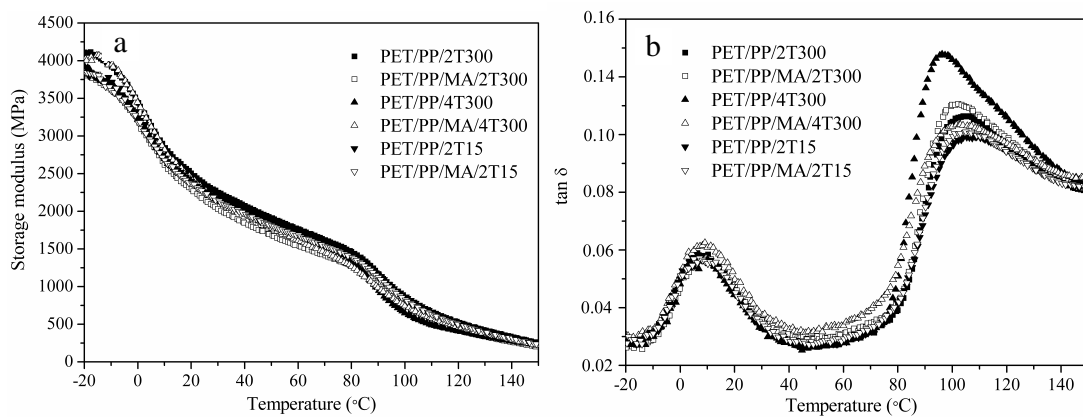
Figure 4.21: Thermal dynamic curves of the PET/PP and PET/PP/TiO$_2$ MFC: (a) storage modulus vs temperature, (b) tan δ vs temperature.

PET-PP 35-65 TiO2-300   5000   6 µm   PET-PP-com 35-62-3 TiO2-300-2v 2000   6 µm
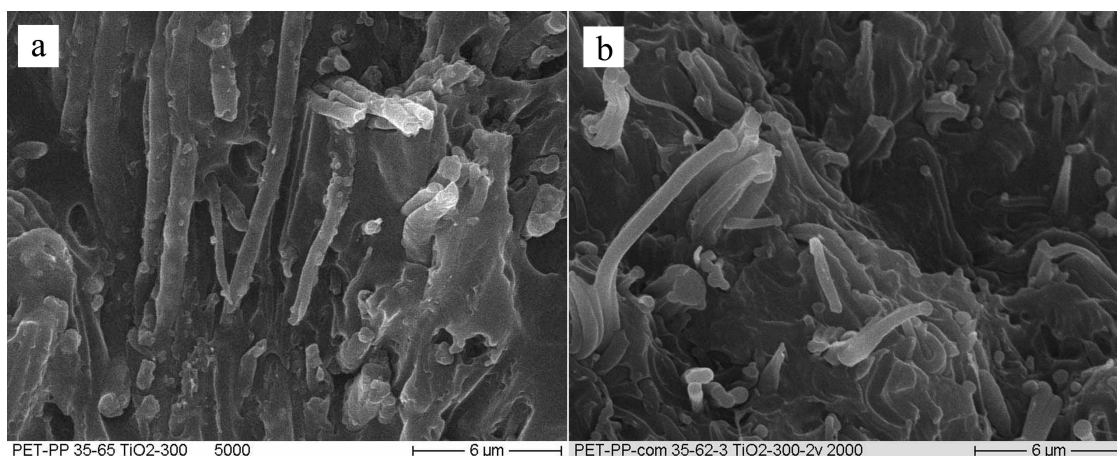
Figure 4.22: Fracture surfaces of (a) PET/PP/2T300 MFC and (b) PET/PP/MA/2T300 MFC.

In the tan δ vs temperature graph, two relaxation peaks are observed at around 6 ℃ and 103 ℃, which correspond to the glass transi tion temperatures (T_g) of PP and PET, respectively [129, 131]. The temperature maximum of the relaxation peaks of PP and PET is given in Table 4.2. It is interesting to notice that for the PET/PP/2T300 and PET/PP/4T300 MFC, the maximum of PP relaxation peak appears at the same position as that for the PET/PP MFC (at around 6 ℃); while for the PET/PP/MA/2T300 and PET/PP/MA/4T300 MFC, the maximum of PP relaxation peak shifts to a higher temperature (at around 9 ℃). However, the temperature maximum of PET relaxation peak in the PET/PP/TiO$_2$ MFC shows the opposite result. The PET relaxation peak in the compatibilized MFC (PET/PP/MA/2T300 and PET/PP/MA/4T300) reaches its maximum at around 103 ℃ which is also the temperature maximum of PET rel axation peak for PET/PP MFC. For the PET/PP/2T300 MFC (the uncompatibilized MFC) the tan δ maximum of PET appears at 105.1 ℃ which is 2 ℃ hi gher than that of the PET in the PET/PP MFC. However, for the PET/PP/4T300 MFC the tan δ maximum is at around 97 ℃ which is surprisingly lower compare d with other PET/PP/TiO$_2$ MFC.

Table 4.2: Glass transition temperatures (T_g) of PP and PET in PET/PP and PET/PP/TiO$_2$ MFC

Specimen	T_g of PP (°C)	T_g of PET (°C)
PET/PP	6.1	103.0
PET/PP/2T300	6.3	105.1
PET/PP/MA/2T300	9.3	102.2
PET/PP/4T300	6.1	96.7
PET/PP/MA/4T300	9.1	103.0
PET/PP/2T15	7.1	105.3
PET/PP/MA/2T15	7.2	105.0

The variation of T_g for both PP and PET can be attributed to the preferential location of TiO$_2$ particles. For the compatibilized PET/PP/TiO$_2$ MFC (PET/PP/MA/2T300 and PET/PP/MA/4T300) where the TiO$_2$-300nm particles are preferentially located in the PP matrix, these rigid TiO$_2$ particles restrict the mobility of the PP chains, thus resulting in the increase of T_g for PP [75]. Similarly, for the PET/PP/2T300 MFC, the preferential location of TiO$_2$ particles in the PET fibril also leads to an increase of T_g for PET. The noticeable drop of T_g for PET in the PET/PP/4T300 MFC is not unusual. Calcagno investigated the PP/PET/montmorillonite (MMT) nanocomposites in which the MMT clays were preferentially situated in the in the PET phase and in PP/PET interface. The cited author reported that addition of MMT into the blends results in a decrease in T_g of the PET dispersed phase [132]. Similar result was also reported by Feng who observed a decrease in T_g of PA6 in the PP/PA6/MMT composites [133]. Both authors associated this behavior to the presence of the MMT predominantly situated in the PET (or PA6) phase and in the interface that affected the chain mobility. In the present study, as discussed before the TiO$_2$ particles are more prone to protrude out of the PET fibrils at high TiO$_2$ loading (4 vol.%), resulting increased interactions between PP and PET. Consequently the T_g of PET in the PET/PP/4T300 MFC shifts to lower temperature.

For the PET/PP/2T15 and PET/PP/MA/2T15 MFC the T_g of PP and PET is not influenced by preferential location of TiO$_2$-15nm particles. The tan δ peak of PP for both specimens appears at around 7 °C, the maximum of PET relaxation

peak is at around 105 °C. In both MFC, the TiO$_2$-15nm particles are always found in the PET fibrils despite of the difference in concentrations, which contributes to the elevation of T$_g$ for PET.

4.2.3 Mechanical Properties of MFC

Tensile properties and impact strength of the injection molded PET/PP/TiO$_2$ and PET/PP MFC are given in Table 4.3. The tensile strength of PET/PP MFC is slightly higher than that of the pure PP. Incorporation of TiO$_2$ particles results in a decrease in the tensile strength of MFC. The PET fibrils are expected to be the reinforcement in the MFC. However, the experimental result indicates that the reinforcement effect of PET fibrils is not pronounced, which can be explained from the following three aspects. Firstly, in the injection molded MFC specimens the PET fibrils lose their orientation, and become quite randomly distributed in the PP matrix. Secondly, the low injection molding temperature (200 °C) results in poor interfacial adhesion between PET fibrils and PP matrix. Thirdly, as shown in Figure 4.13a-d, the PET fibrils become much shorter and thicker after injection molding, resulting in a less effective reinforcement effect.

Table 4.3: Tensile properties and impact strength of PET/PP and PET/PP/TiO$_2$ MFC

Specimen	Tensile Strength (MPa)	Tensile Modulus (MPa)	Impact Strength (kJ/m^2)
Neat PP	29.1 ± 1.0	1521.0 ± 58.3	11.1 ± 1.7
PET/PP	30.1 ± 1.7	1995.4 ± 73.0	19.0 ± 2.3
PET/PP/MA	31.2 ± 2.0	2190.0 ± 80.5	24.5 ± 4.1
PET/PP/2T300	26.3 ± 2.6	2382.5 ± 97.3	5.6 ± 1.3
PET/PP/MA/2T300	29.6 ± 1.6	2311.4 ± 63.8	16.3 ± 1.6
PET/PP/4T300	27.0 ± 0.7	2462.6 ± 71.6	4.0 ± 1.1
PET/PP/MA/4T300	30.3 ± 2.0	2318.0 ± 86.9	9.6 ± 2.1
PET/PP/2T15	28.9 ± 2.0	2488.4 ± 100.4	13.2 ± 3.8
PET/PP/MA/2T15	30.0 ± 1.7	2406.0 ± 50.6	18.6 ± 1.0

It is interesting to notice that the compatibilized PET/PP/TiO$_2$ MFC usually exhibit higher tensile strength compared with the uncompatibilized PET/PP/TiO$_2$ MFC.

As seen in Figure 4.22a, the residual PET fibrils are "damaged" by the TiO_2-300nm particles; while in the PET/PP/MA/2T300 MFC the PET fibrils are well preserved (Figure 4.22b). Therefore in the PET/PP/2T300 MFC, the reinforcement effect of the PET/TiO_2-300nm fibrils becomes less effective in comparison to the PET fibrils in the PET/PP/MA/2T300 MFC. In addition, for the PET/PP/MA/2T300 MFC, the interfacial adhesion between the PET fibrils and PP matrix is improved by incorporating compatibilizer, which also promotes the stress transfer from the matrix to the fibril reinforcement and leads to an increase in tensile strength [134].

The tensile modulus of PET/PP and PET/PP/TiO_2 MFC is dramatically improved compared with the pure PP. The PET fibrils which are much stiffer and tougher than the PP contribute to this modulus improved [63]. The incorporation of TiO_2 particles further increases the modulus of MFC irrespective of their preferential location. Comparing the PET/PP/TiO_2 MFC with different TiO_2 loadings (2 vol.% and 4 vol.%), one can notice that the tensile properties of PET/PP/TiO_2 MFC are not much influenced by the concentration of the TiO_2 particles.

The impact strength of PET/PP MFC is higher than that of the pure PP. Li [135] also observed an increase in the essential work of fracture of PET/PE MFC compared with pure PE. However, other researchers reported that the impact strength of PET/PP MFC is lower than pure PP, which is opposite to our finding [54, 55]. In the PET/PP MFC, the tough PET fibrils enhance the impact strength despite of the poor interfacial adhesion between the PET fibrils and PP.

The addition of TiO_2 particles decreases the impact strength of the MFC, the impact strength decreases more with increasing loading of TiO_2. Similar findings were also reported by other researchers who incorporated nanofillers into polymer blends [97, 136, 137]. In the PET/PP/TiO_2 MFC, irrespective of their preferential location the rigid TiO_2 particles act as weak points or stress concentrations. The stress can not be effectively transferred between the fibrils

and matrix when the specimens suffer from sudden impact energy, and the impact strength drops accordingly [75, 136]. Similar to the tensile strength results, the impact strength of the umcompatibilized PET/PP/TiO$_2$ MFC is much lower compared with the compatibilized PET/PP/TiO$_2$ MFC. In a composite material, effective energy dissipation is influenced heavily by the interfacial bonding between the matrix and dispersed phase [138]. In the uncompatibilized PET/PP/TiO$_2$ MFC, the TiO$_2$ particles are exclusively located in the PET fibrils. As noticed in Figure 4.22a, the protruding TiO$_2$ particles severely damage the PET/PP interface, thus resulting in debonding between the fibrils and matrix. Consequently, the crack easily initiates and propagates through the polymer/fiber interface under impact load, which results in a sharp decrease in impact strength [139, 140]. In addition, the damaged PET fibrils also contribute to the droplet of the impact strength. At higher loading of TiO$_2$ particles (4 vol.%) the damage of interface and PET fibrils is more severe, a further decrease in impact strength is thereby observed for the PET/PP/4T300 MFC. In the compatibilized PET/PP/TiO$_2$ MFC the TiO$_2$ particles are dispersed in the PP matrix, the PET fibrils are well preserved. The PET fibril/PP matrix interface is less likely to be damaged since the TiO$_2$ particles are less prone to protrude out of the isotropic PP. Therefore higher impact strength of the compatibilized PET/PP/TiO$_2$ MFC is observed in comparison to the uncompatibilized PET/PP/TiO$_2$ MFC.

4.3 PET/PP/TiO$_2$ nanocomposites

4.3.1 PET/PP/TiO$_2$-300nm composite

4.3.1.1 Dispersion of TiO$_2$ particles

Figure 4.23a-d show the dispersion of TiO$_2$ in the PET/PP/TiO$_2$ and PET/PP/PP-g-MA/TiO$_2$ composites prepared with Blending Procedures 1 and 2. Interestingly, for both blending procedures, without PP-g-MA the TiO$_2$ particles are exclusively located in the PET dispersed phase (Figure 4.23a and c), and in the PP matrix if PP-g-MA is incorporated (Figure 4.23b and d). For Blending Procedure 1 this is not difficult to understand since the PET/PP/TiO$_2$ (or PET/PP/PP-g-MA/TiO$_2$) composite is made by melt blending of the precompounded PP/TiO$_2$ composite with PET (or PET together with PP-g-MA) via a second step extrusion procedure. During Blending Procedure 2, although all the components were fed simultaneously into the hopper, the PP incorporates the TiO$_2$ as it melts prior to the PET. Therefore blending procedure 1 and 2 are essentially the same. Based on this analysis it is believed that in both blending procedures (i.e. 1 and 2) the TiO$_2$ particles migrate from the PP to the PET phase during extrusion in absence of PP-g-MA. In the composites containing PP-g-MA, the migration of TiO$_2$ does not take place, and all the TiO$_2$ particles stay in the PP. Therefore it is reasonable to infer that the presence of PP-g-MA influences the preferential location of TiO$_2$.

For (PET/T)/PP and (PET/T)/PP/MA, which are prepared with Blending Procedure 3, the TiO$_2$ particles are dispersed in the PET phase as displayed in Figure 4.23e and f. The presence of PP-g-MA does not influence the location of TiO$_2$. Figure 4.23g shows the dispersion of TiO$_2$ in the (PET/PP/MA)/T which was prepared with Blending Procedure 4. It is interesting to notice that the PET droplets are covered with a layer enriched in TiO$_2$ particles.
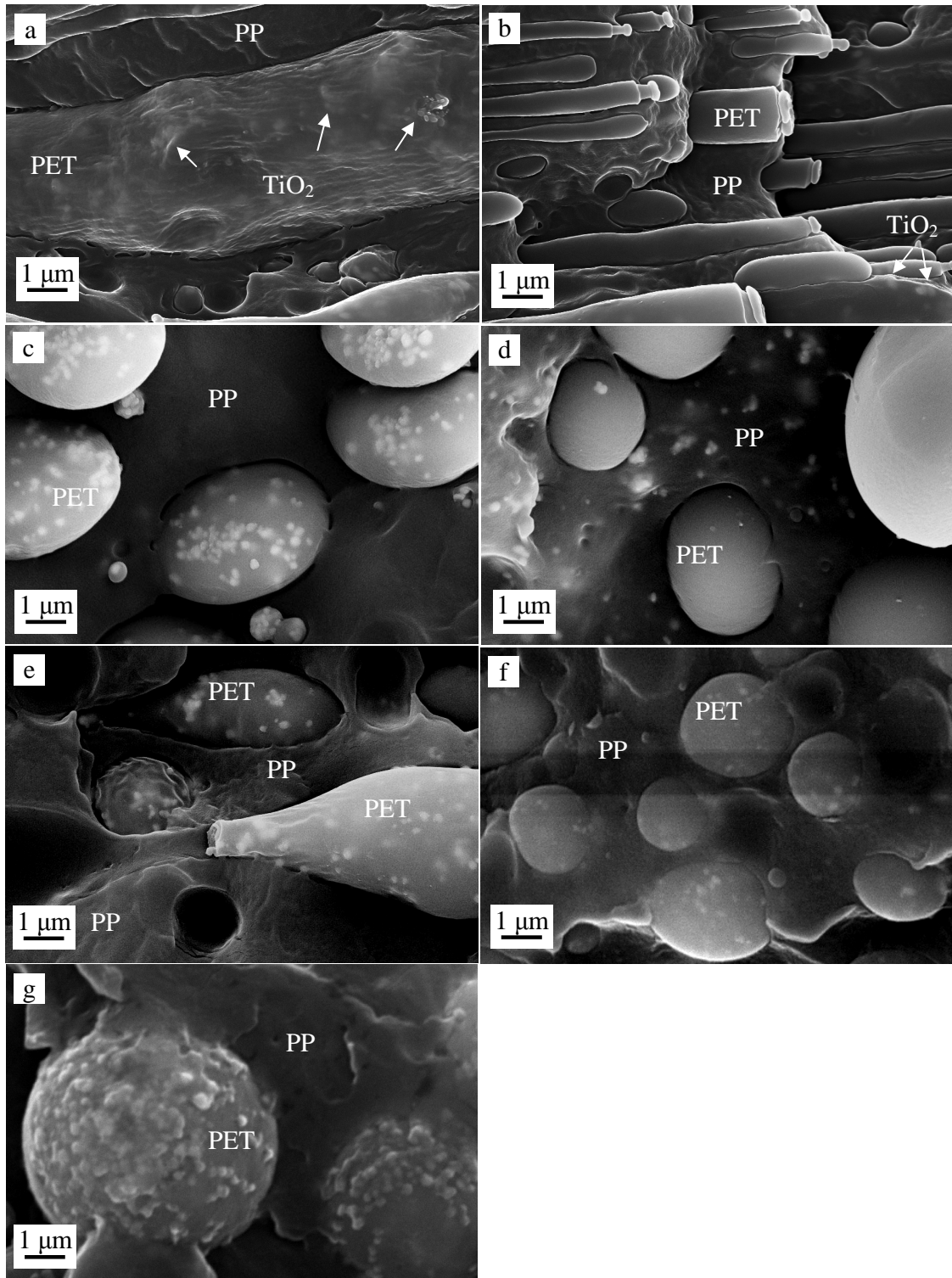
Figure 4.23: Dispersion of TiO$_2$ in PET/PP/TiO$_2$ and PET/PP/PP-g-MA/TiO$_2$ composites prepared with different blending procedures: (a) (PP/T)/PET and (b) (PP/T)/PET/MA prepared with Blending Procedure 1, (c) PP/PET/T and (d)

PP/PET/MA/T prepared with Blending Procedure 2, (e) (PET/T)/PP and (f) (PET/T)/PP/MA prepared with Blending Procedure 3, (g) (PET/PP/MA)/T prepared with Blending Procedure 4.

To further confirm the preferential location of TiO_2 particles in the blends, the PP/PET/T, PP/PET/MA/T and (PET/PP/MA)/T composites were etched by hot xylene to remove the PP. The morphologies are shown in Figure 4.24. In the composites PP/PET/T, PP/PET/MA/T and (PET/PP/MA)/T the TiO_2 particles are preferentially located in PET, PP and at the interface, respectively. For PP/PET/T, as shown in Figure 4.24a, the TiO_2 particles are observed in the PET droplets. However, for PP/PET/MA/T most of the TiO_2 particles removed by hot xylene. Therefore, they were preferentially located in the PP. Only a small amount of TiO_2 particles remained at the surface of PET droplets (Figure 4.24b). In (PET/PP/MA)/T, even after removing the PP matrix, the TiO_2 particles still cover the PET droplets (Figure 4.24c). The TiO_2 particles on the PET surface in this nanocomposite are clearly viewed in Figure 4.24d.
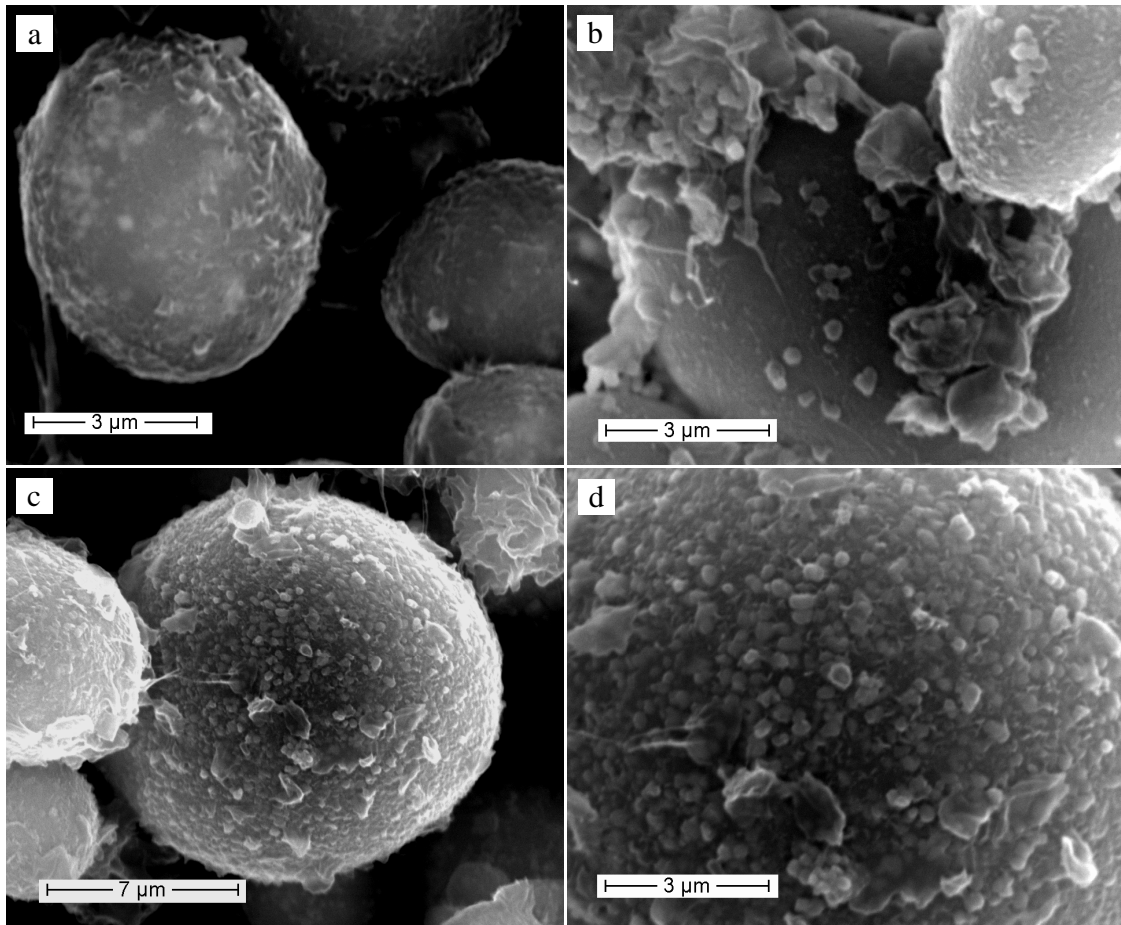
Figure 4.24: Morphology of PET/PP/TiO$_2$ and PET/PP/PP-g-MA/TiO$_2$ composites, PP was selectively etched by xylene: (a) PP/PET/T, (b) PP/PET/MA/T, (c) (PET/PP/MA)/T, (d) (PET/PP/MA)/T at high magnification.

The effects of PP-g-MA and blending sequence on the location of TiO$_2$ are summarized in Table 4.4. In absence of PP-g-MA, the TiO$_2$ are always dispersed in the PET phase irrespective of the blending procedures. However, in presence of PP-g-MA, the location of TiO$_2$ is governed by the blending sequence.

Table 4.4: Location of TiO_2 in the $PET/PP/TiO_2$ and $PET/PP/PP-g-MA/TiO_2$ composites prepared with different blending procedures

Blending Procedure	Location of TiO_2	
	$PET/PP/TiO_2$	$PET/PP/PP-g-MA/TiO_2$
Blending Procedure 1	PET	PP
Blending Procedure 2	PET	PP
Blending Procedure 3	PET	PET
Blending Procedure 4	-	TiO_2 layer on PET droplets

Inorganic fillers in polymer blends tend to interact more favorably with one particular phase, especially if the polarities of the two polymers are different. Therefore inorganic fillers usually migrate during melt blending. It is widely accepted that the competitive interaction between inorganic fillers and polymers is the thermodynamic driving force for the fillers' migration which results in their preferential location in one of the blend components. This competitive interaction can be predicted by the Young's equation [84]:

$$\omega = \frac{\gamma_{N-A} - \gamma_{N-B}}{\gamma_{A-B}} \qquad (4.2)$$

where ω is the wetting parameter; γ_{N-A} and γ_{N-B} are the interfacial tensions between filler and polymer A, and filler and polymer B, respectively. If $\omega > 0$, that is, $\gamma_{N-A} > \gamma_{N-B}$, inorganic fillers are dispersed in polymer B or at the interface; if $\omega < 0$, that is, $\gamma_{N-A} < \gamma_{N-B}$, the fillers are in polymer A or at the interface.

The interfacial tension between the inorganic filler and polymer can be computed by the geometric-mean equation [141]:

$$\gamma_{N-A} = (\sqrt{\gamma_N^d} - \sqrt{\gamma_A^d})^2 + (\sqrt{\gamma_N^p} - \sqrt{\gamma_A^p})^2 \qquad (4.3)$$

where the superscripts d and p stand for the dispersive and polar contributions to the surface tension, respectively. At 270 ℃ (the e xtrusion temperature) γ_{PP} is much lower than γ_{PET}, and the surface tension values are listed in Table 4.5 [140]. Materials such as metals, metal oxides and inorganic compounds (oxides, nitrides, silica) are high-energy materials. They usually have surface tensions in the range of 200-5000 mN/m. Organic polymers are low-energy materials, their surface tensions are generally bellow 100 mN/m [141]. For nanoparticles higher

values of the surface energy values than the corresponding bulk material have been reported. This is because of the missing bonds (or ruptured bonds) on the surface which give rise to a positive excess surface energy. In the present study, the surface energy of the TiO_2 particles at 270 °C is unknown, however, being a nano-sized inorganic material, these particles likely exhibit very high surface energy values [142, 143]. For the composite without PP-g-MA, one can presume that $\gamma_{TiO2-PP} > \gamma_{TiO2-PET}$. Therefore it is not surprising that the TiO_2 particles are located in the PET in the systems (Figure 4.24a, c, and e).

Table 4.5: Surface tension of PET and PP at 270 °C

Material	Surface tension at 270 °C (mN/m)		
	γ	γ^d	γ^p
PET	28.3	22.0	6.3
PP	15.7	15.7	0

Maleic anhydride (MA) is known to be an excellent ligand for metal oxides, it can be easily adsorbed onto the TiO_2 surface by electronic donation [144, 145]. The number of hydroxyl groups (OH) of the TiO_2 particles depends on the crystal structure of the TiO_2 as well as an interactions with visible or UV-light respectively (Figure 4.25) [146]. But independent of those facts, the OH groups are always found at the TiO_2 surface which are able to react with the MA functional groups to build up chemical bonds (as described in Figure 4.26). Breaking up of the anhydride structure of the PP-g-MA leads to carboxyl groups which are able to form a complex structure via acid-base inter actions, Homo/Lumo inter actions, respectively [147]. A reevaluation of the blending procedures reveals that during the preparation of (PP/T)/PET/MA (Blending Procedure 1) and PP/PET/MA/T (Blending Procedure 2), the PP-g-MA melts before the PET although the two components are incorporated simultaneously. This is just due to the difference in the melting ranges between PP-g-MA and PET. Therefore the PP-g-MA chains may be absorbed onto the surface of TiO_2 particles. Surrounded by the PP segments of PP-g-MA the TiO_2 particles become

"compatible" with the PP. As a consequence, they are staying in the PP instead of migrating to the PET phase.
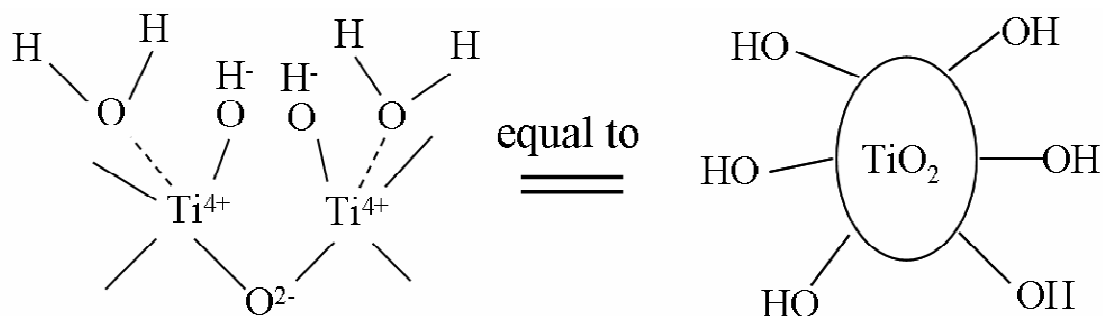
Figure 4.25: OH groups on the surface of TiO_2 particles.
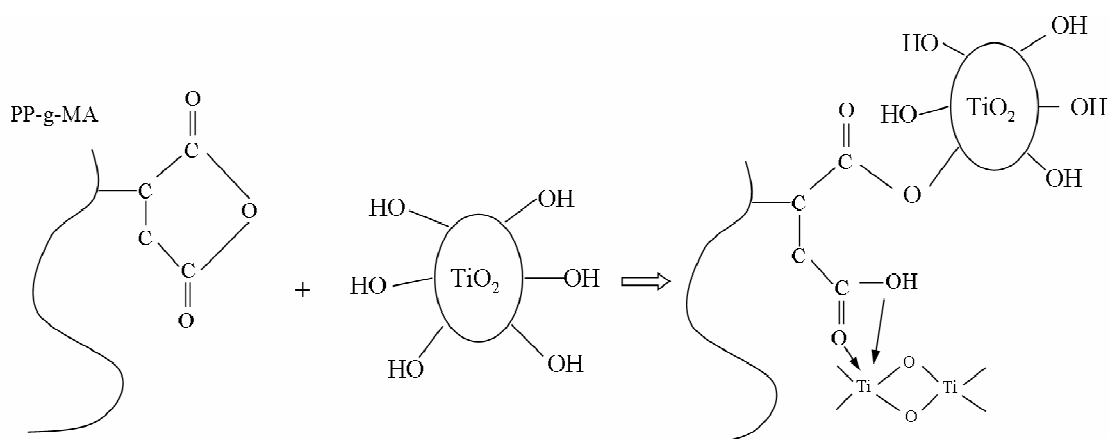
Figure 4.26: Possible interactions between the PP-g-MA and TiO_2.

For the (PET/T)/PP/MA prepared with Blending Procedure 3, the TiO_2 particles are precompounded with the PET. Consequently they are surrounded by the PET chains in the beginning of the second step extrusion. Therefore the incorporated PP-g-MA mostly reacts with the PET (via the maleic anhydride/PET terminal hydroxyl reaction) instead of interacting with the TiO_2. Accordingly, the TiO_2 particles remain in the PET phase.

The reaction time generally required for two reactive polymers is less than 5 minutes (the typical processing time) [148, 149]. With Blending Procedure 4, the

PET, PP and PP-g-MA were fed simultaneously during the first step extrusion performed with an estimated residence time of about 2 min. Aliphatic amine/anhydride and aliphatic amine/aromatic isocyanate reactions are extremely fast, having complete conversion within less than 30 s. Aromatic amine/anhydride and carboxylic acid/epoxy also have significant reaction conversion (about 10%) at short times (2 min) [149]. The maleic anhydride/hydroxyl is known to be less reactive than the aliphatic amine/anhydride and aliphatic amine/aromatic isocyanate. Nevertheless, even during the first step extrusion the chemical reaction between PP-g-MA and PET may take place. This was proved by the following strategy. PET/PP (35/65) blends with 0 vol.%, 1 vol.%, 3 vol.% and 6 vol.% of PP-g-MA were prepared under the same processing conditions. These blends were etched by hot xylene for 6 hours to remove the PP matrix. The morphology of the remaining PET phase in these blends is shown in Figure 4.27. It is seen from Figure 4.27a that the surface of PET phase in the uncompatibilized PET/PP blend is quite smooth. However, for the blends with increasing content of PP-g-MA, the surface of PET becomes rougher. This can be attributed to grafted PP chains and the accumulation of MA groups at the PET/PP interface (Figure 4.27b-d). Favorably interacted with the MA, the incorporated TiO_2 particles should also be located at the interface.
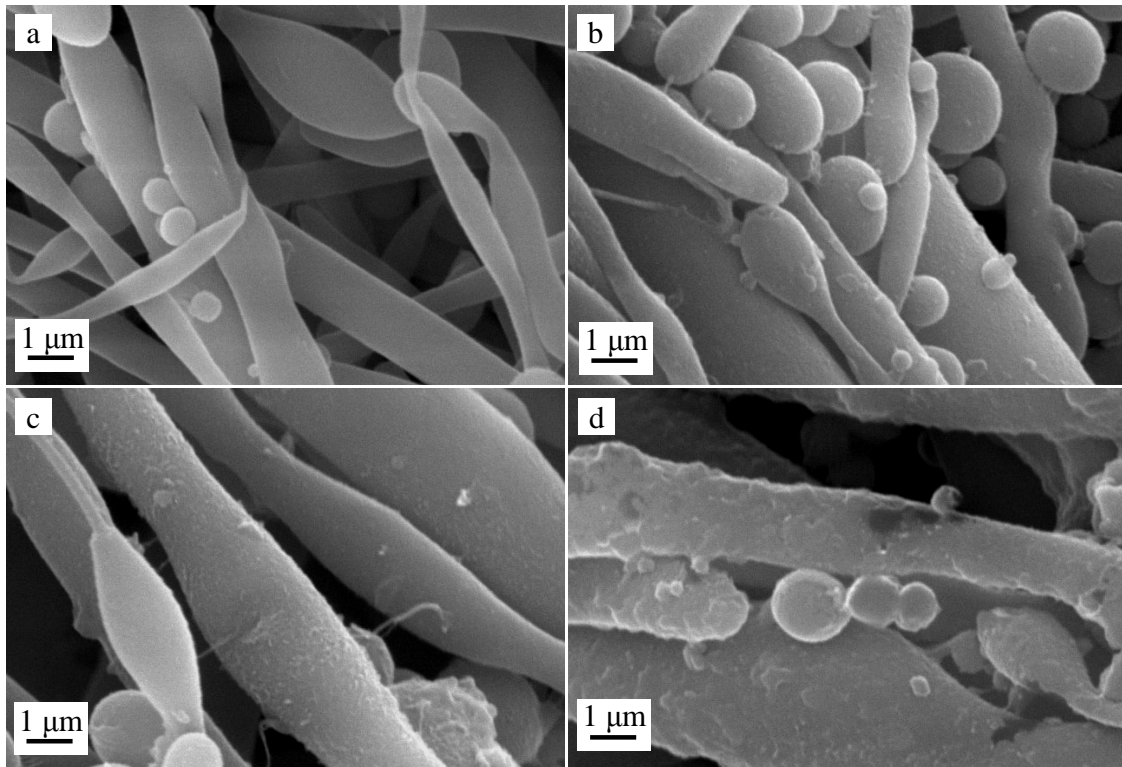
Figure 4.27: Morphology of PET dispersed phase in the PET/PP blends with (a) 0 vol.%, (b) 1 vol.%, (c) 3 vol.% and (d) 6 vol.% of PP-g-MA.

4.3.1.2 Phase morphology of PET/PP/TiO$_2$ composites

As discussed earlier, blending Procedures 1 and 2 are essentially the same, therefore the investigation is focused on the composites prepared with blending Procedures 2 and 3. As shown in Figure 4.28, the PP/PET/T (blending Procedure 2) and (PET/T)/PP (blending Procedure 3) in which the TiO$_2$ particles are preferentially located in the PET, show a similar morphology (Figure 4.28a and c). The PET droplets are large and exhibit broad size distribution ranging from 5 μm to 25 μm. In the PP/PET/MA/T (blending Procedure 2) the size of PET droplets are much smaller and the size distribution is narrower (Figure 4.28b). For the (PET/T)/PP/MA (blending Procedure 3), very fine PET droplets are observed as displayed in Figure 4.28d.

PET/PP(35-65) TiO2(300nm)-2v% 500 ⊢—— 60 µm ——⊣   PET/PP(35-65) TiO2(300nm)-2v% 500 ⊢—— 60 µm ——⊣

PET-PP-com 300-2v 500 ⊢—— 60 µm ——⊣   PET+TiO2-PP-com 300-2v 500 ⊢—— 60 µm ——⊣
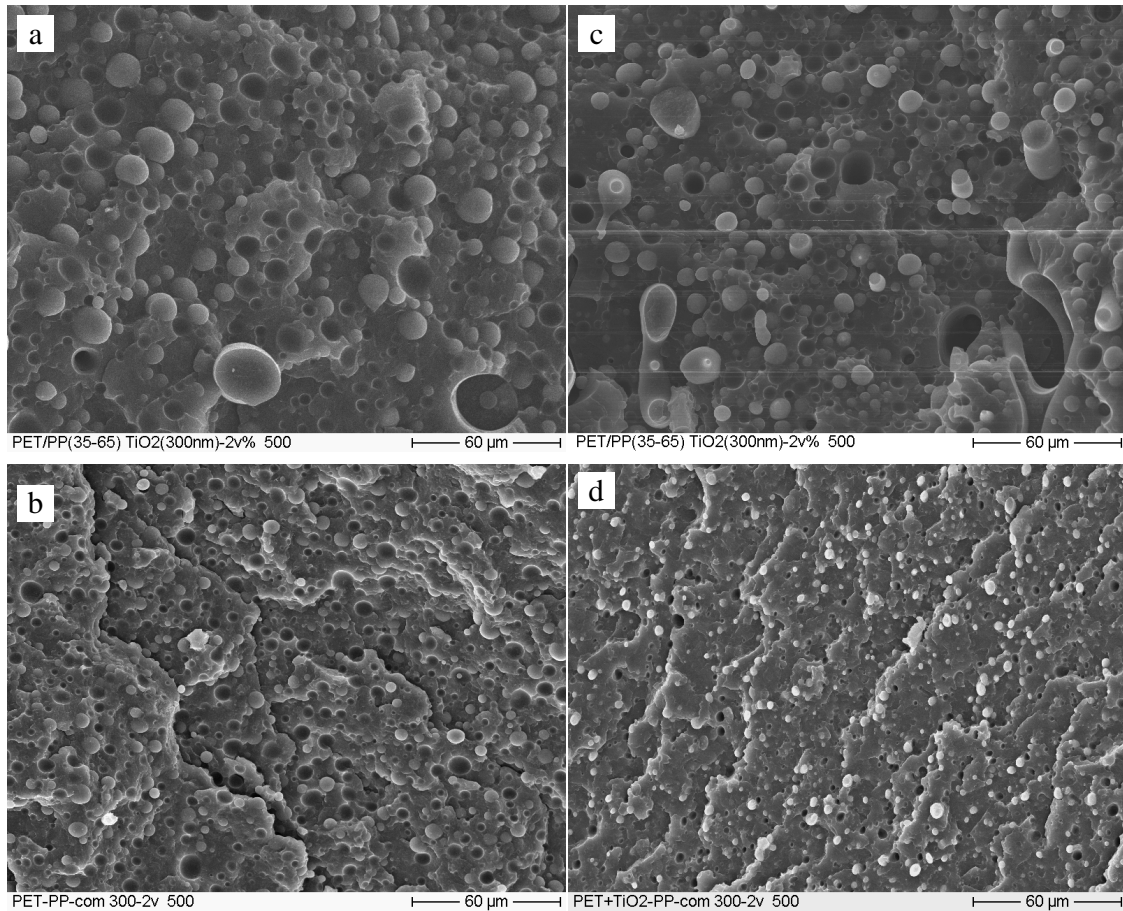
Figure 4.28: Morphology of PET/PP/TiO$_2$ and PET/PP/PP-g-MA/TiO$_2$ composites prepared with blending Procedure 2 and 3. (a) PP/PET/T and (b) PP/PET/MA/T prepared with blending Procedure 2, (c) (PET/T)/PP and (d) (PET/T)/PP/MA prepared with blending Procedure 3.

During melt blending of two immiscible polymers, under a certain shear rate, the viscosity ratio (λ) between the dispersed phase and the matrix is defined as follows:

$$\lambda = \frac{\eta_d}{\eta_m} \tag{4.4}$$

where η_d is the viscosity of the dispersed phase and η_m is the viscosity of the matrix. It is generally accepted that a viscosity ratio of 1 leads to the smallest diameter of the dispersed phase and the finest morphology of the polymer blends. However, other researchers [150, 151] reported that a low viscosity ratio is more

favorable for a finer morphology, because high viscous matrix enhances droplets break up by exerting an efficient shear stress transfer toward the dispersed phase. Note that a low viscosity matrix often acts as a lubricant for the dispersed phase, and thus reduces the droplets break up.

As is already known, in the PET/PP/T extrudate the TiO_2 particles are dispersed exclusively in the PET phase. Therefore, the concentrations of TiO_2 particles in the PET and PP phases are 8 and 0 vol. %, respectively. For the PET/PP/MA/T extrudate, upon addition of the PP-g-MA, the particles are exclusively located in the PP phase. So their concentration is 3 vol. % in the PP matrix and 0 vol. % in the PET dispersed phase. To calculate the viscosity ratio of the PET/PP/T and PET/PP/MA/T systems, two additional composites (PET/TiO_2 (300 nm)-8 vol.% and PP/TiO_2 (300 nm)-3 vol.%) were prepared. The viscosity of these two composites and the neat PET and PP was measured. To subject all the materials to the same thermodynamic history, the neat PET and PP were extruded under the same conditions which were set for preparing the PET/TiO_2 (300 nm)-8 vol.% and PP/TiO_2 (300 nm)-3 vol.% composites.

The viscosity curves for pure PET, PP and PET/TiO_2-8 vol.% and PP/TiO_2-3 vol.% composites are shown in Figure 4.29. It is evident that the viscosities of PET and PP are increased in presence of the TiO_2. During extrusion the shear rate ($\dot{\gamma}$) inside the extruder can be calculated by the following equation:

$$\dot{\gamma} = \frac{n \pi D}{H} \qquad (4.5)$$

Where n is the screw rotation speed, D is the screw diameter and H is the channel depth. Under the screw speed of 40 rpm, which is adopted during the extrusion of PET/PP/T and PET/PP/MA/T blends, the shear rate inside the extruder is estimated to be 13 s^{-1}. At this shear rate, the viscosity ratio of the PET/PP/T system (η_{PET}/η_{PP}) is 0.122, which is two times higher than that of the corresponding value in the PET/PP/MA/T (Table 4.6). As discussed earlier, a lower viscosity ratio between the dispersed phase and matrix will result in a finer

morphology. This is the reason why the PET droplet size in PET/PP/MA/T extrudate is much smaller than that of the PET droplets in the PET/PP/T.
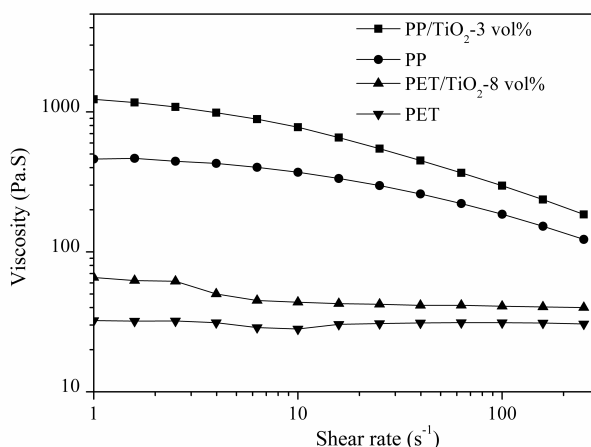
Figure 4.29: Viscosity of pure PP, PET, PP/TiO$_2$ (300 nm)-3 vol.% and PET/TiO$_2$ (300 nm)-8 vol.% composites at 275 °C as a function of the shear rat e.

Table 4.6: Viscosity ratio (η_{PET}/η_{PP}) in the PET/PP/T and PET/PP/MA/T

Material	Viscosity ratio	
PET/PP/T (TiO$_2$ in PET)	0.122	between PET/TiO$_2$ (300 nm)-8 vol.% and PP
PET/PP/MA/T (TiO$_2$ in PP)	0.040	between PET and PP/TiO$_2$ (300 nm)-3 vol.%

As discerned before the PP/PET/MA/T and (PET/T)/PP/MA composites, the PP-g-MA acts as compatibilizer for the PET and PP phases. Although the viscosity of PET is increased by TiO$_2$, PET is still very finely dispersed in these two composites because of the presence of PP-g-MA.

4.3.1.3 DSC analysis of PET/PP/TiO$_2$ composites

The crystallization temperatures (T$_c$) and crystallinities (X$_c$) of PP and PET in the PET/PP blend and the composites are listed in Table 4.7. Compared with pure PP, the T$_c$ of PP in both polymer blend and composites is increased, but the crystallinity of PP is not much influenced. During cooling, the already solidified

PET dispersed phase promotes the heterogeneous nucleation of the molten PP. Note that for (PP/T)/PET/MA, the presence of TiO_2 in the PP matrix does not affect the T_c of PP.

Table 4.7: Crystallization temperatures and crystallinities of PP and PET

Specimen		PP		PET	
		T_c (°C)	X_c (%)	T_c (°C)	X_c (%)
Neat PP		117.2	42.2	-	-
PET/PP		122.6	43.5	195.1	12
(PP/T)/PET	(TiO_2 in PET)	123.4	42.0	199.8	18.3
(PP/T)/PET/MA	(TiO_2 in PP)	122.2	45.0	-	-
(PET/T)/PP	(TiO_2 in PET)	122.7	43.1	204.8	16.7
(PET/T)/PP/MA	(TiO_2 in PET)	121.6	41.4	204.3	15.6
(PET/PP/MA)/T	(TiO_2 on PET)	121.1	44.8	191.2	17.1

For (PP/T)/PET, (PET/T)/PP and (PET/T)/PP/MA, in which the TiO_2 are preferentially located in the PET, the T_c of PET is higher than that of PET in PET/PP. More interestingly, the T_c of PET in (PET/T)/PP and (PET/T)/PP/MA is about 5 °C higher than that of the PET in the (PP/T)/PET. For the latter two composites, the TiO_2 particles were extruded with PET in the first step extrusion, whereby the TiO_2 are well dispersed in PET phase. On the other hand, in (PP/T)/PET the TiO_2 particles migrate from the PP into the PET. This migration can hardly guarantee a good dispersion of the TiO_2 particles in the PET phase. At the same concentration of TiO_2, the well dispersed TiO_2 particles easily incorporate in the surrounding PET chains and lead to an earlier crystallization of the later (i.e. PET). In the (PET/PP/MA)/T, the TiO_2 particles are generally located on the surface of the PET. Therefore the heterogeneous nucleation effect of TiO_2 on the PET crystallization is less effective (Table 4.7).

Generally, the incorporation of nanofillers is reported to elevate the T_c of polymers, however, it does not necessarily help to increase the crystallinity [152-154]. The incorporated nanofillers accelerate the crystallization kinetics which leads to an early crystallization of the polymer, but it can also result in a structure with low crystallinity, as the nanofillers may inhibit the crystallization resulting in

reduced crystallinity [153, 154]. In the present study, the crystallinity of PET phase is not influenced by the incorporation of TiO_2. At the early stage of the crystallization process of PET, the incorporated TiO_2 particles promote the crystallization of PET. However, later they inhibit the crystalline development of PET.

4.3.1.4 Tensile Properties of PET/PP/TiO$_2$ composites

Tensile properties of the PET/PP/TiO$_2$ composites are shown in Figure 4.30. For comparison purpose, the tensile properties of neat PP and PET/PP blend are also indicated. Compared with neat PP, the tensile modulus of PET/PP is improved because of the high modulus of PET. The tensile modulus of the composites is moderately increased compared with the PET/PP blend due to the high stiffness of the TiO_2 particles. The tensile strength of the composites is not much influenced by the incorporation of TiO_2 except for the (PET/T)/PP/MA whose tensile strength reaches as high as 38.5 MPa. Note that for this composite the TiO_2 particles were incorporated into PET at the first step extrusion. As discussed earlier, during the second step extrusion the PP-g-MA reacts with PET, resulting improved interfacial adhesion between PET and PP. Therefore, the tensile strength increases accordingly.
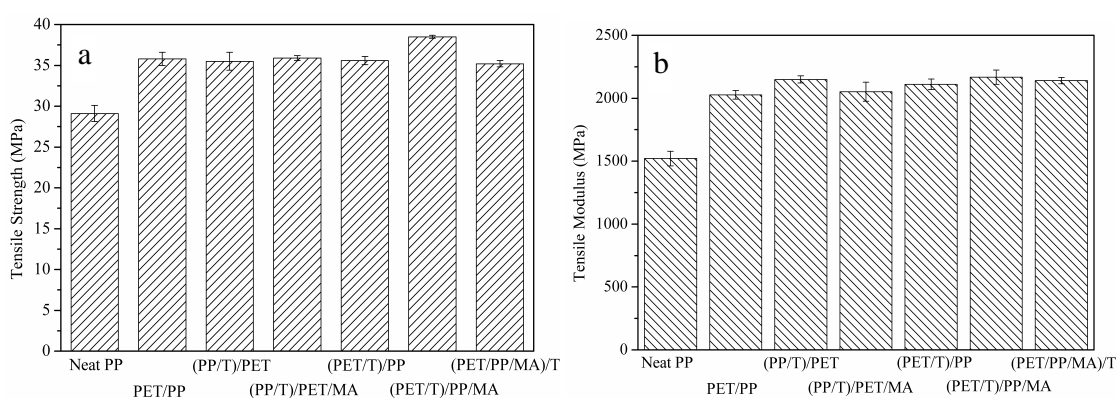

Figure 4.30: Tensile strength (a) and tensile modulus (b) of the blend and composites.

4.3.2 PET/PP/TiO$_2$-15nm nanocomposites

4.3.2.1 Preferential location of TiO$_2$ nanoparticles

SEM images in Figure 4.31 show the dispersion of TiO$_2$ nanoparticles in the PET/PP/2T and PET/PP/4T nanocomposite. The TiO$_2$ nanoparticles are exclusively located in the dispersed PET phase. To confirm further the dispersion of TiO$_2$, TEM image was taken of the PET/PP/2T nanocomposite (Figure 4.32). The dark continuous and bright dispersed phases correspond to the PP and PET, respectively. Figure 4.32 reveals that the TiO$_2$ nanoparticles are mainly dispersed at the PET/PP interface, and to a lesser extent in the PET droplets. Note that the PET/PP/2T nanocomposite was prepared by melt blending of the precompounded PP/TiO$_2$ nanocomposite with PET. Therefore the preferential locations of TiO$_2$ at the interface and in PET indicate that during extrusion of PET/PP/2T the TiO$_2$ nanoparticles migrate from the PP to the PET.
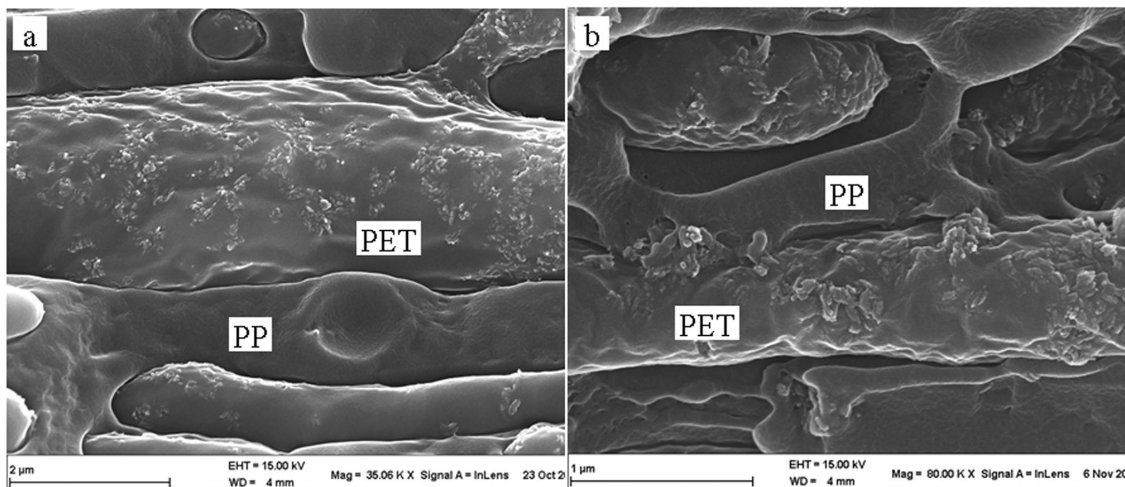
Figure 4.31: SEM images of (a) PET/PP/2T and (b) PET/PP/4T nanocomposites.
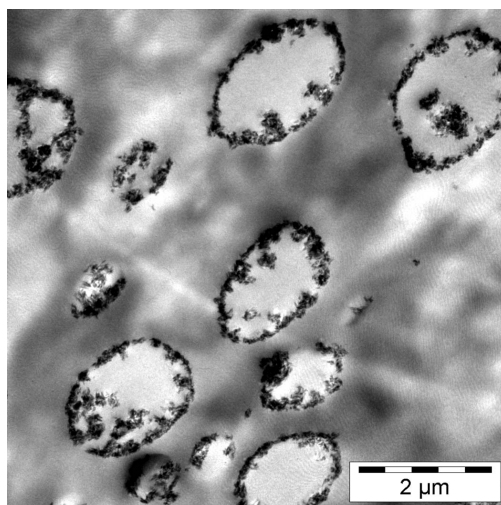
Figure 4.32: TEM image of PET/PP/2T nanocomposite.

Figure 4.33a is a TEM image of the PET/PP/3MA/2T nanocomposite which gives a general view of the dispersion of TiO_2 nanoparticles. Some PET droplets are covered with TiO_2 nanoparticles (although not completely covered, Figure 4.33b). However, most of the TiO_2 nanoparticles are dispersed in the PP phase (Figure 4.33c). This result suggests that upon addition of 3 vol.% of PP-g-MA, only a part of TiO_2 nanoparticles migrate to the PET phase. When the concentration of the PP-g-MA compatibilizer is increased to 6 vol.%, the PET phase is not affected, small agglomerates of TiO_2 are found only in the PP matrix (Figure 4.33d).
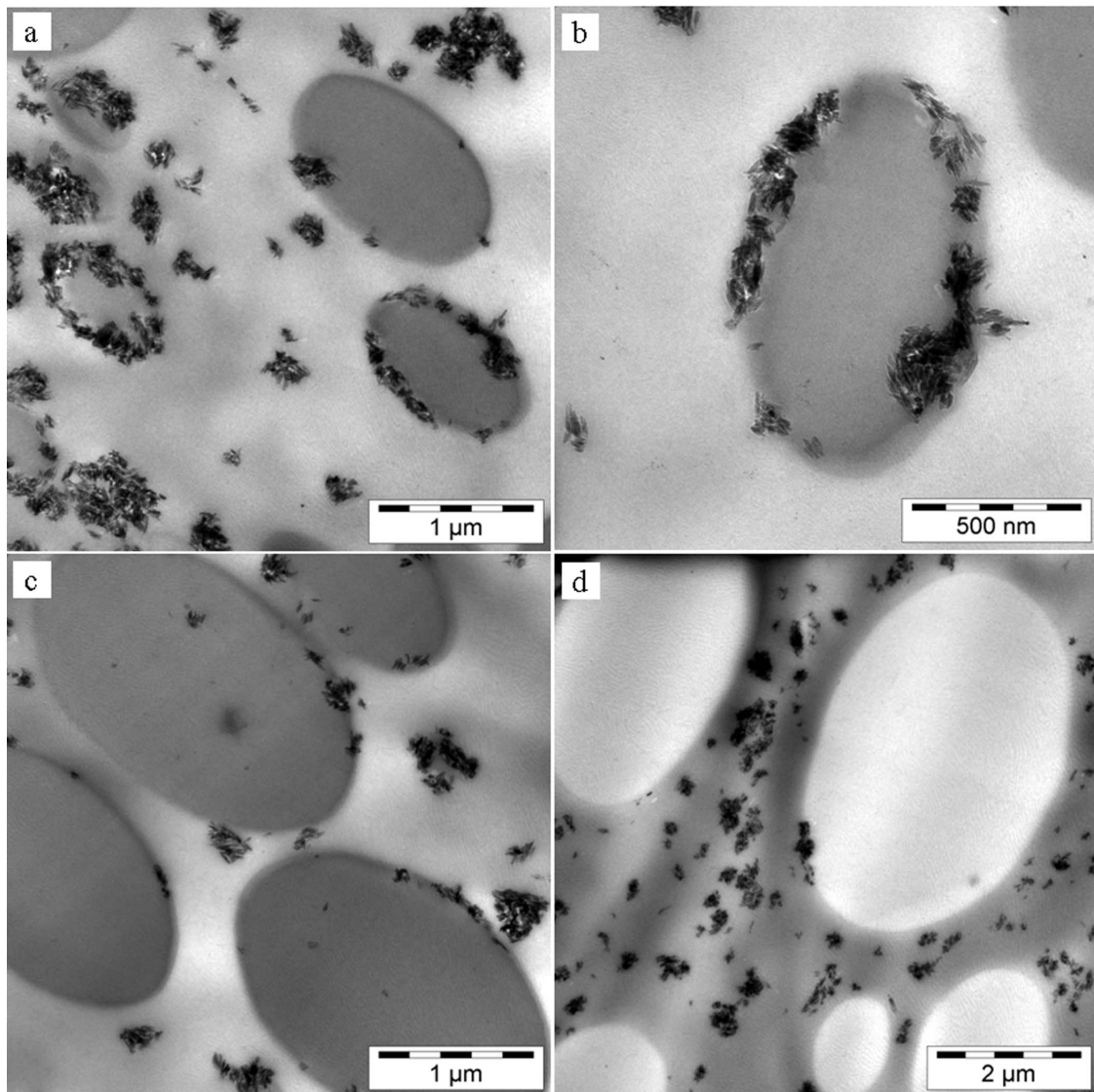
Figure 4.33: TEM images of PET/PP/3MA/2T and PET/PP/6MA/2T nanocomposites: (a)-(c) PET/PP/3MA/2T, (d) PET/PP6MA/2T.

Treated with polyalcohol, the TiO_2 nanoparticles favorably interact with PET via the reaction between the hydroxyl and carboxyl groups (Figure 4.34a). Therefore during extrusion of the PET/PP/2T and PET/PP/4T nanocomposites, the TiO_2 nanoparticles are driven into the preferred PET phase. The final location of TiO_2 nanoparticles is generally considered to represent the thermodynamic equilibrium state. However, during melt blending the equilibrium may never be reached because of the short mixing time and the very low diffusion coefficient of the

nanoparticles in viscous media [155]. It is therefore also possible that the location of the TiO_2 nanoparticles at the PET/PP interface represents an intermediate state in the morphology development.
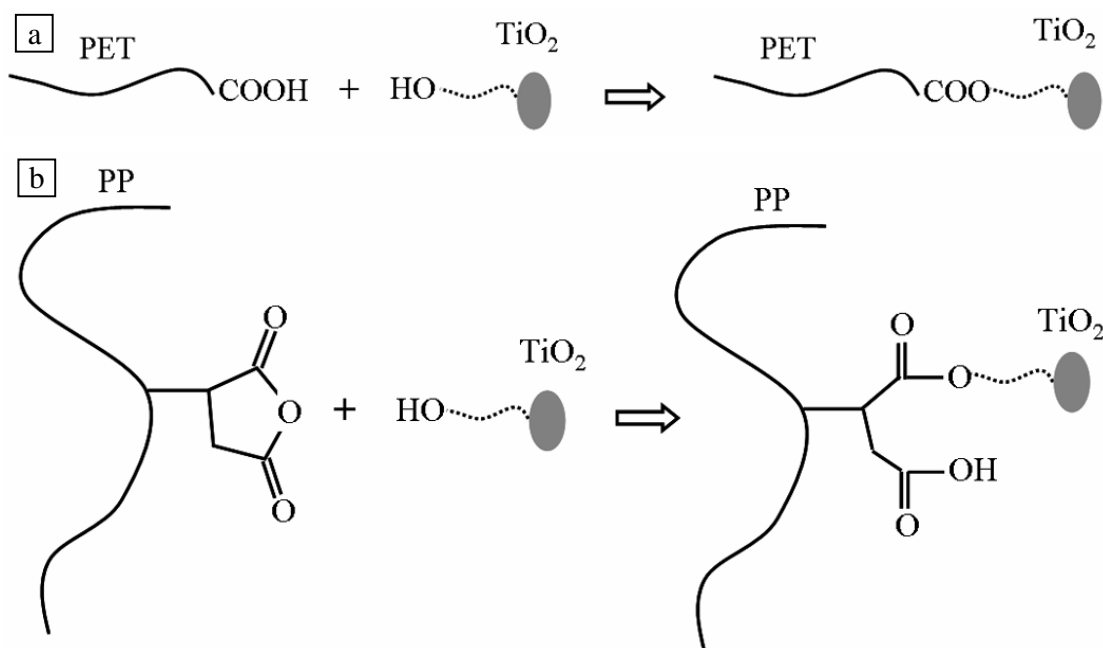
Figure 4.34: Possible chemical reactions between (a) PET and coated TiO_2 nanoparticles, (b) PP-g-MA and coated TiO_2 nanoparticles.

The PP-g-MA can also react with the treated TiO_2 nanoparticles through the reaction between the anhydride and hydroxyl groups (Figure 4.34b). The surface of TiO_2 is thereby covered with PP chains, which makes the TiO_2 nanoparticles compatible with PP and this forces them to stay in the PP phase. However, the location of TiO_2 in the PP phase does not necessarily mean that the TiO_2 nanoparticles are more prone to interact with the PP-g-MA than with the PET. In fact, the location of TiO_2 is determined by the blending procedure. Recall that during extrusion of the PET/PP/3MA/2T and PET/PP/6MA/2T nanocomposites, the PP/TiO_2, PET and PP-g-MA were simultaneously fed into the extruder. Having a lower melting temperature than the PET, the PP and PP-g-MA melt first, therefore the TiO_2 nanoparticles may be "coated" by PP-g-MA before the PET

itself melts. The grafted PP chains on the surface of the TiO_2 nanoparticles favor the stay of the TiO_2 in the PP phase.

The influence of the amount of PP-g-MA on the location of TiO_2 nanoparticles is schematically shown in Figure 4.35. It is already known that the concentration of trimethylolpropane in the TiO_2 nanoparticles is 1.0 wt. % and the concentration of MA in the PP-g-MA is 1.0 wt.%. For the nanocomposite with 2 vol.% of TiO_2 and 3 vol.% of PP-g-MA, the ratio between the hydroxyl groups (from the TiO_2) and the maleic anhydride groups (OH/MA) is calculated to be 6.0/2.4. Considering the agglomeration of the TiO_2 nanoparticles, there will be less OH groups available to react with the anhydride of MA. Therefore at low concentration of PP-g-MA (3 vol.%), some hydroxyl groups of the coating do not react with PP-g-MA, as the PP-g-MA concentration is not high enough to "coat" all the TiO_2 nanoparticles. The "uncoated" TiO_2 nanoparticles, more exactly the free hydroxyl groups of their coating can react with PET. Therefore a small amount of TiO_2 nanoparticles migrate to the PET, and locate at the inner surface of PET droplets (Figure 4.33a). When the concentration of PP-g-MA increases to 6 vol.%, all the TiO_2 nanoparticles are likely covered by PP chains, yielding that all the TiO_2 nanoparticles remain in the PP phase (Figure 4.35b).
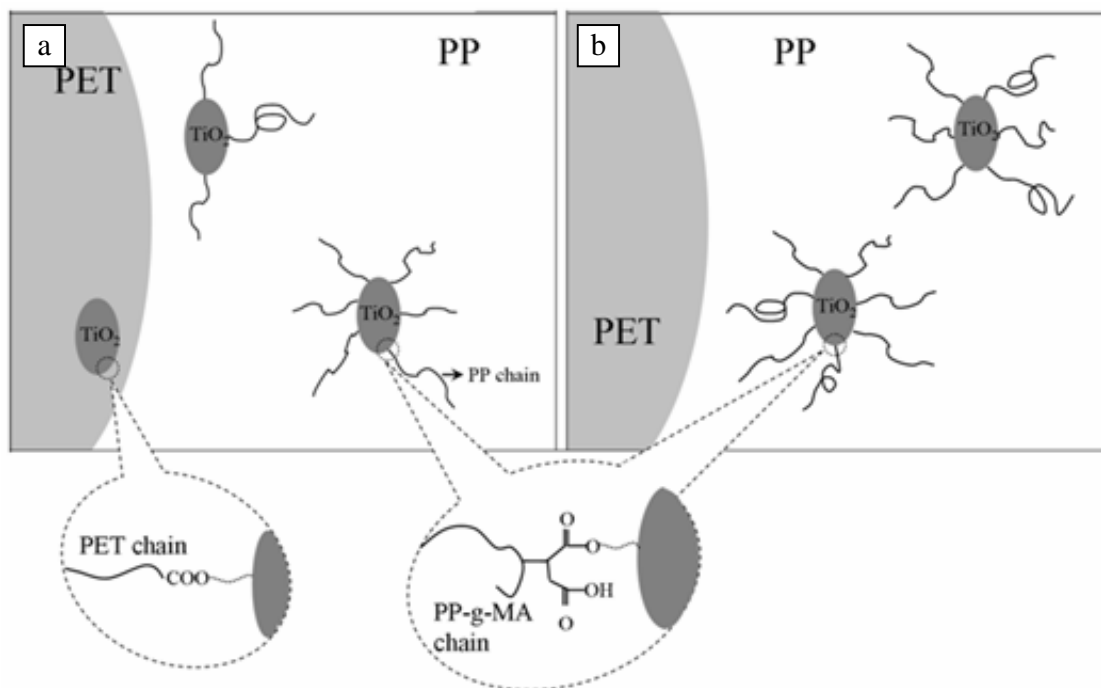
Figure 4.35: Scheme of the morphology development in (a) PET/PP/3MA/2T and (b) PET/PP/6MA/2T nanocomposites.

4.3.2.2 Compatibilization effect of the TiO$_2$ nanoparticles

SEM pictures in the morphology of PET/PP blends and PET/PP/TiO$_2$ nanocomposites are shown in Figure 4.36. The fracture surfaces of PET/PP and PET/PP/MA blends clearly demonstrate a two-phase morphology (PET droplets in the PP matrix). This reflects the expected immiscibility between the two components (Figure 4.36a and b). The number average diameter and diameter range of PET droplets in the PET/PP blends and PET/PP/TiO$_2$ nanocomposites are listed in Table 4.8. The droplet size of PET in the PET/PP/MA is smaller than that in the PET/PP, which is attributed to the compatibilization effect of the PP-g-MA.
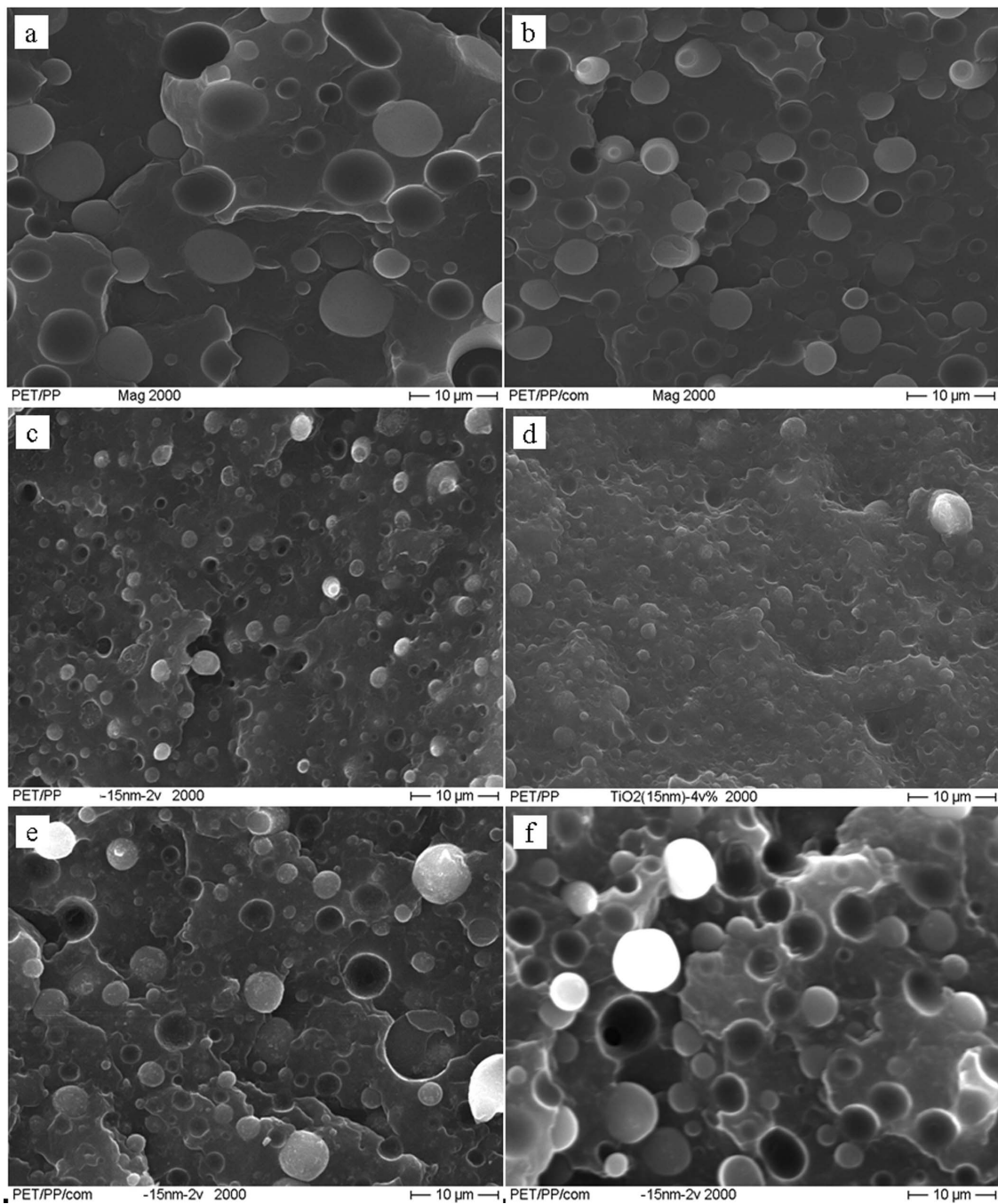
Figure 4.36: SEM images of the fracture surface of PET/PP blends and PET/PP/TiO$_2$ nanocomposites: (a) PET/PP, (b) PET/PP/MA, (c) PET/PP/2T, (d) PET/PP/4T, (e) PET/PP/3MA/2T, (f) PET/PP/6MA/2T.

Upon addition of 2 vol.% of TiO$_2$ nanoparticles into the PET/PP blend, the size of PET droplets is greatly decreased (Figure 4.57c). The number average diameter

is 1.4 µm. Addition of 4 vol.% of TiO_2 nanoparticles causes a further decrease in the PET droplet size (Figure 4.57d), especially for PET/PP/4T whose interface can not be easily distinguished. For the PET/PP/3MA/2T and PET/PP/6MA/2T nanocomposites, as shown in Figure 4.57e and f, the number average diameters of PET droplets are 2.0 and 3.8 µm, respectively. These values are higher than that of the PET droplets in the PET/PP/2T and PET/PP/4T nanocomposites, but still much lower compared to the PET droplets in the PET/PP blend. Furthermore, a narrowing in the size distribution of PET droplets can be observed in PET/PP/TiO_2 nanocomposites, especially in the PET/PP/2T and PET/PP/4T nanocomposites.

Table 4.8: Number average diameter and diameter range of PET droplets in PET/PP and PET/PP/TiO_2 nanocomposites

Materials	PET droplets	
	Number average diameter (µm)	Diameter range (µm)
PET/PP	5.4	2.0 ~ 9.2
PET/PP/MA	3.4	1.6 ~ 5.6
PET/PP/2T	1.4	0.5 ~ 5.4
PET/PP/4T	1.1	0.6 ~ 4.5
PET/PP/3MA/2T	2.0	0.7 ~ 8.7
PET/PP/6MA/2T	3.8	1.5 ~ 7.8

By comparing the phase morphologies of PET/PP/TiO_2 nanocomposites and PET/PP blend, it can be concluded that that the PET/PP/2T and PET/PP/4T nanocomposites display the best compatibilization characteristics, i.e. the finest dispersion of the PET droplets. In these two nanocomposites, the incorporated TiO_2 nanoparticles reduce the dispersed domain size (cf. Table 4.8) and stabilize the phase morphology. To some degree, the compatibilization effect of TiO_2 nanoparticles is also observed in the PET/PP/3MA/2T nanocomposite, and to a lesser extent in the PET/PP/6MA/2T nanocomposite (cf. Figure 4.36 and Table 4.8). These differences in the compatibilization effect of TiO_2 nanoparticles offer insight into the overall compatibilization mechanisms depending on the location of TiO_2 nanoparticles.

According to equation 4.4, the affinity of the two polymers and nanofillers determines the compatibilization effect of nanofillers. In the PET/PP/2T and PET/PP/4T nanocomposites, the TiO_2 nanoparticles are mostly located at the PET/PP interface. PET is already known to be strongly absorbed onto the TiO_2 nanoparticles, which means a negative value for the term of $\Delta G_{PET-TiO2}$. The non-polar PP has no affinity to the TiO_2 nanoparticles or to their coating polyalcohol, indicating a positive value of $\Delta G_{PP-TiO2}$. It is presumed that the $|\Delta G_{PET-TiO2}|$ > $|\Delta G_{PP-TiO2}|$. Therefore the ΔG_m is decreased upon the addition of TiO_2 nanoparticles, the compatibility of the system is thereby improved [99, 100]. In the filled polymer blends, the nanofillers at the interface are usually considered as physical barriers that inhibit or prevent drop coalescence [88, 156]. In the present study, for the PET/PP/2T and PET/PP/4T nanocomposites, the TiO_2 nanoparticles at the PET/PP interface prevent the coalescence of the dispersed PET droplets. This results in a small PET droplet size.

For the PET/PP/6MA/2T nanocomposite, the TiO_2 nanoparticles are "coated" with the PP chains because of the reaction between PP-g-MA and TiO_2. These "coated" TiO_2 nanoparticles become a part of the PP matrix, and thus do not interact with the PET. In this nanocomposite, the PET droplets size is still noticeable smaller than that of the PET droplets in the binary PET/PP blend (cf. Figure 4.36 and Table 4.8). However, the compatibilization mechanism of the TiO_2 nanoparticles is different from that of the PET/PP/2T nanocomposite. In the PET/PP/6MA/2T nanocomposite, the TiO_2 nanoparticles are exclusively located in the PP matrix, the TiO_2 content in this phase is calculated to be 3 vol.%. The viscosity curves for the pure PET, PP and PP/TiO_2 (15 nm)-3 vol.% nanocomposite are shown in Figure 7. Recall that the pure PP was subjected to the same thermodynamic history as that of PP/TiO_2 nanocomposite (i.e. the pure PP was also extruded with the Berstorff extruder before measuring the viscosity). The viscosity of PET is much lower compared with the pure PP and the PP/TiO_2 (15 nm)-3 vol.% nanocomposite. The incorporation of nanofillers is known to influence the rheological behavior of the polymers. A solid like behavior of the

nanocomposites is usually observed due to the polymer-particles and/or particle - particle interactions. In the present experiment, the viscosity of the PP/TiO$_2$ (15 nm)-3 vol.% nanocomposite is significantly higher than the pure PP, especially at low shear rate range.
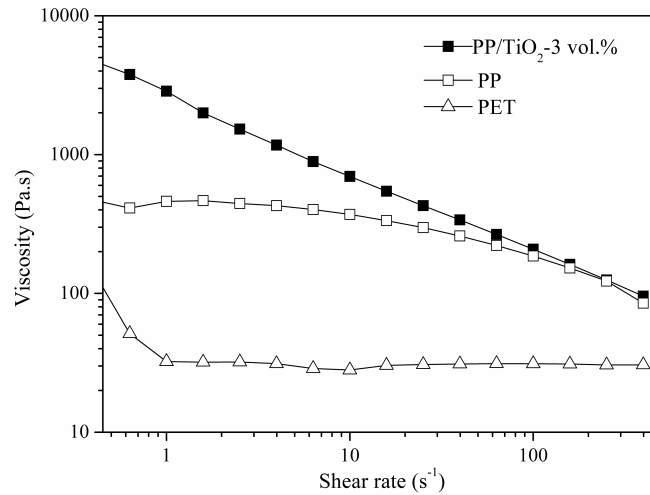
Figure 4.37: Viscosities of pure PP, PET and PP/TiO$_2$ (15 nm)-3 vol.% nanocomposite.

For the PET/PP blend, the viscosity ratio λ between the dispersed PET and PP matrix is given as follows:

$$\lambda_{PET/PP} = \frac{\eta_{PET}}{\eta_{PP}} \tag{4.6}$$

While for the PET/PP/6MA/2T nanocomposite in which the TiO$_2$ nanoparticles are preferentially located in the PP, the viscosity ratio between the dispersed PET phase and PP/TiO$_2$ matrix is

$$\lambda_{PET/PP/6MA/2T} = \frac{\eta_{PET}}{\eta_{PP/TiO2}} \tag{4.7}$$

During extrusion of the PET/PP blend and PET/PP/TiO$_2$ nanocomposite, at the shear rate of 13 s^{-1} (the estimated shear rate at the screw speed of 40 rpm), the viscosity of PP/TiO$_2$ is higher than that of the pure PP, but the viscosity of the PET in PET/PP blend and PET/PP/TiO$_2$ nanocomposite is the same. Therefore the $\lambda_{PET/PP}$ is higher than $\lambda_{PET/PP/6MA/2T}$. With decreasing viscosity ratio, the

deformability of dispersed droplets increases, resulting in a finer dispersion of the minor phase, PET. Equation 4.7 suggests that the PP-g-MA compatibilizer does not influence the morphology of either PP or PET. This assumption is acceptable in PP/PET/6MA/2T nanocomposites, since PP-g-MA does not act as compatibilizer for PET and PP, instead it interacts with TiO_2 (Figure 4.35b).

Fenouillot [100] summarized the compatibilization mechanisms of the nanofillers for the nanocomposites: 1) reduction of the interfacial energy, 2) inhibition of coalescence by the presence of a solid barrier around the minor polymer drops, 3) changes in the viscosities of the phases due to the uneven distribution of the filler, 4) immobilization of the dispersed drops (or of the matrix) by the creation of a physical network of particles when the concentration of solid is above the percolation threshold, and 5) strong interaction of polymer chains with the solid particles inducing steric hindrance. In the present study, depending on the location of the TiO_2 nanoparticles, two compatibilization mechanisms are proposed for the for the PET/PP/2T nanocomposites: (1) increase in the thermodynamic stability (i.e. the decrease in free energy of mixing) by the TiO_2 nanoparticles at the interface; (2) the physical barrier effect the TiO_2 at the interface preventing the coalescence of the PET droplets. For the PET/PP/6MA/2T nanocomposite a further compatibilization mechanism may be at work: decreasing viscosity ratio due the TiO_2 dispersed in the PP matrix which enhances the droplet breakup of PET.

In the PET/PP/3MA/2T nanocomposite, the TiO_2 nanoparticles were dispersed in the PP matrix, as well as at the interface. All the above mentioned three compatibilization mechanisms are applicable to this nanocomposite. However, for this nanocomposite the effects of the former two mechanisms (thermodynamic stability, physical barrier) are not as significant as for the PET/PP/2T nanocomposite. On the other hand, the effect of the third compatibilization mechanism (viscosity ratio) is less remarkable for PET/PP/3MA/2T than for the PET/PP/6MA/2T system.

4.4 Application of MFC

The applicability of the MFC approach to polyolefin, as well as other polymer blends fall into the following three categories.

Recycling friendly use

The environmental pollution caused by plastic materials due to the huge volume of litter makes recycling a very important issue for manufacturers and processors worldwide. A normally adopted approach for polymer recycling is called thermomechanical recycling [157]. This technique first involves mechanical recycling where the thermoplastics are granulated followed later by techniques as extrusion or thermoforming. In this case, blending and alloying of structurally different polymers offer an opportunity to convert the waste plastics into high performance polymer materials with specific applications. However, the majority of polymer blends are immiscible and results in poor mechanical properties compared with the raw materials. The manufacturing of in-situ microfibrillar blends is a promising method to enhance the properties of general purpose polymers to meet engineering specifications. Waste polymers, such as recycled polyolefin based commodities, polyester beverage containers, edible oil bottles and film can be used for the preparation of MFC, which brings a great reduction in the cost of materials. The MFC made from waste polymers can be re-processed and completely recycled.

Food packaging

Prevention and control of the permeation of gases and liquids through plastic film and membranes are required in food packaging and industrial application. The general approach in formulating high performance barriers is to use materials having low diffusivity and low solubility of the permeant. Most of polymers have varying levels of effectiveness in barrier properties, but polymer-polymer blending offers a simple and economical approach for permeability control. For a blend, the barrier properties will be strongly influenced by the morphology. The

structures that can be obtained range from fully laminar systems, where the dispersed polymer phase is present as a continuous layer, over interleaved sheets and lamellar or fibrillar morphologies to particulate systems. In Figure 4.38 the barrier properties of a blend as a function of the morphology is schematically illustrated.
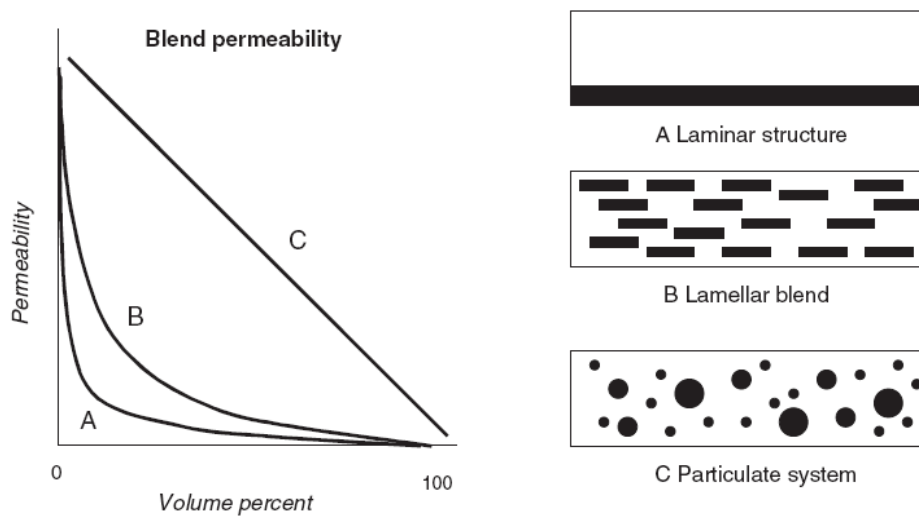
Figure 4.38: Schematic illustration of the permeability of a blend of a high-barrier material in a low-barrier matrix as a function of the morphology [158].

Compared with PP and PE, PET is of low oxygen permeability. The oxygen barrier property of polyolefin materials might be improved by incorporating PET and developing a lamellar blend as shown in Figure 5.1. Bhattacharyya et al. prepared a range of MFC films from PET/PE (30/70 by weight) blends. All the MFC films have been shown to possess superior oxygen barrier properties compared to the neat PE films. Furthermore, the film that contains microfibrils combined with plates of PET has even lower permeability than microfibril-only films because of its higher effective gas blocking area [159].

Tissue scaffolding application

The MFC concept can be applied in the in the area of tissue engineering. The purpose of scaffolding is usually to (1) support differentiated cell function and

growth; (2) transport cells, cell nutrients and biochemical factors, and (3) provide mechanical support to maintain a space for tissue to form [52]. In the MFC for tissue scaffolding application, the microfibrils are usually biodegradable polymers such as poly(lactic acid) (PLA) and poly(glycolic acid) (PGA). After extraction of the matrix polymer, the remaining biodegradable polymers are expected to sustain the growth of living cells. The use of toxic organic solvents to dissolve the matrix materials may have a negative influence on the seeded living cells, therefore the matrix materials are required to be water soluble or soluble in non-toxic solvent.

Most recently, the PLA/PVA MFC was developed. It was found that after extraction of the PVA matrix, the PLA micro- and/or nanofibrils were interconnected, forming a three-dimensional network. Figure 4.39 shows the morphology of the PLA fibrils prepared by stretching the PLA/ ethylene vinyl alcohol (EVOH) (40/60) blend. The diameter of these fibrils is in range of 400nm to 1 μm. Such a spatial arrangement of microfibrils resulted in the formation of extremely porous material where the pores had sizes in the nano range. The living cells attached rather well to the microfibrils, proliferated and grew further forming continuous tissue [52].
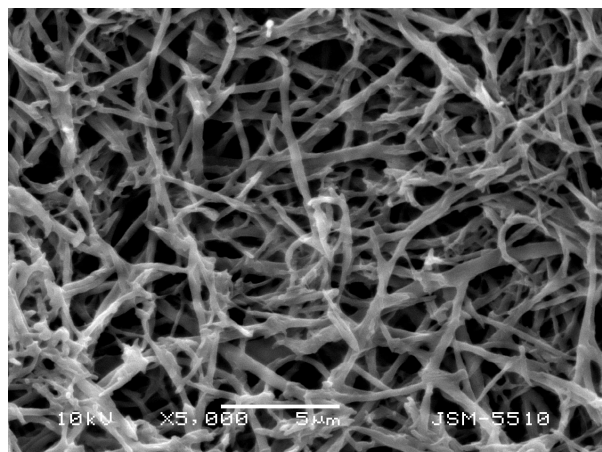

Figure 4.39: PLA fibrils prepared by stretching the PLA/EVOH (40/60) blend, EVOH fraction was removed.

5 Conclusions

The current work was devoted to the preparation, characterization of PET/PP, PET/PP/TiO$_2$ microfibrillar composites and PET/PP/TiO$_2$ ternary nanocomposites. PET/PP and PET/PP/TiO$_2$ MFC were prepared by melt blending of the polymer blends, stretching of the extrudates and compression molding or injection molding of the drawn strands and their granules. PET/PP/TiO$_2$ ternary nanocomposites were prepared by using different blending procedures. The morphology, crystallization behavior, thermodynamic mechanical property and mechanical properties of the MFC and ternary nanocomposites were investigated. The results and conclusions obtained in this work are summarized as follows:

PET/PP MFC

PET/PP blends with different concentrations of PET and PP-g-MA (serving as compatibilizer) were extruded under different screw speeds. The effects of blend composition, compatibilizer and processing parameters on the blend morphology were studied. The main results deduced can be summarized as follows:

- Melt blending of PET and PP with different compositions at a constant screw speed of 40 rpm, resulted in phase inversion (from the PP matrix to PET matrix) when the concentration of PET reaches 40 wt.%. Maintaining the same PET concentration, a gradual increase of screw speed from 20 rpm to 80 rpm also leads to a change in the matrix is overtaking this role from PP. This is attributed to the accelerated coalescence of PET droplets as a result of the extensive shear. However, keeping the screw speed at 80 rpm, the coalescence of the PET droplets in the PET/PP (40/60) blend can be completely suppressed by incorporating 6 wt.% of PP-g-MA as compatibilizer.

- The phase structure of "the PET droplets in PP matrix" is the desired structure for preparing PET/PP MFC. Therefore the PET/PP (30/70), PET/PP (40/60) (extruded at 20 rpm) and PET/PP/PP-g-MA (40/54/6)

(extruded at 80 rpm) combinations which possess this kind of structure were stretched into strands and MFC were prepared from them accordingly.

- The tensile properties of the compression molded PET/PP MFC show a great improvement compared with the neat polymers because of the reinforcing effect of the PET fibrils. The tensile properties are improved with increasing content of the PET fibrils.

PET/PP/TiO$_2$ MFC

TiO$_2$ particles with different sizes (300 nm and 15 nm) were incorporated into PET/PP blend. Uncompatibilized and compatibilized (PP-g-MA as compatibilizer) PET/PP/TiO$_2$ MFC were prepared by injection molding of the pelletized PET/PP/TiO$_2$ drawn strands. Major conclusions of this part of the study can be drawn as follows:

- In the uncompatibilized PET/PP/TiO$_2$ extrudates, the TiO$_2$ particles migrate from the PP matrix to the PET dispersed phase during melt blending of PP/TiO$_2$ and PET; while in the compatibilized extrudates, the TiO$_2$ particles stay in the PP matrix.

- The T_c of the PP in drawn strands is dramatically increased because of heterogeneous nucleation of the PET fibrils. The T_c of the PET in the uncompatibilized PET/PP strands is also elevated because the TiO$_2$ particles act as nucleation agent for PET.

- Incorporation of the TiO$_2$ particles into the drawn strands results in a decrease of the storage modulus compared with the PET/PP drawn strand. In presence of the TiO$_2$ particles, defects appear at the interface between the PET fibrils and the PP matrix, which leads to poor stress transfer and thereby a drop of E′.

- In the injection molded PET/PP/TiO$_2$ microfibrillar composites, the PET fibrils become shorter and thicker compared with those fibrils in the drawn strands. However, the preferential location of TiO$_2$ particles is preserved.

- The glass transition temperatures of the PP in the PET/PP/TiO$_2$ MFC are greatly influenced by the preferential location of TiO$_2$ particles: exclusively located in the PP matrix, the T$_g$ of PP in the compatibilized PET/PP/TiO$_2$ MFC is 3 °C higher than that of PP in the uncompatibilized PET/PP/TiO$_2$ MFC and the PET/PP MFC.

- The tensile strength and impact strength of the PET/PP/TiO$_2$ MFC are lower compared with the PET/PP MFC, since the incorporated TiO$_2$ particles either damage the PET fibrils or result in defects at the interface. However, an increase in tensile modulus for the PET/PP/TiO$_2$ MFC is observed compared to the PET/PP MFC.

PET/PP/TiO$_2$ ternary nanocomposites

PET/PP/TiO$_2$-300nm composites

TiO$_2$ particles (300 nm in diameter) were incorporated in 2 vol.% into PET/PP blend in presence and absence of PP-g-MA with four different blending procedures. The effects of PP-g-MA and blending sequence on the location of TiO$_2$ particles in the PP-based (ca. 70 vol.%) composites were studied. The conclusions were deduced as follows:

- In the PET/PP/TiO$_2$ composites, the TiO$_2$ particles are always located in the PET phase irrespective of blending procedures. However, in PET/PP/PP-g-MA/TiO$_2$ composites the location of TiO$_2$ depends on the blending sequence: firstly blended with PP or with PET and PP simultaneously (Blending Procedure 1 and 2), the TiO$_2$ particles are dispersed in the PP phase. Firstly blended with PET (Blending Procedure 3), the TiO$_2$ particles stay in the PET. When blended with the

precompounded PET/PP/PP-g-MA (Blending Procedure 4), the TiO_2 particles are located on the surface of the dispersed PET.

- In absence of PP-g-MA, the TiO_2 particles are driven into the thermodynamically preferred PET because of the interfacial tension difference ($\gamma_{TiO2\text{-}PET}$ is lower than $\gamma_{TiO2\text{-}PP}$). However, the MA of PP-g-MA is easily absorbed onto the surface of TiO_2. In case of the blends with PP-g-MA, whether the interaction between TiO_2 and PP-g-MA can take place is governed the blending sequence. If the PP-g-MA/TiO_2 interaction is at work then the TiO_2 particles are covered by PP chains of PP-g-MA, which favors the stay of TiO_2 in the PP phase.

- For the PET/PP/TiO_2 composites in which the TiO_2 particles are located in the PET, the T_c of PET is elevated due to the heterogeneous nucleation effect of the TiO_2. Better dispersion of the TiO_2 leads to further increase in the T_c of PET.

- The tensile modulus of the composites is moderately increased compared with the PET/PP blend due to the high stiffness of the TiO_2 particles. The tensile strength of the composites is not much influenced by the incorporation of TiO_2 except for the (PET/T)/PP/MA whose tensile strength reaches 38.5 MPa.

PET/PP/TiO_2-15nm nanocomposites

PET/PP/TiO_2 nanocomposites were prepared by compounding a PP/TiO_2 nanocomposite premix with PET in absence and presence (up to 6 vol.%) of (PP-g-MA. The influence of PP-g-MA concentration on the location of TiO_2 nanoparticles and the compatibilization effect of TiO_2 nanoparticles on the phase morphology were investigated. The main results concluded are as follows:

- In the PET/PP/TiO_2 nanocomposites, the TiO_2 nanoparticles are generally located at the PET/PP interface and in the dispersed PET droplets. Upon addition of 3 vol.% of PP-g-MA, the TiO_2 nanoparticles are found to be

dispersed in the PP matrix as well as at the interface. With 6 vol.% of PP-g-MA, the TiO_2 nanoparticles are exclusively located in the PP.

- The incorporated TiO_2 nanoparticles exert a compatibilization effect on the PET/PP blend irrespective of their locations. However, locating at the interface, the TiO_2 nanoparticles exhibit a more remarkable compatibilization effect than those dispersed in the PP matrix. One the one hand, the TiO_2 nanoparticles at the interface stabilize the morphology by decreasing the free energy of mixing; on the other hand, these nanoparticles also act as physical barriers preventing the coalescence of the PET droplets. Both of the compatibilization mechanisms contribute to a finer blend morphology of the PET/PP/2T nanocomposite in which the TiO_2 nanoparticles are located at the interface.

6 Summary and Outlook

In the present work, PET/PP, PET/PP/TiO$_2$ microfibrillar composites and PET/PP/TiO$_2$ ternary composites were prepared. In the PET/PP, PET/PP/TiO$_2$ microfibrillar composites, the micro-sized PET fibrils demonstrate large aspect ratio and exist in the PP matrix as the reinforcement, which enhances the tensile properties of the compression molded composites. Phase structure of the extrudate determines the structure of the drawn strands and further influences the mechanical properties of the composites. Therefore, special attention was paid to investigate the influence of material composition, the amount of incorporated PP-g-MA and the processing parameters on the morphology of the extrudates.

In the PET/PP/TiO$_2$ nanocomposites, the incorporated TiO$_2$ particles are preferentially located in the PET phase. However, in PET/PP/PP-g-MA/TiO$_2$ composites the location of TiO$_2$ depends on the blending sequence because of the interaction between the OH from the TiO$_2$ and MA groups from the PP-g-MA. The incorporated TiO$_2$ particles do not help to enhance the tensile properties of the composites, however, they greatly reduce the droplet size of the PET dispersed phase and exert a compatibilization effect on the phase morphology. This interest finding offers an insight to develop new composites which are compatibilized by nanoparticles with enhanced mechanical properties.

As continuation of the present work, the following aspects should be considered:

- For the purpose of mass production of microfibrillar composites, the processing parameters should be optimized to solve the cutting problem of the drawn strands and the feeding problem during injection molding.

- During injection molding (or compression molding), the processing temperature was set between the melting temperature of PET and PP. At

this temperature, PP melts but PET stays in solid state. This low processing temperature results in poor interfacial adhesion between the fibrils and matrix. In addition, the difference in the thermal expansion coefficient and Poisson number between PET and PP may also lead to poor interfacial adhesion. Therefore it is necessary to develop a method for improving the interfacial adhesion which will lead to improvement in mechanical properties of the MFC.

- It is possible and interesting to obtain nanofibrils by adjusting the extrusion and stretching parameters. The development of nanofibrils reinforced composites may open a new perspective for enhancing the material properties.

- It is necessary to explore other polymer blends and compatibilizer for developing new types of MFC. Far more important is to use such nanofillers as carbon nanotubes and carbon nanofibers which align themselves during stretching.

7 References

[1] Robeson L. M.: Polymer blends-a comprehensive review, Hanser, Munich, 2007, Chapter 4.

[2] Evstatiev, M., Fakirov, S.: Microfibrillar reinforcement of polymer blends. Polymer 33 (1992), pp. 877-880.

[3] Si, M., Araki, T., Ade, H., Kilcoyne, A. L. D., Fisher, R., Sokolov, J. C., Rafailovich, M. H.: Compatibilizing bulk polymer blends by using organoclays. Macromolecules 39 (2006), pp. 4793-4801.

[4] Koning, C., Van Duin, M., Pagnoulle, C., Jerome, R.: Strategies for compatibilization of polymer blends. Progress in Polymer Science 23 (1998), pp. 707-757.

[5] Harrats, C., Thomas, S., Groeninckx, G.: Micro- and nanostructured multiphase polymer blend systems phase morphology and interfaces. Boca Raton London New York: Taylor & Francis Group, Inc 2006.

[6] Macosko, C. W.: Morphology development and control in immiscible polymer blends. Macromolecular Symposia 149 (2000), pp. 171-184.

[7] Macosko, C. W., Guegan, P., Khandpur, A. K.: Compatibilizers for melt blending: premade block copolymers. Macromolecules 29 (1996), pp. 5590-5598.

[8] Sundararajs, U., Macosko, C. W.: Drop breakup and coalescence in polymer blends: the effects of concentration and compatibilization. Macromolecules 28 (1996), pp. 2647-2657.

[9] Chen, C. C., White, J. L.: Compatibilizing agents in polymer blends: interfacial tension, phase morphology, and mechanical properties. Polymer Engineering and Science 33 (1993), pp. 923-930.

[10] Hellmann, G. P., Dietz, M.: Random and block copolymers as compatibilizers, directly compared. Macromolecular Symposia 170 (2001), pp. 1-8.

[11] Mark, H. F.: Encyclopedia of polymer science and technology, John Wiley & Sons, New York, 2005.

[12] Kalfoglou, N. K., Kallitsis, J. K., Lambert, J. C., Vanderstappen, L., Skafidas D. S.: Comparison of compatibilizer effectiveness for PET/HDPE blends. Polymer 36 (1995), pp. 4453-4462.

[13] Moly, K. A., Oommenm, Z., Bhagawan, S. S., Groeninckx, G., Thomas, S.: Melt rheology and morphology of LLDPE/EVA blends: effect of blend ratio, compatibilization, and dynamic crosslinking. Journal of Applied Polymer Science 86 (2002), pp. 3210-3225.

[14] Papadopoulou, C. P., Kalfoglou, N. K.: Comparison of compatibilizer effectiveness for PET/PP blends: their mechanical, thermal and morphology characterization. Polymer 41 (2000), pp. 2543-2555.

[15] Shi, D., Ke, Z., Yang, J., Gao, Y. Wu, J., Yin, J.: Rheology and morphology of reactively compatibilized PP/PA6 blends. Macromolecules (35) 2002, pp. 8005-8012.

[16] Zhang, X., Li, G., Wang, D., Yin, Z., Yin, J., Li, J.: Morphological studies of polyamide 1010/polypropylene blends. Polymer 39 (1998), pp. 15-22.

[17] Loyens, W., Groeninckx, G.: Phase morphology development in reactively compatibilised polyethylene terephthalate/elastomer blends. Macromolecular Chemistry and Physics 203 (2002), pp. 1702-1714.

[18] Vocke, C., Anttila, U., Seppälä, J.: Compatibilization of polyethylene/ polyamide 6 blends with oxazoline-functionalized polyethylene and styrene ethylene/butylene styrene copolymer (SEBS). Journal of Applied Polymer Science 72 (1999), pp. 1443-1450.

[19] Vocke, C., Anttila, U., Heino, M., Hietaoja, P., Seppälä, J.: Use of oxazoline functionalized polyolefins and elastomers as compatibilizers for thermoplastic blends. Journal of Applied Polymer Science 70 (1998), pp. 1923-1930.

[20] Park, J., Kim, D., Suh, K.: Blends of polyethylene terephthalate with EPDM through reactive mixing. Journal of Applied Polymer Science 78 (2000), pp. 2227-2233.

[21] Lin, X. D., Cheung, W. L.: Study of poly(ethylene terephthalate)/ polypropylene microfibrillar composites. I. Morphological development in

melt extrusion. Journal of Applied Polymer Science 89 (2003), pp. 1743-1752.

[22] Lin, X. D., Cheung, W. L.: Study on PET/PP microfibrillar composites. I. Morphological development in melt extrusion. Journal of Applied Polymer Science 88 (2003), pp. 3100-3109.

[23] Lee, J. K., Han, C. D.: Evolution of polymer blend morphology during compounding in an internal mixer, Polymer 40 (1999), pp. 6277-6296.

[24] Paul, D. R., Bucknall, C. B.: Polymer blends, John Wiley&Sons, New York, 2000, Chapter 16.

[25] Sundararaj, U., Macosko, C. W., Rolando, R. J., Chan, H. T.: Morphology development in polymer blends. Polymer Engineering and Science 32 (1992), pp.1814-1823

[26] Utracki, L. A., Sammut, P.: Rheological evaluation of polystyrene/ polyethylene blends. Polymer Engineering and science 28 (1988), pp. 1405-1415.

[27] Deyrail, Y., Fulchiron, R., Cassagnau, P.: Morphology development in immiscible polymer blends during crystallization of the dispersed phase under shear flow. Polymer 43 (2002), pp. 3311-3321.

[28] Lepers, J. C., Favis, B. D.: Interfacial tension reduction and coalescence suppression in compatibilized polymer blends. AIChE Journal 45 (1999), pp. 887-895.

[29] Monticciolo, A., Cassagnau P., Michel, A.: Fibrillar morphology development of PE/PBT blends: rheology and solvent permeability. Polymer Engineering and Science 38 (1998), pp. 1882-1889.

[30] Elmendorp, J. J., Maalcke, R. J.: A study on polymer blending microrheology: Part 1. Polymer Engineering and Science 25 (1985), pp. 1041-1047.

[31] Lee, J. K., Han, C. D.: Evolution of polymer blend morphology during compounding in a twin-screw extruder. Polymer 41 (2000), pp. 1799-1815.

[32] Gregor-Svetec, D.: High modulus polypropylene fibers. II. influence of fiber preparation upon structure and morphology. Journal of Applied Polymer Science 100 (2006), pp. 1067-1082.

[33] Gupta, V. B., Sett, S. K., Venkataraman, A.: Flow-drawing of poly(ethylene terephthalate). Polymer Engineering and Science 30 (1990), pp. 1252-1257.

[34] Clark, E. S., Scott, L. S.: Superdrawn crystalline polymers: a new class of high-strength fiber, Polymer Engineering and Science, 14 (1974), pp. 682-686.

[35] Taylor, W. N., Clark, E. S.: Superdrawn filaments of polypropylene. Polymer Engineering and Science, 18 (1978), pp. 518-526.

[36] Kardos, J. L., Raisoni, J.: The potential mechanical response of macromolecular systems-a composite analogy. Polymer Engineering and Science 15 (1975), pp. 183-190.

[37] Nicolov, N., Evstatiev, M., Fakirov, S.: Morphology of microfibrillar reinforced composites PET/PA 6 blend. Polymer 37 (1996), pp. 4455-4463.

[38] Mehta, A., Isayev, A. I.: Rheology, morphology, and mechanical characteristics of poly(etherether keton)-liquid crystalline polymer. Polymer Engineering and Science 31 (1991), pp. 971-980.

[39] Tjong, S. C., Liu, S. L., Li, R. K. Y.: Structure and mechanical properties of the extruded blends of a liquid crystalline polymer with polypropylene. Journal of Materials Science 30 (1995), pp. 353-360.

[40] Tjong, S. C., Liu, S. L., Li, R. K. Y.: Mechanical properties of injection moulded blends of polypropylene with thermotropic liquid crystalline polymer. Journal of Materials Science 31 (1996), pp. 479-484.

[41] Wang, H., Yi, X., Hinrichsen, G.: Influence of drawing down on the properties of thermotropic liquid crystalline polymer/polyether sulfone composites. International Polymer Processing 1 (1997), pp. 26-37.

[42] Kim, S. H., Park, S. W., Gil, E. S.: Crystallization kinetics of poly (ethylene terephthalate) with thermotropic liquid crystalline polymer blends. Journal of Applied Polymer Science 67 (1998), pp. 1383-1392.

[43] Kozlowski, M., La Mantia, F.P.: Study on compatibilization of polypropylene-liquid crystalline polymer blends. Journal of Applied Polymer Science 66 (1997), pp. 969–980.

[44] Machiels, A. G. C., Dam, J. V., Boer, A. P. D., Norder, B.: Stability of blends

of thermotropic liquid crystalline polymers with thermoplastic polymers. Polymer Engineering and Science 37 (1997), pp. 1512-1525.

[45] Evstatiev, M., Fakirov, S., Bechtold, G., Friedrich, K.: Structure-property relationships of injection and compression molded microfibrillar-reinforced PET/PA-6 composites. Advances in Polymer Technology 19 (2000), pp. 249-259

[46] Fakirov, S., Evstatiev, M., Schultz, J. M.: Microfibrillar reinforced composites from drawn poly(ethylene terephthalate)/nylon-6 blend. Polymer 34 (1993), pp. 4669-4679.

[47] Fakirov, S., Evstatiev, M., Petrovich, S.: Microfibrillar reinforced composites from binary and ternary blends of polyesters and nylon-6. Macromolecules 26 (1993), pp. 5219-5226.

[48] Fakirov, S., Evstatiev, M.: Microfibrillar reinforced composites-new matrials from polymer blends. Advanced Materials 6 (1994), pp. 395-398.

[49] Evstatiev, M., Fakirov, S., Friedrich, K.: Effect of blend composition on the morphology and mechanical properties of microfibrillar composites. Applied Composite Materials 2 (1995), pp. 93-106.

[50] Evstatiev, M., Fakirov, S., Krasteva, B., Friedrich, K., Covas, J., Cunha, A.: Recycling of poly(ethylene terephthalate) as polymer-polymer composites. Polymer Engineering and Science 42 (2002), pp. 826-835.

[51] Fakirov, S., Bhattacharyya, D., Lin, R. J. T., Fuchs, C., Friedrich, K.: Contribution of coalescence to microfibril formation in polymer blends during cold drawing. Journal of Macromolecular Science, Part B 46 (2007), pp. 183-194.

[52] Shields, R. J., Bhattacharyya, D., Fakirov, S.: Fibrillar polymer–polymer composites: morphology, properties and applications. Journal of Materials Science 43 (2008), pp. 6758-6770.

[53] Shen, J., Huang, W., Zuo, S.: In-situ fiberized poly(ethylene terephthalate) as a reinforcement to poly(propylene) matrix. Macromolecular Materials and Engineering 288 (2003), pp. 658-664.

[54] Taepaiboon, P., Junkasem, J., Dangtungee, R., Amornsakchai, T., Supaphol,

P.: In Situ microfibrillar-reinforced composites of isotactic polypropylene/ recycled poly(ethylene terephthalate) system and effect of compatibilizer. Journal of Applied Polymer Science 102 (2006), pp. 1173-1181.

[55] Jayanarayanan, K., Thomas, S., Joseph, K.: Morphology, static and dynamic mechanical properties of in situ microfibrillar composites based on polypropylene/poly(ethylene terephthalate) blends. Composites: Part A 39 (2008), pp. 164-175.

[56] Fuchs, C., Bhattacharyya, D., Fakirov, S.: Microfibril reinforced polymer-polymer composites: application of tsai-hill equation to PP/PET composites. Composites Science and Technology 66 (2006), pp. 3161-3171.

[57] Li, Z. M., Li, L. B., Shen, K. Z., Yang, W., Huang, R., Yang, M. B.: Transcrystalline morphology of an in situ microfibrillar poly(ethylene terephthalate)/poly(propylene) blend fabricated through a slit extrusion hot stretching-quenching process. Macromolecular Rapid Communications 25 (2004), pp. 553-558.

[58] Li, Z. M., Li, L. B., Shen, K. Z., Yang, M. B., Huang R.: In-situ microfibrillar PET/iPP blend via slit die extrusion, hot stretching, and quenching: Influence of hot stretch ratio on morphology, crystallization, and crystal structure of iPP at a fixed PET concentration. Journal of Polymer Science Part B: Polymer Physics 42 (2004), pp. 4095-4106.

[59] Li, Z. M., Lu, A., Lu, Z. Y., Shen, K. Z., Li, L. B., Yang, M. B.: In-situ microfibrillar PET/iPP blend via a slit die extrusion, hot stretching and quenching process: Influences of PET concentration on morphology and crystallization of iPP at a fixed hot stretching ratio. Journal of Macromolecular Science Part B: Physics 44 (2005), pp. 203-216.

[60] Li, Z. M., Yang, W., Li, L. B., Xie, B. H., Huang, R., Yang, M. B.: Morphology and nonisothermal crystallization of in situ microfibrillar poly(ethylene terephthalate)/polypropylene blend fabricated through slit-extrusion, hot-stretch quenching. Journal of Polymer Science Part B: Polymer Physics 42 (2004), pp. 374-385.

[61] Li, Z. M., Yang, M. B., Huang, R.: Poly(ethylene terephthalate)/polyethylene

composite based on in-situ microfiber formation. Polymer-Plastics Technology and Engineering 41 (2002), pp. 19-32.

[62] Dai, K., Xu, X. B., Li, Z. M.: Electrically conductive carbon black (CB) filled in situ microfibrillar poly(ethylene terephthalate) (PET)/polyethylene (PE) composite with a selective CB distribution. Polymer 48 (2007), pp. 849-859.

[63] Friedrich, K., Evstatiev, M., Fakirov, S., Evstatiev, O., Ishii, M., Harrass, M.: Microfibrillar reinforced composites from PET/PP blends: processing, morphology and mechanical properties. Composites Science and Technology 65 (2005), pp. 107-116.

[64] Fakirov, S., Kamo, H., Evstatiev, M., Friedrich, K.: Microfibrillar reinforced composites from PET/LDPE blends: morphology and mechanical properties. Journal of Macromolecular Science Part B: Physics 43 (2004), pp. 775-789.

[65] Lin, X. D., Jia, D., Leung, F. K. P., Cheung, W. L.: Study on poly(ethylene terephthalate)/polypropylene microfibrillar composites. II. solid-state drawing behavior. Journal of Applied Polymer Science 93 (2004), pp. 1989-2000.

[66] Evstatiev, M., Schultz, J. M., Petrovich, S., Georgiev, G., Fakirov, S., Friedrich, K.: In situ polymer/polymer composites from poly(ethylene terephthalate), polyamide-6, and polyamide-66 blends. Journal of Applied Polymer Science 67 (1998), pp. 723-737.

[67] Pesneau, I., Ait Kadi, A., Bousmina, M., Cassagnau, Ph., Michel, A.: From polymer blends to in situ polymer/polymer composites: morphology control and mechanical properties. Polymer Engineering and Science 42 (2002), pp. 1990-2004.

[68] Huang, W., Shen, J., Chen, X., Chen, H.: Factors influencing the fiberization and mechanical properties of polypropylene/polyamide 66 in situ composites. Polymer International 52 (2003), pp. 1131-1135.

[69] Quan, H., Zhong, G., Li, Z. M., Yang, M. B., Xie, B. H.: Morphology and mechanical properties of poly (phenylene sulfide)/isotactic polypropylene in situ microfibrillar blends. Polymer Engineering and Science 45 (2005), pp. 1303-1311.

[70] Xu, H. S., Li, Z. M., Pan, J. L.: Morphology and rheological behaviors of

polycarbonate/high density polyethylene in situ microfibrillar blends. Macromolecular Materials and Engineering 289 (2004), pp. 1087-1095.

[71] Biswas, M., Ray, S. S.: Recent progress in synthesis and evaluation of polymer-montmorillonite nanocomposites. Advances in Polymer Science 155 (2001), pp. 167-221.

[72] Ray, S. S., Okamoto, M.: Polymer/layered silicate nanocomposites: a review from preparation to processing. Progress in Polymer Science 28 (2003), pp. 1539-1641.

[73] Giannelis, E. P.: Polymer-layered silicate nanocomposites: synthesis, properties and applications. Applied Organometallic Chemistry 12 (1998), pp. 675-680.

[74] Messersmith, P. B., Giannelis, E. P.: Synthesis and barrier properties of poly(1-caprolactone)-layered silicate nanocomposites. Journal of Polymer Science Part A: Polymer Chemistry 33 (1995), pp. 1047-1057.

[75] Qu, C., Yang, H., Liang, D., Cao, W., Fu, Q.: Morphology and properties of PET/PA-6/SiO$_2$ ternary composites. Journal of Applied Polymer Science 104 (2007), pp. 2288-2296.

[76] Hong, J. S., Kim, Y. K., Ahn, K. H., Lee, S.: Shear-induced migration of nanoclay during morphology evolution of PBT/PS blend. Journal of Applied Polymer Science 108 (2008), pp. 565-575.

[77] Chow, W. S., Mohd Ishak, Z. A., Karger-Kocsis, J.: Morphological and rheological properties of polyamide 6/poly(propylene)/organoclay nanocomposites. Macromolecular Materials and Engineering 290 (2005), pp. 122-127.

[78] Chow, W.S., Mohd Ishak, Z. A., Karger-Kocsis, J.: Atomic force microscopy study on blend morphology and clay dispersion in polyamide-6/polypropylene/organoclay systems. Journal of Polymer Science Part B: Polymer Physics 43 (2005), pp. 1198-1204.

[79] Austin, J. R., Kontopoulou, M.: Effect of organoclay content on the rheology, morphology and physical properties of polyolefin elastomers and their blends with polypropylene. Polymer Engineering and Science 46 (2006), pp.

1491-1501.

[80] Chow, W. S., Abu Bakar, A., Mohd Ishak, Z. A., Karger-Kocsis, J., Ishiaku, U. S.: Effect of maleic anhydride-grafted ethylene–propylene rubber on the mechanical, rheological and morphological properties of organoclay reinforced polyamide 6/polypropylene nano-composites. European Polymer Journal 41 (2005), pp. 687-696.

[81] Sumita, M., Sakata, K., Asai, S., Miyasaka, K., Nakagawa, H.: Dispersion of fillers and the electrical-conductivity of polymer blends filled with carbon-black. Polymer Bulletin 25 (1991), pp. 265-271.

[82] Al-Saleh, M. H., Sundararaj, U.: An innovative method to reduce percolation threshold of carbon black filled immiscible polymer blends. Composites Part A: Applied Science and Manufacturing 39 (2008), pp. 284-293.

[83] Feng, J. Y., Chan, C. M., Li, J. X.: A method to control the dispersion of carbon black in an immiscible polymer blend. Polymer Engineering and Science 43 (2003), pp. 1058-1063.

[84] Elias, L., Fenouillot, F., Majeste, J. C., Cassagnau, Ph.: Morphology and rheology of immiscible polymer blends filled with silica nanoparticles. Polymer 48 (2007), pp. 6029-6040.

[85] Wu, G. Z., Asai, S., Sumita, M.: Entropy penalty-induced self-assembly in carbon black or carbon fiber filled polymer blends. Macromolecules 35 (2002), pp. 945-951.

[86] Lee, M. W., Hu, X., Li, L., Yue, C. Y., Tam, K. C.: Flow behaviour and microstructure evolution in novel SiO_2/PP/LCP composites: effects of filler properties and mixing sequences. Polymer International 52 (2003), 276-284.

[87] Gubbels, F., Jerome, R.: Kinetic and thermodynamic control of the selective localization of carbon black at the interface of immiscible polymer blends. Chemistry of Materials 10 (1998), pp. 1227-1235.

[88] Fenouillot, F., Cassagnau, P., Majeste, J. C.: Uneven distribution of nanoparticles in immiscible fluids: Morphology development in polymer blends. Polymer 50 (2009), pp. 1333-1350.

[89] Elias, F., Fenouillot, F., Majeste, J. C., Martin. G., Cassagnau, P.: Migration

of nanosilica particles in polymer blends. Journal of Polymer Science Part B: Polymer Physics 46 (2008), pp. 1976-1983.

[90] Larson R. G.: The structure and rheology of complex fluids, Oxford University Press, 1999,Chapter 6.

[91] Callan, J. E., Hess, W. M., Scott, C. E.: Elastomer blends-compatibility and relative response to fillers. Rubber Chemistry and Technology 44 (1971), pp. 814-837.

[92] Sircar, A. K., Lamond, T. G.: Carbon black-polymer composites: the physics of electrically conducting compsites. Rubber Chemistry and Technology 46 (1973), pp. 178-190.

[93] Clarke, J., Clarke, B., Freakley, P. K., Sutherland, I.: Compatibilising effect of carbon black on morphology of NR–NBR blends. Plastics, Rubber and Composites 30 (2001), pp. 39-44.

[94] Zhu, S. M., Liu, Y., Rafailovich, M., Sokolov, J., Gersappe, D., Winesett, D. A., Ade, H.: Abstracts of Papers of American Chemical Society 218 (1999), pp. U431-U431.

[95] Ferreiro, V., Douglas, J. F., Amis, E. J., Karim, A.: Phase ordering in blend films of semi-crystalline and amorphous polymers. Macromolecular Symposia 167 (2001), pp. 73-88.

[96] Liu, Y., Kontopoulou, M.: The structure and physical properties of polypropylene and thermoplastic olefin nanocomposites containing nanosilica. Polymer 47 (2006), pp. 7731-7739.

[97] Zhang, Q., Yang, H., Fu, Q.: Kinetics-controlled compatibilization of immiscible polypropylene/polystyrene blends using nano-SiO_2 particles. Polymer 45 (2004), pp.1913-1922.

[98] Ray, S. S., Bousmina, M.: Effect of organic modification on the compatibilization efficiency of clay in an immiscible polymer blend. Macromolecular Rapid Communications 26 (2005), pp. 1639-1646.

[99] Nesterov, A. E., Lipatov, Y. S.: Compatibilizing effect of a filler in binary polymer mixtures. Polymer 40 (1999), pp. 1347-1349.

[100] Lipatov, Y. S.: Polymer blends and interpenetrating polymer networks at the

interface with solids. Progress in Polymer Science 27 (2002), pp. 1721-1801.

[101] Khatua, B. B., Lee, D. J., Kim, H. Y., Kim, J. K.: Effect of organoclay platelets on morphology of nylon-6 and poly(ethylene-ran-propylene) rubber blends. Macromolecules 37 (2004), pp. 2454-2459.

[102] Wang, K., Wang, C., Li, J., Su, J., Zhang, Q., Du, R., Fu, Q.: Effects of clay on phase morphology and mechanical properties in polyamide 6/EPDM-g-MA/organoclay ternary nanocomposites. Polymer 48 (2007), pp. 2144-2154.

[103] Hong, J. S., Kim, Y. K., Ahn, K. H., Lee, S. J., Kim, C.: Interfacial tension reduction in PBT/PE/clay nanocomposite. Rheologica Acta 46 (2007), pp. 469-478.

[104] Vo, L. T., Giannelis, E. P.: Compatibilizing poly(vinylidene fluoride)/nylon-6 blends with nanoclay. Macromolecules 40 (2007), pp. 8271-8276.

[105] Li, Y., Shimizu, H.: Novel morphologies of poly(phenylene oxide) (PPO)/polyamide 6 (PA6) blend nanocomposites. Polymer 45 (2004), pp. 7381-7388.

[106] Hong, J. S., Namkung, H., Ahn, K. H., Lee, S. J., Kim, C.: The role of organically modified layered silicate in the breakup and coalescence of droplets in PBT/PE blends. Polymer 47 (2006), pp. 3967-3975.

[107] Ma, C. G., Mai, Y. L., Rong, M. Z., Ruan, W. H., Zhang, M. Q.: Phase structure and mechanical properties of ternary polypropylene/elastomer/nano-CaCO$_3$ composites. Composites Science and Technology 67 (2007), pp. 2997-3005.

[108] Utracki, L. A., Shi, Z. H.: Development of polymer blend morphology during compounding in a twin screw extruder. part I: droplet dispersion and coalescence-a review. Polymer Engineering and Science 32 (1992), pp. 1824-1833.

[109] Everaerta, V., Aerts, L., Groeninckx, G.: Phase morphology development in immiscible PP/(PS/PPE) blends influence of the melt-viscosity ratio and blend composition. Polymer 40 (1999), pp. 6627-6644.

[110] Shi, Z. H., Utracki, L. A.: Development of polymer blend morphology during compounding in a twin-screw extruder. Part II: theoretical derivations.

Polymer Engineering and Science 32 (1992), pp. 1834-1845.

[111] Willis, J. M., Favis, B. D.: Reactive processing of polystyrene-co-maleic anhydride/elastomer blends: processing-morphology-property relations hips. Polymer Engineering and Science 30 (1990), pp. 1073-1084.

[112] Luciani, A., Jarrin, J.: Morphology development in immiscible polymer blends. Polymer Engineering and Science 36 (1996), pp. 1619-1626.

[113] Bae, T. Y., Park, K. Y., Kim, D. H.: Poly(ethylene terephthalate)/ polypropylene reactive blends through isocyanate functional group. Journal of Applied Polymer Science 81 (2001), pp. 1056-1062.

[114] Paul, D. R., Bucknall, C. B.: Polymer blends, John Wiley&Sons, New York, 2000, Chapter 33.

[115] Friedrich, K., Ueda, E., Kamo, H., Evstatiev, M., Fakirov, S.: Direct electron microscopic observation of transcrystalline layers in microfibrillar reinforced polymer-polymer composites. Journal of Materials Science 37 (2002), pp. 4299-4305.

[116] Evstatiev, M., Fakirov, S., Evstatiev, O., Friedrich, K.: Effect of blend composition on the structure-properties relationships of nanostructured polymer composites from polycondensate/polyolefin blends. International Journal of Polymeric Materials 53 (2004), 211-227.

[117] Friedrich, K.; Fakirov, S.; Zhang, Z.: Polymer composites: from nano- to macro-scale, Springer, New York, 2005, Chapter 9.

[118] Evstatiev, M., Schultz, J. M., Fakirov, S., Friedrich, K.: In situ fibrillar reinforced PET/PA-6/PA-66 blend. Polymer Engineering and Science 41 (2001), pp. 192-204.

[119] Ma J., Zhang S., Qi Z., Li G., Hu Y.: Crystallization behaviors of polypropylene/montmorillonite nanocomposites. Journal of Applied Polymer Science 83 (2002), pp. 1978-1985.

[120] Othman N., Hassan A., Rahmat A. R., Wahit M. U.: Preparation and characterisation of polyethylene-octene grafted maleic anhydride-toughened 70:30 PA6/PP/MMT nanocomposites. Polymers and Polymer Composites 15 (2007), pp. 217-227.

[121] Fornes, T. D., Paul, D. R.: Crystallization behavior of nylon 6 nanocomposites. Polymer 44 (2003), pp. 3945-3961.

[122] Sui, G., Zhong, W. H., Fuqua, M. A., Ulven, C. A.: Crystalline structure and properties of carbon nanofiber composites prepared by melt extrusion. Macromolecular Chemistry and Physics 208 (2007), pp. 1928-1936.

[123] Rong, M. Z., Zhang, M. Q., Pan, S. L., Friedrich, K.: Interfacial effects in polypropylene-silica nanocomposites. Journal of Applied Polymer Science 92 (2004), pp. 1771-1781.

[124] Chow, W. S., Mohd-Ishak, Z. A., Karger-Kocsis, J., Apostolov, A. A, Ishiaku, U. S.: Compatibilising effect of maleated polypropylene on the mechanical properties and morphology of injection molded polyamide6/polypropylene/ organoclay nanocomposites. Polymer 44 (2003), pp. 7427-7440.

[125] Karger-Kocsis, J., Wanjale, S. D., Abraham, T., Bárány, T., Apostolov, A. A.: Preparation and characterization of polypropylene homocomposites: exploiting polymorphism of PP homopolymer. Journal of Applied Polymer Science, in press.

[126] Pothan, L. A.; Oommen, Z.; Thomas, S.: Dynamic mechanical analysis of banana fiber reinforced polyester composites. Composites Science and Technology 63 (2003), pp. 283-293.

[127] Heino, M., Kirjava, J., Hietaoja, P., La, J. S.: Compatibilization of polyethylene terephthalate/polypropylene blends with styrene-ethylene/ butylene-styrene (SEBS) block copolymers. Journal of Applied Polymer Science 65 (1997), pp. 241-249.

[128] Papke, N., Karger-Kocsis, J.: Thermoplastic elastomers basedon compatibilized poly(ethylene terephthalate) blends: effect of rubber type and dynamic curing. Polymer 42 (2001), pp. 1109-1120.

[129] Mohanty, S., Verma, S. K., Nayak, S. K.: Dynamic mechanical and thermal properties of MAPE treated jute/HDPE composites. Composites Science and Technology 66 (2006), pp. 538-547.

[130] Li, W.; Schlarb, A. K.; Evstatiev, M.: Study of PET/PP/TiO$_2$ microfibrillar-structured composites: Part 1. preparation, morphology and dynamic

mechanical analysis of fibrillized Blends. Journal of Applied Polymer Science 113 (2009), pp. 1471-1479

[131] DA Silva, L., Bretas, R. E. S.: Blends of a bottle grade polyethylene terephthalate copolymer and a liquid crystalline polymer. Part I: injection molding morphology and rheological properties. Polymer Engineering and Science 2000, 40, 1414-1428.

[132] Calcagno, C. I. W., Mariani, C. M., Teixeira, S. R., Mauler, R. S.: The role of the MMT on the morphology and mechanical properties of the PP/PET blends. Composites Science and Technology 68 (2008), pp. 2193-2200.

[133] Feng, M., Gong, F., Zhao, C., Chen, G., Zhang, S., Yang, M.: Effect of clay on the morphology of blends of poly(propylene) and polyamide 6/clay nanocomposites. Polymer International 53 (2004), pp. 1529-1537.

[134] Champagne, M. F., Huneault, M. A., Row, C., Peyrel, W.: Reactive compatibilization of polypropylene/polyethylene terephthalate blends. Polymer Engineering and Science 39 (1999), pp. 976-984.

[135] Li, Z. M., Yang, W., Huang, R., Fang, X. P., Yang, M. B.: Essential work of fracture parameters of in-situ microfibrillar poly(ethylene terephthalate)/polyethylene blend: influences of blend composition. Macromolecular Materials and Engineering 289 (2004), pp. 426-433.

[136] Li, X., Park, W., Lee, J., Ha, C.: Effect of blending sequence on the microstructure and properties of PBT/EVA-g-MAH/organoclay ternary nanocomposites. Polymer Engineering and Science 42 (2002), pp. 2156-2164.

[137] Premphet, K., Horanont, P.: Phase structure and property relationships in ternary polypropylene/elastomer/filler composites: Effect of elastomer polarity. Journal of Applied Polymer Science 76 (2000), pp. 1929-1939.

[138] Lee, B. S., Chun, B. C.: Effect of nylon66 addition on the mechanical properties and fracture morphology of poly(phenylene sulfide)/glass fiber composites. Polymer Composites 24 (2003), pp. 192-198.

[139] Li, Z. M., Yang, M. B., Feng, J. M., Huang, R.: Fibre formation based toughening in polycarbonate/polyethylene alloy compatibilized with diallyl

bisphenol A ether grafted polyethylene. Journal of Materials Science 36 (2001), pp. 2013-2018.

[140] Jiang, C., Zhong, G., Li, Z. M.: Recyclability of in situ microfibrillar poly(ethylene terephthalate)/high-density polyethylene blends. Macromolecular Materials and Engineering 292 (2007), pp. 362-372.

[141] Wu, S.:Polymer surface and ahhesion, Marcel Dekker, New York 1982.

[142] Nanda, K. K., Maisels, A., Kruis, F. E., Fissan, H., Stappert,S.: Higher surface energy of free nanoparticles, Physical Review Letters , 91 (2003), pp. 106102.

[143] Ranade, M. R., Navrotsky, A., Zhang, H. Z.: Energetics of nanocrystalline TiO_2. Proceedings of the National Academy of Sciences 99 (2002), 6476-6481.

[144] Wilson, J. N., Titheridge, D. J., Kieu, L., Idriss, H.: Reactions of maleic anhydride over TiO_2 (001) single crystal surfaces. The Journal of Vacuum Science and Technology A 18 (2000), pp. 1887-1892.

[145] Xu, J., Sun, K., Zhang, L., Ren, Y., Xu, X.: A highly efficient and selective catalyst for liquid phase hydrogenation of maleic anhydride to butyric acid. Catalysis Communications 6 (2005), pp. 462-465.

[146] Kaneko, M., Okura, I.: Photocatalysis science and technology: Kodansha-Springer Verlag, 2002.

[147] Nikolova D.: Charakterisierung und Modifizierung der Grenzflächen im Polymer-Metall-Verbund, Dissertation, 2005.

[148] Macosko, C. W., Jeon, H. K., Hoye, T. R.: Reactions at polymer-polymer interfaces for blend compatibilization Source. Progress in Polymer Science 30 (2005), pp. 939-947.

[149] Oyama, H. T., Ougizawa, T., Inoue, T., Weber, M., Tamaru, K.: Interfacial coupling between immiscible polymers: reactive interface between polysulfone and amorphous polyamide. Macromolecules 34 (2001), pp. 7017-7024.

[150] Favis, B. D., Chalifoux, J. P.: The effect of viscosity ratio on the morphology of polypropylene/polycarbonate blends during processing. Polymer

Engineering and Science 27 (1987), pp. 1591-1600.

[151] Everaert, V., Aerts, L.: Phase morphology development in immiscible PP/(PS/PPE) blends influence of the melt-viscosity ratio and blend composition. Polymer 40 (1999), pp. 6627-6644.

[152] Sánchez-Solís, A., Romero-Ibarra, I., Estrada, M. R., Calderas, F., Manero, O.: Mechanical and rheological studies on polyethylene terephthalate-montmorillonite nanocomposites. Polymer Engineering and Science, 44 (2004), 1094-1102.

[153] Huang, Y., Liu, Y., Zhao, C.: Morphology and properties of PET/PA-6/E-44 blends. Journal of Applied Polymer Science 69 (1998), pp. 1505-1515.

[154] Todorov, L. V., Viana, J. C.: Characterization of PET nanocomposites produced by different melt-based production methods. Journal of Applied Polymer Science, 106 (2007), pp. 1659-1669.

[155] Elias L., Fenouillot F., Majest J. C., Alcouffe P., Cassagnau P.: Immiscible polymer blends stabilized with nano-silica particles: Rheology and effective interfacial tension. Polymer 49 (2008), pp. 4378-4385

[156] Clegg, P. S.: Fluid-bicontinuous gels stabilized by interfacial colloids: low and high molecular weight fluids. Journal of Physics: Condensed Matter 20 (2008), pp. 113101.

[157] Avila, A. F., Duarte, M. V.: A mechanical analysis on recycled PET/HDPE composites. Polymer Degradation and Stability 80 (2003), pp. 373-382.

[158] Lange, B. J., Wyser Y.: Recent innovations in barrier technologies for plastic packaging-a review. Packaging Technology and Science 16 (2003), pp. 149-158.

[159] Shields, R. J., Bhattacharyya D., Fakirov, S.: Oxygen permeability analysis of microfibril reinforced composites from PE/PET blends. Composites Part A-Applied Science and Manufacturing 39 (2008), pp. 940-949.

8 List of Publications

Journal Papers

1. Li, W., Schlarb, A. K., Evstatiev, M.: Effect of viscosity ratio on the morphology of PET microfibrils in uncompatibilized and compatibilized drawn PET/PP/TiO$_2$ blends. Journal of polymer Science Part B: Polymer Physics, 47 (2009), pp. 555-562.

2. Li, W., Schlarb, A. K., Evstatiev, M.: Study of PET/PP/TiO$_2$ microfibrillar-structured composites: Part 1. preparation, morphology and dynamic mechanical analysis of fibrillized blends, Journal of Applied Polymer Science, 113 (2009), pp. 1471-1479.

3. Li, W., Karger-Kocsis, J., Schlarb, A. K.: Dispersion of TiO$_2$ particles in PET/PP/TiO$_2$ and PET/PP/PP-g-MA/TiO$_2$ composites prepared with different blending procedures, Macromolecular Materials and Engineering, 294 (2009), pp. 582-589.

4. Li, W., Schlarb, A. K., Evstatiev, M.: Influence of the processing window and weight ratio on the morphology of the extruded and drawn PET/PP blends, Polymer Engineering and Science, 49 (2009), pp. 1929-1936.

5. Li, W., Schlarb, A. K., Evstatiev, M.: Study of PET/PP/TiO$_2$ microfibrillar-structured composites: Part 2. morphology and mechanical properties, Journal of Applied Polymer Science, 113 (2009), pp. 3300-3306.

6. Li, W., Schlarb, A. K., Weber, M., Evstatiev, M.: Deformation of dispersed PA66 phase in drawn PA66/SAN blend, Polymer Bulletin (2009), in press.

Conference and Symposium Proceedings

1. Li, W., Schlarb, A. K.: Influence of PP-g-MA on the migration of TiO$_2$ nanoparticles in PET/PP blend, Polymer Research Division, BASF SE, Ludwigshafen, Germany, April, 2008.

2. Li, W., Schlarb, A. K.: Preparation and properties of PET/PP microfibrillar composites, 8th IVW Kolloquium, Kaiserslautern, Germany, September, 2008.

3. Li, W., Schlarb, A. K.: PET/PP/TiO$_2$ microfibrillar composites, Graduiertenkolleg 814, Johanniskreuz, Germany, November, 2008.

4. Li, W.: Preferential location of TiO$_2$ particles in PET/PP blend, submitted to 17th International Conference on Composite Materials, Edinburgh, UK, 27-31 July, 2009.

Curriculum Vitae

Personal

Family name: Li

First name: Wenjing

Nationality: Chinese

Date of birth: September 24, 1982

Place of birth: Shan Dong, China

Correspondence address: Goeschenstrasse 11

                      21073, Hamburg, Germany

E-mail address: lwjsmiling@gmail.com

Education

10/2006-09/2009   Institut für Verbundwerkstoffe, Kaiserslautern, Germany

                   PhD student

09/2004-07/2006   Harbin Institute of Technology, Harbin, China

                   M.S. in Materials Science

09/2000-07/2004   Qiqihar University, Qiqihar, China

                   B.S. in Materials Science